UNIVERSITY OF NAIROBI

DEPARTMENT OF GEOLOGY

MSc IN GEOLOGY

**SUBSURFACE STRUCTURES AND CHARACTERIZATION OF THE SILALI
GEOTHERMAL SYSTEM, KENYA RIFT.**

By

Kangogo Deflorah Jerobon

Reg No: I56/77008/09

**A dissertation submitted to the University of Nairobi in partial fulfillment of the
requirements for the Degree of Master of Science in Geology (Applied Geophysics).**
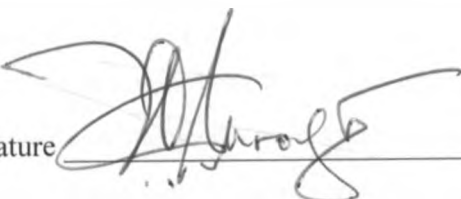
2011

DECLARATION

I certify that although I may have conferred with others in preparing for this assignment, and drawn upon a range of sources cited in this work, the content of this thesis report is my original work and has not been presented for a degree in any other university or any other award.

Signature _____ Date: ___5ᵀᴴ AUGUST, 2011___

Deflorah Kangogo

I confirm that the candidate under our supervision has undertaken the work in this dissertation report.

Signature _____ Date: 8/8/2011

Prof. Justus Barongo

Department of Geology, University of Nairobi.

ABSTRACT

Electrical resistivity methods are widely applied in geothermal exploration and are the cheapest means of acquiring subsurface data. Further detailed surveys like exploratory drilling which is cost intensive in an area under study is always based on accurate surface exploration results. Several exploration methods are applicable in geophysical prospecting of geothermal resources; however, this study focuses mainly on application of electromagnetic methods namely Transient Electromagnetic (TEM) and Magnetotelluric (MT). During the detailed exploration surveys of Silali geothermal prospect situated in the floor of the Northern Kenya rift, MT and TEM methods were applied. The survey was to map out the subsurface resistivity, which is then interpreted so as to provide information such as fluid filled fractures, the reservoir and the heat source. Joint one dimensional (1-D) inversions of MT and TEM data were done so as to correct for static shift in MT soundings. Results of the joint 1-D inversion of MT and TEM data revealed four main resistivity zones; A shallow high resistivity zone (> 100 Ωm) to about 300 m below the surface which is as a result of unaltered rocks, 2) An intermediate low resistivity zone (10 Ωm) to depths of about 1 km which is as a result of low temperature hydrothermal alteration minerals, 3) A deeper high resistivity (> 50 Ωm), up to 3-4 km depth indicating high temperature minerals occurring at depth. The shallow boundary between an upper, low resistive layer and the underlying intermediate resistivity zone at depths of 800-3500 m appears to mark the change in clay mineralogy from low grade alteration mineralogy represented by smectite to high grade alteration mineralogy represented by chlorite, epidote and actinolite, which is interpreted as the geothermal reservoir zone of this study area, and 4) a deeper low resistivity region, at a depth of about 5000 m below sea level is inferred to be magmatic material or intrusion i.e., the heat source of this study area. The resultant 2-D resistivity models showed significant variations in the resistivity distribution both vertically and horizontally on all profiles indicating major structural controls of the geothermal system. This study concludes that a geothermal resource exists in Silali caldera and the nearly vertical conductors in the resistive zones are fluid filled fracture systems/faults and are best targets for exploratory drilling. It is, therefore, recommended that deep exploration wells be drilled within the caldera floor and outside the caldera to the east to further confirm the nature and potential of the resource at Silali.

ACKNOWLEDGEMENT

TABLE OF CONTENTS

List of Figures

List of Tables

List of Plates

Acronyms

AFREPREN	African Energy Policy Research Network
ASAL	Arid and Semi-Arid Lands
EM	Electromagnetic
g.u	Gravity Unit
GDC	Geothermal Development Company
GoK	Government of Kenya
ISOR	Iceland GeoSurvey
Ka	Kilo annum
KenGen	Kenya Electricity Generating Company
KNBS	Kenya National Bureau of Statistics
KPLC	Kenya Power and Lighting Company
KRV	Kenya Rift Valley
Ma	Mega annum
MoE	Ministry of Energy
MT	Magnetotelluric
MW	Mega Watt
TEM	Transient Electromagnetic

CHAPTER ONE

1.0 INTRODUCTION

Silali geothermal prospect, herein referred to as the study area, is the largest and the most spectacular trachytic caldera volcano in the axis of the northern Kenya Rift Valley (KRV). It is a broad, low angle shield, with an elliptical shape slightly elongated in a N-S direction (Figure 1.1). The volcanic shield covers an area of about 900 km^2 and rises to 760 m above the rift floor. The summit of the volcano is at 1528 masl and is occupied by a caldera that measures 7.5 km by 5 km and is bounded by 300 m cliffs. The latest activity from a satellite vent on the northern slopes of Silali is basaltic in composition and to the east is trachytic in composition and was erupted about 200-300 years ago. The young activity associated with the volcano indicates that the magmatic body under the volcano is still hot and able to sustain a geothermal system. This means that there is a remarkable geothermal potential in the region and therefore presents an opportunity for major geothermal power developments in the region which requires geophysical exploration for detailed mapping of the subsurface structure and characterization of the geothermal system.

In the past few decades, application of geo-electrical methods in geothermal prospecting has proven to be a powerful tool. The use of electromagnetic (EM) resistivity methods has become increasingly more effective in characterizing and delineating potential geothermal reservoirs to an extent that even prospects with no surface manifestations have been resolved and delineated. Resistivity methods determine the variations in electrical resistivity of the subsurface both laterally and with depth. Therefore, methods such as (MT) and (TEM) based on the principles of naturally varying magnetic field and controlled magnetic field source techniques, respectively, have been used in this study in mapping the subsurface structure.
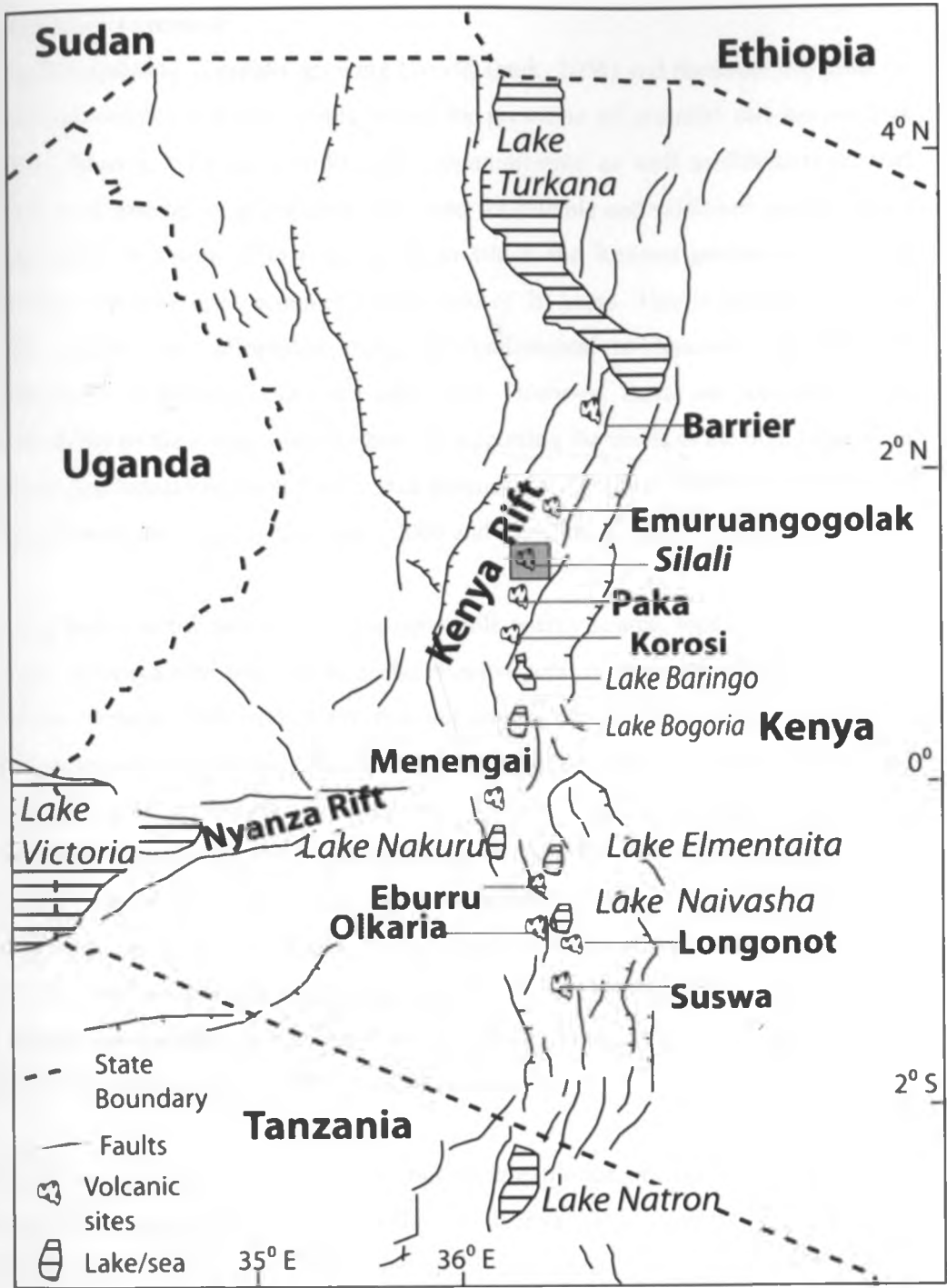
Figure 1.1: Map showing the Kenya rift and the volcanic centers and lakes. Silali (shaded box) is the volcanic center in focus for this study.

1.1 Problem statement

Kenya's population is rapidly growing (World Bank, 2006) and therefore the need for affordable, reliable and dependable power for provision of essential services such as lighting, heating, cooking, mobility and communication as well as driving industrial growth is of paramount importance. The need for reliable and sufficient energy source is stipulated in Vision 2030 (blue print) in which the Kenyan government aims at achieving a middle class economy in a period of 20 years. This is in agreement that secure, reliable and affordable energy is fundamental to economic stability and development at household and national level. However, there are concerns in the sustainability of the energy resource base in supporting the needs as the high population pressure and industrialization has exerted pressure on already available energy sources (Kenya Power and Lighting Company, 2006 and Ministry of Energy, 2002).

Though hydroelectric power source, a renewable energy source, tops the list of energy sources in Kenya with 646.1 MW of the effective total output (African Energy Policy Research Network 2004 and 2005), it is not reliable since Kenya's river systems and their catchments have suffered serious degradation due to extensive deforestation. This implies that a hydropower-dominated power system is vulnerable to large variations in rainfall and climate change and this has proved to be a big challenge in the recent past with the failure of long rains that resulted in power and energy shortfalls. It is also a big challenge for a hydro project if people have to be relocated incase the proposed hydro project area is densely populated. There is thus need to conserve and reduce use of foreign exchange by avoiding, where possible, importation of basic needs like energy, electricity supply or fuel to generate electricity.

Geothermal energy is vast, available, but underexploited, alternative energy source potential for boosting energy supplies in Kenya. The country's geology and hydrogeology favor economic exploitation of geothermal resources. Located on the East African Rift, Kenya boasts massive geothermal potential, as high as 7,000 MW by some estimates. While financial obstacles have hindered development, geothermal is a primary focal point of the country's strategy for energy stability. Kenya currently exploits 167 MW of geothermal power at the Olkaria Geothermal Field and is fast-tracking programs to increase the country's renewable energy capacity, of which

geothermal energy resources could contribute 490 MW by 2012. According to the state-run GDC, Kenya is moving to expand geothermal generating capacity by 5,000 MW by 2030. GDC currently reports a total in-development geothermal capacity of 490 MW coming from six geothermal projects in Olkaria and Menengai (where drilling begun in October, 2010). Construction of four 70 MW geothermal plants in Olkaria and Naivasha commenced in early 2010.

Despite all the merits earmarked by the energy sector, geothermal power production, on the other hand, though constant, is not feasible to step it up at a short notice in addition to its high cost of equipment and in technology (AFREPREN, 2005a). Drilling and exploration for deep resources is very expensive. Forecasts for the future of geothermal power depend on assumptions about technology, energy prices, subsidies, and interest rates.

The appropriate utilization of energy resources has not been possible and its scarcity has still remained an issue of great concern. This fact is attributable to various geothermal exploration problems whereby optimal site location for drill holes in order to provide the best chance of intersecting productive thermal fluid channels and reservoirs deep beneath the subsurface has been a great challenge.

It is in this regard that this study seeks to employ geophysical techniques, i.e, joint TEM and MT imaging to image the subsurface for the existence of electrically conductive zones that form the geothermal reservoirs and geological structures which will form a basis into the future understanding of the geothermal regime of the area in its various aspects because they relate directly to the properties that characterize geothermal systems. These structures could be possible conduits for geothermal fluids indicating the presence of heat sources. This will go a long way in ensuring proper exploitation and management of geothermal resource at the Silali caldera towards sustainable development in the country in that, effective mapping of the extent, location of the heat source and guidance on optimal site location for drill holes to provide the best chance of intersecting productive thermal fluid channels and reservoirs deep beneath the subsurface will be based on the geophysical methods.

1.2 Research motivation

Electromagnetic measurements provide information on the distribution of the electrical resistivity in the subsurface. In geothermal systems, electrical resistivity variations are predominantly caused by hydrothermal alteration zones. The hot fluids of a geothermal system lead to the formation of a sequence of hydrothermal alteration products depending on the temperature. At the top of a high enthalpy geothermal system, a clay cap with expandable clay minerals does occur. Its resistivity is generally lower than the overlying rocks exposed to lower subsurface temperatures. Below the clay cap, a higher resistive core is to be found representing the geothermal reservoir. Thus, the succession of a low resistive region (the clay cap) and a high resistive surrounding (the core below and low temperature alterations above) are somehow indicative of a geothermal reservoir. Electrical resistivity methods are suitable to detect this pattern.

1.3 Aim and objectives

Aim

To determine the sub-surface structures, the areal extent and location of the geothermal reservoir and the possible heat source in the Silali area based on magnetotelluric and transient electromagnetic mapping.

1.3.1 Specific objectives

- To map the subsurface structures of Silali geothermal prospect based on magnetotelluric and transient electromagnetic methods.
- To locate and determine the extent of the geothermal reservoir/heat source in the study area.
- To develop a geothermal model of the study area showing structures and fluid flow patterns.

1.3.2 Justification and significance

The predictive capability for subsurface resource location is an important aspect of a geothermal exploration tool. Geophysical methods have long received attention for this purpose due to their ability to provide structural images of the underground from data taken at the surface. Of the various physical properties of the earth, electrical resistivity is one which can be strongly affected by geothermal processes. Since an increased fluid content in the earth's subsurface due to fracturing, and the development of more

conductive alteration minerals (clays, etc.), can give rise to an electrical resistivity contrast. EM methods of probing have been applied for many years. The reliable mapping of electrical resistivity should increase chances of discovering blind geothermal resources, in defining the location and extent of geothermal reservoirs, in imaging controlling structures for geothermal systems, and in locating and characterizing permeable fracture zones. The magnetotelluic method, in particular, is a preferred geophysical method for geothermal exploration due to its potential to probe greater depth than any other resistivity methods (e.g, Arnason et al., 2010; Onacha, 2006; Newman et al., 2008; Cumming and Mackie, 2010). In addition, magnetotelluric methods have been hailed for their ability to image subsurface conductors (Wannamaker, 1999; Jones et al., 2003; Newman et al., 2008; Spichak and Manzella, 2009; Berktold, 1983; Ingham, 2004).

In geothermal sites, these conductors are often indicators of fluid filled reservoir, concentration of low temperature (above 70^0C and less than 220^0C), conductive minerals like smectite and zeolite, and the heat source (magmatic intrusion). However, at temperatures above 240^0C, minerals such as chlorite and illite which resist the flow of electrical currents are produced (Flovenz et al., 2005; Cumming and Mackie, 2010). These features are the basis of our interpretations.

1.4 Literature review

Limited geophysical studies have been conducted around Silali. On a regional scale, Swain (1976) and, later, Mariita (2003), observed that location of the volcanic centers in Kenya, including Silali volcano, are coincident with the Bouguer gravity high of amplitude more than 200 g.u. along the rift axis. Other volcanic centers like Barrier, Paka, Korosi, Menengai, and Suswa also coincide with the gravity high axis along the Kenya rift (Simiyu and Keller, 1997). This gravity high has been interpreted to represent a shallow magma chamber along the rift. The gravity data station distribution, however, is sparse (about 5 km spacing) and hence could not adequately resolve structures around Silali that are relevant to geothermal development.

1.4.1 Seismology

Since the early 1970's, both passive and active source seismic investigations have been used in trying to understand the formation and structure of the Kenyan part of the East African rift valley (Achauer, 1992; Achauer, 1994; Hamilton et al., 1973; Henry, 1987; Henry et al., 1990; Keller et al., 1994; Keller, 1994; Slack et al., 1994; Tongue et al., 1992; Tongue et al., 1994; Fairhead and Stuart, 1982). Figure 1.2 shows seismicity distribution from the networks deployed. Some of these results have been applied in the search for geothermal energy in Kenya. The United States Geological Survey carried out seismic studies at Lake Bogoria and Olkaria in 1972 and located earthquakes of magnitude 2 or less that were restricted mainly within the fields along fault zones (Hamilton and Muffler, 1972). The resulting time distance plots indicated the Lake Bogoria and Olkaria areas are underlain by a three layer volcanic sequence of about 3.5 km thick. This sequence is, in turn, underlain by a layer with a P-wave velocity of 6.3 km/s. Their interpreted model shows a structure with velocities higher than the average upper crustal velocities within the rift. Further, fewer events were recorded in Lake Bogoria compared to Olkaria.

In 1986/87, a micro-earthquake network was setup in the Lake Bogoria region in an area of about 25 km diameter in the Molo graben, Ndoloita graben and Kamaachj horst comprising 15 recording stations. Results from the survey appeared to suggest that most of the activity was associated with larger, older faults of the rift flanks rather than younger grid faults cross-cutting the rift. The earthquake depth distribution showed that most activities occurred above a depth of 12 km and no 'normal' activity takes place below 15 km, implying a deep brittle-ductile transition zone.

During the KRISP Project, the University of Leicester carried out micro-seismic monitoring at Lake Bogoria geothermal prospect (Young et al., 1991). Results from here, too, indicated that seismicity is confined to faulted zones.

1.4.2 Gravity and ground magnetics

The Bouguer gravity data comprising over 60,000 stations from East Africa, and a subset for the central Kenya rift was extracted by Kenya Electricity Generating Company Limited (KenGen) from the University of Texas at El Paso's (UTEP) database (Mariita, 2003) and also from reports by workers and thesis work of students for this part of the rift (Fairhead, 1976; Simiyu and Keller, 1997; Swain, 1992; Swain, et al., 1994; Swain et al., 1981; Swain and Khan, 1978). The data was reduced to Bouguer values using a density of 2.67 g/cm^3 and adjusted to a common IGSN71 gravity datum.

Analysis of this (Figure 1.3) data showed a large positive anomaly, located in the central part of the area (between Lake Baringo and Emuruangogolak volcanic centre) running in a N-S direction. This could be related to the axial high anomaly that could be a heat source for a possible geothermal system. However, the data is too sparse to give a detailed picture of localized anomalies.
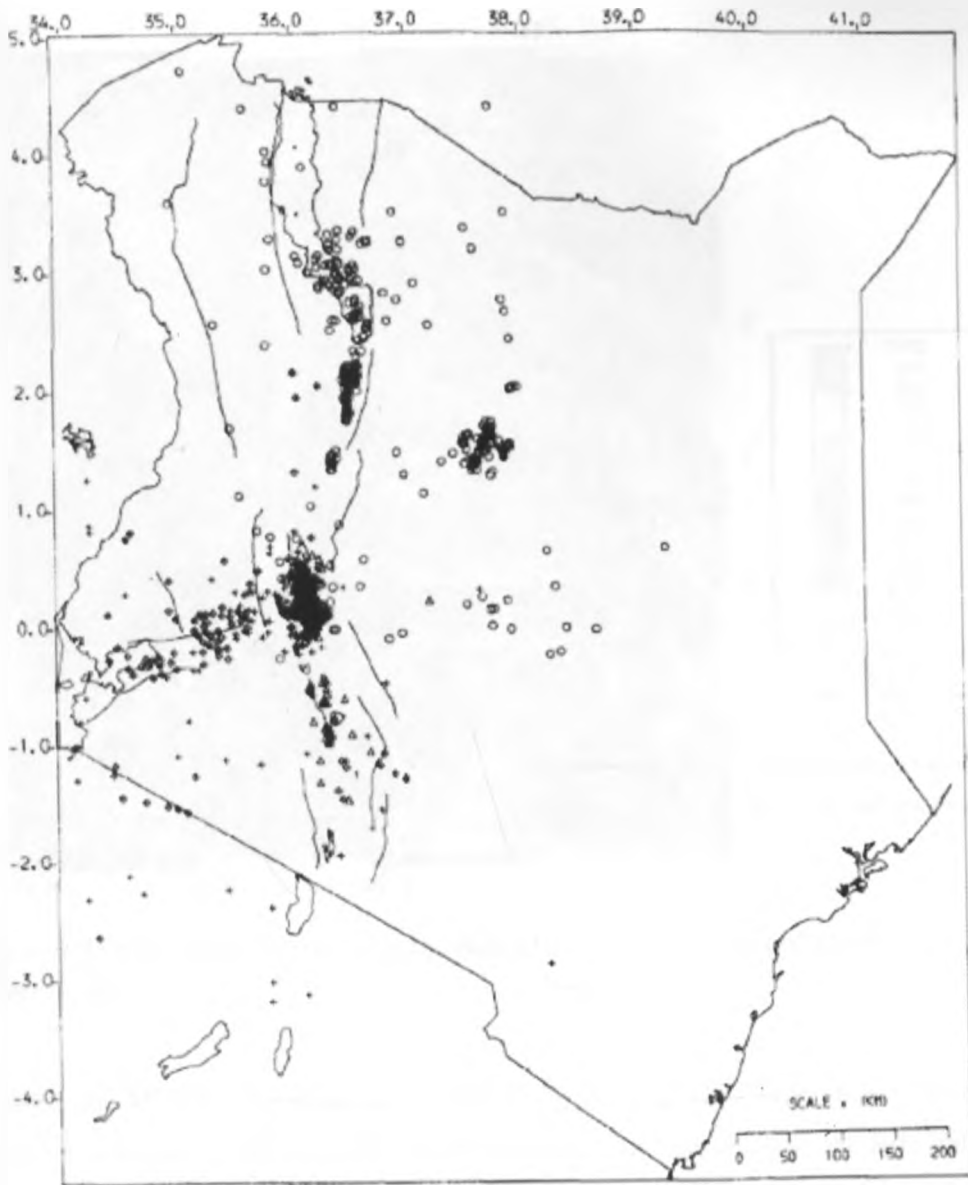
Figure 1.2. Seismicity distribution in Kenya from temporary local networks. Δ = Hamilton's Networks 1985; □ = Kaptagat Array 1976; O = Ngurunit Array 1981; + = KRISP'85 Bogoria Network 1985. (Tongue et al., 1992).
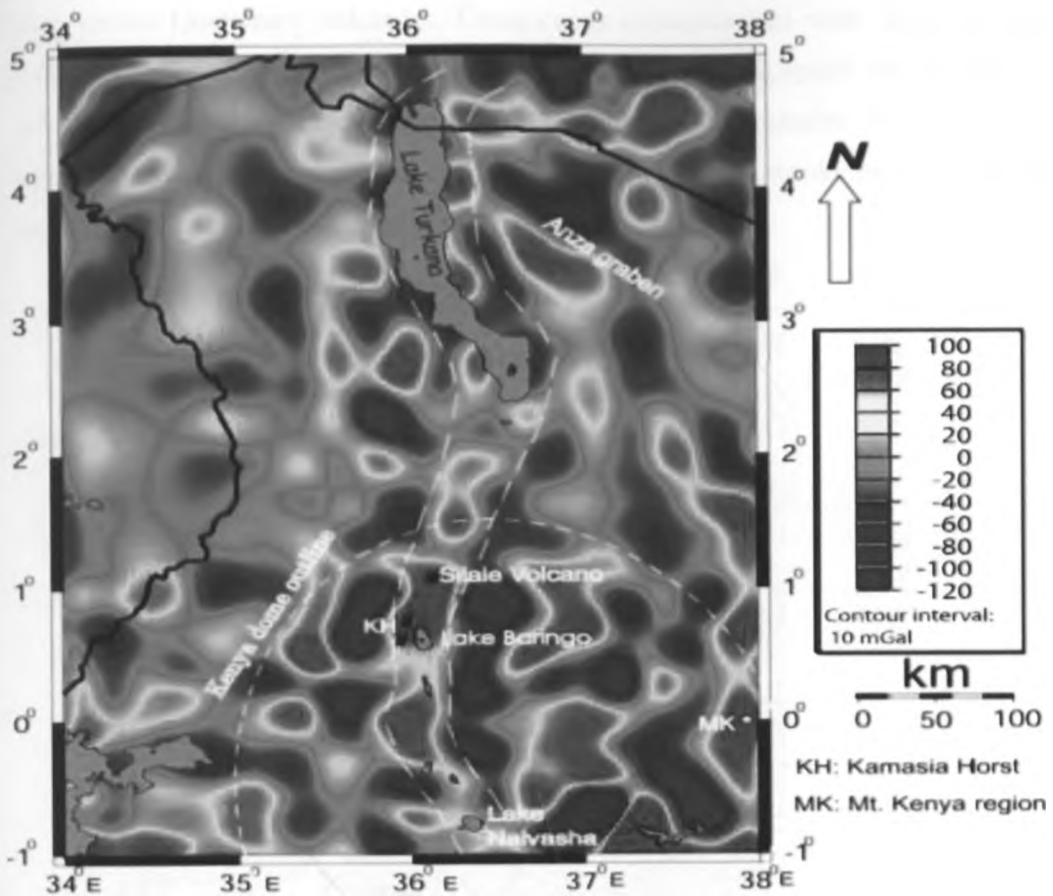
Figure 1.3. Band-pass filtered gravity map of the northern part of the Kenya rift, (Mariita, 2003).

In 1987, the Ministry of Energy, on behalf of the National Oil Corporation of Kenya (NOCK), contracted CGG to carry out an aero-magnetic survey along the Rift Valley (NOCK, 1987). The data was collected at a terrain clearance of 2996 m.a.s.l. Various data reduction techniques were applied to these data, producing different contour maps. KenGen reviewed and evaluated the residual anomalies after reduction to the pole, since qualitative information could be derived from such maps to provide clues as to the geology and structure of a broad region from an assessment of the shapes and trends of the anomalies (Mariita, 2003). They marked the area by a series of high amplitude magnetic anomalies. The wavelengths of these anomalies were less than 2.5 km, their amplitudes showed broad peaks reaching several hundred gammas and their shapes were either isometric or oval (Figure 1.4). This magnetic field was very typical of what is observed over basic volcanics, i.e., basalts. The positive anomalies coincide closely

10

with known Quaternary volcanoes. Conspicuous examples that were noted include positive anomalies coinciding with the Korosi, Silali, Emuruangogolak and the Barrier volcanoes. These high magnetic markers would suggest massive basalts in the subsurface (if not exposed), whereas the overlying terrain would have negligible susceptibility compared to that of basalt.
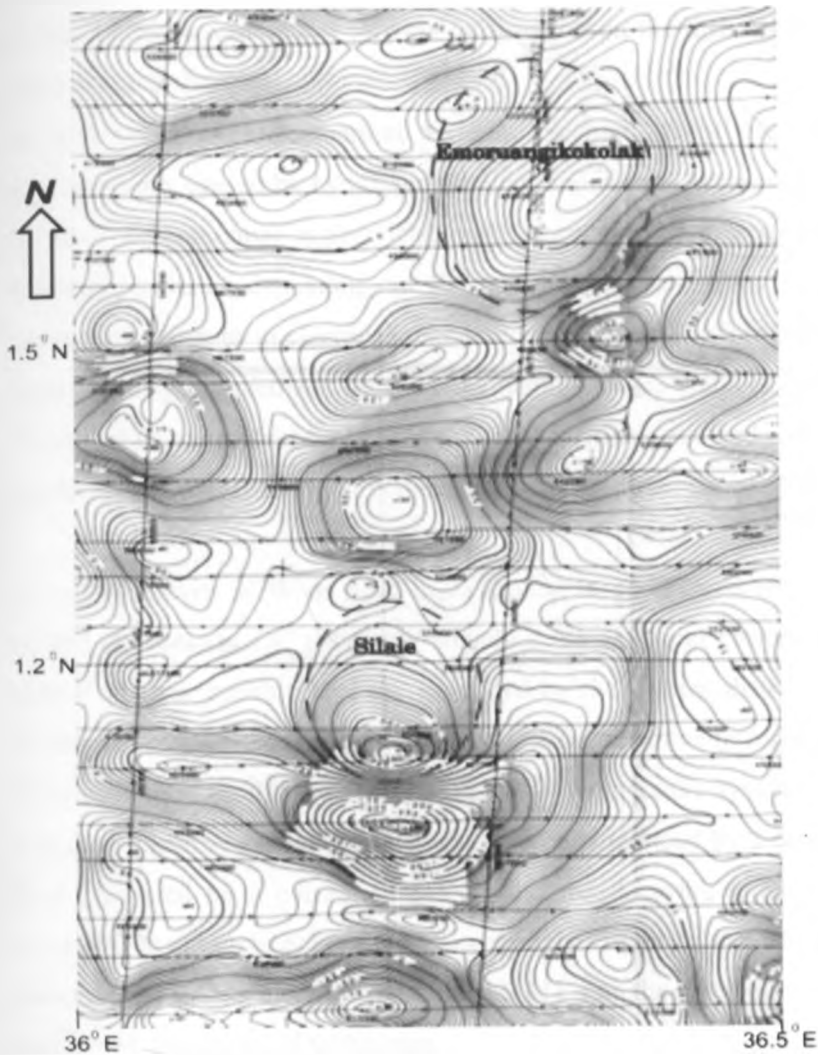
Figure 1.4. Aeromagnetic residual field intensity contour map for areas around Korosi-Chepchuk, Silali and Emuruangogolak volcanic centres. Regional field correction used IGRF 1985 and updated to 1987. (Modified from NOCK, 1987).

1.5 Application of resistivity methods in geothermal exploration

Electrical resistivity methods have proven to be useful tools in geothermal exploration for a long time now. This is because they relate directly to the properties that characterize geothermal systems such as permeability, porosity, salinity, temperature and degree of hydrothermal alteration of the rocks (Hersir and Bjørnsson, 1991). Geoelectrical measurements provide information on the distribution of the subsurface electrical resistivity.

In high temperature geothermal systems, electrical resistivity variations are often predominantly caused by hydrothermal alteration zones (Árnason et al., 2000). The hot fluids of a geothermal system lead to the formation of a sequence of hydrothermal alteration minerals depending on the temperature. Resistivity methods are used to determine variations in electrical conductivity of the sub-surface both laterally and with depth. Among the methods used are the natural-source methods (magnetotelluric) and controlled-source induction methods. Electromagnetic methods are more sensitive to conductive (low-resistivity) structures compared to direct current (DC) techniques.

Several resistivity methods have been applied in geothermal resource assessment for several decades. In DC resistivity sounding, an electrical current is injected into the ground and the potential voltage generated by the current distribution in the earth is measured at the surface. The DC method is more sensitive to resistive structures hence it has been used to identify and delineate high-temperature systems. In the central-loop Transient Electro-Magnetic soundings, current is induced by a time varying magnetic field generated by a current in a loop and the decaying induced magnetic field is monitored at the surface. For the MT method the current in the ground is induced by the natural time varying electromagnetic field. MT soundings have the greatest penetration depth of all the electrical techniques.

1.6 The role of electrical resistivity

Unaltered volcanic rocks generally have high resistivities- which can be changed by hydrothermal activity. Hydrothermal fluids tend to reduce the resistivity of rocks:-

- ❖ by altering the rocks,
- ❖ by increase in salinity or

❖ due to high temperature.

In high enthalpy reservoirs, i.e., fluid temperatures above 200 °C, hydrothermal alteration plays the predominant role (Figures 1.5 and 1.6). In a volcanic terrain, the acid-sulphate waters lead to different alteration products depending on the temperature and thus on the distance from the heat source. With basalts as country rock smectite becomes the dominant alteration product in the temperature range from 100 °C to 180 °C. At higher temperatures mixed layer clays and chlorite become dominant
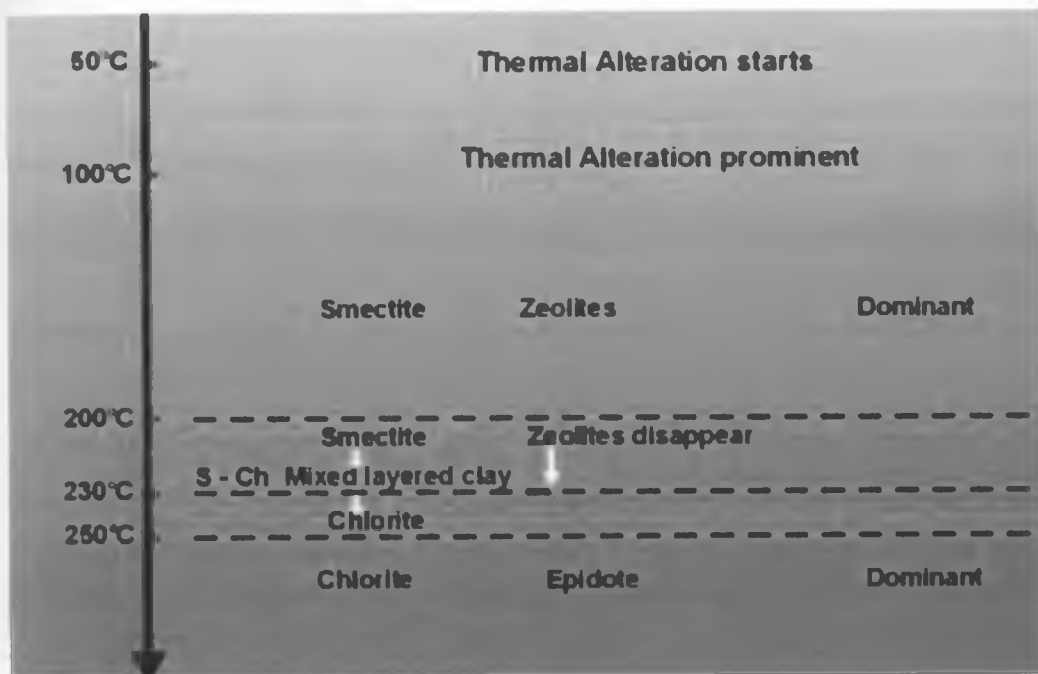
Figure 1.5: Alteration mineralogy with increasing temperature in basaltic country rock. In the temperature range 100°C to 180°C, smectite becomes the dominant alteration product and, generally forms a smectite/bentonite clay cap (source: Geological Survey of Iceland ISOR).
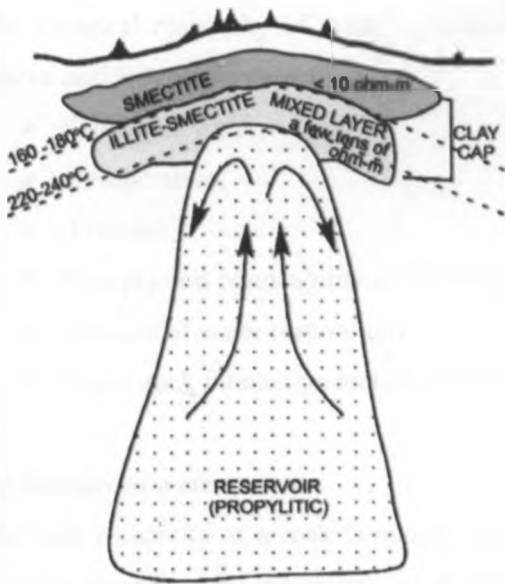
Figure 1.6: Schema of a generalised geothermal system. The smectite cap formed exhibits resistivities in the range of 2 Ohm metre, the mixed layer around 10 Ohm metre.

1.7 Resistivity of rocks

Most rock-forming minerals are electrical insulators. Measured resistivities in the Earth materials are primarily controlled by the movement of charged ions in pore fluids or by conduction of secondary minerals. Although water itself is not a good conductor of electricity, ground water generally contains dissolved compounds that greatly enhance its ability to conduct electricity. Hence, connected porosity and fluid saturation tend to dominate electrical resistivity measurements. In addition to pores, fractures within crystalline rock can lead to low resistivities if they are filled with fluids.

The electrical resistivity of a conductive body is defined as the electrical resistance in Ohms (Ω) between the opposite faces of a unit cube of the conductive material of the material (Kearey and Brooks, 1994). For a conducting cylinder of resistance (R), length (L) and cross-sectional area (A), the resistivity is given by:

$$\rho = RA/L, \qquad (2.1)$$

where, ρ is the specific resistivity (Ωm),

R is the resistance (Ω),

A is area (m^2),

14

L is length (m).

The electrical resistivity of rocks is influenced mainly by the following parameters (Hersir and Björnsson, 1991):-

> Salinity of water,
> Temperature,
> Pressure,
> Porosity and permeability of the rock,
> Amount of water (saturation),
> Water-rock interaction and alteration.

1.8 Salinity of water

The bulk resistivity of a rock is mainly controlled by the resistivity of the pore fluid which is dependent on the salinity of the fluid (Figure 1.7). An increase in amount of dissolved solids in the pore fluid can increase the conductivity by large amounts (conduction in solutions is largely a function of salinity and mobility of the ions present in the solution). Therefore, the conductivity, σ, of a solution may be determined by considering the current flow through a cross-sectional area of $1m^2$ at a voltage gradient of 1 V/m. This is expressed in the equation (2.2) (Hersir and Björnsson, 1991):-

$$\sigma = 1/\rho = F\, (c_1q_1m_1 + c_2q_2m_2 + \cdots), \qquad (2.2)$$

where ,

σ = Conductivity (S/m),

F= Faraday's number (9.65×10^4 C),

c_i = Concentration of ions,

q_i = Valence of ions,

m_i = Mobility of ions.
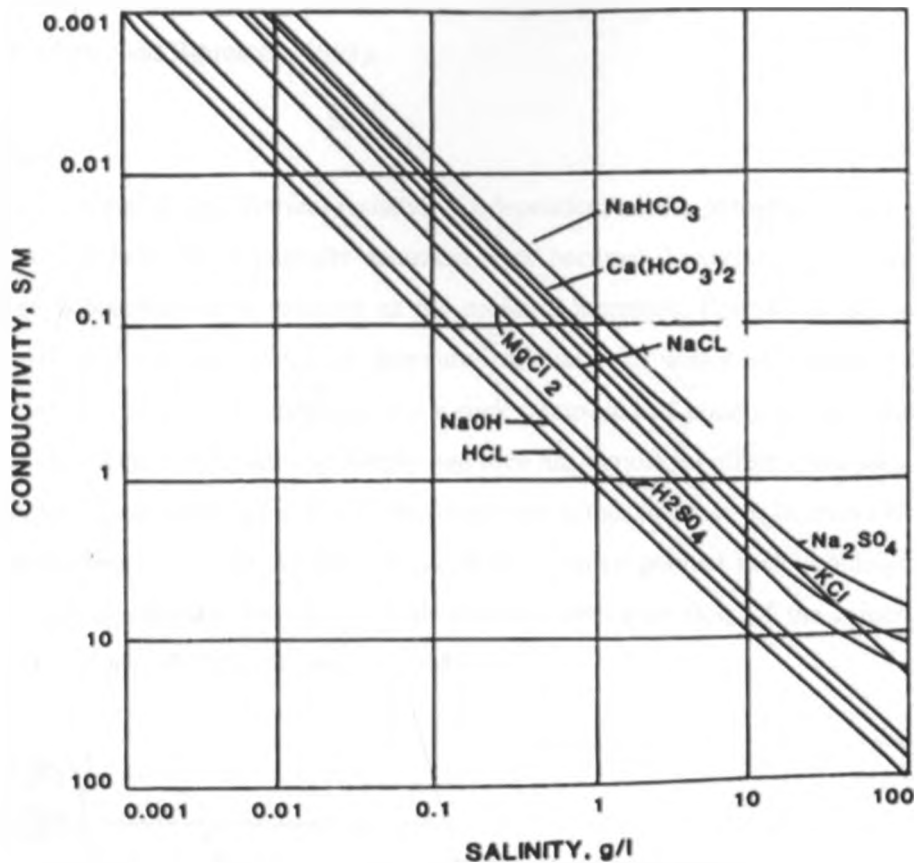
Figure 1.7: Pore fluid conductivity vs. Salinity for a variety of electrolytes (from Keller and Frischknecht, 1966).

1.9 Temperature

At moderate temperatures, 0-200°C, the resistivity of aqueous solutions decreases with increasing temperature. This is due to an increase in ion mobility caused by a decrease in the viscosity of the water. This relationship has been described by Dakhnov (1962) as:

$$\rho_w = \rho \, w_0 \, /(1 + \alpha \, (T - T_0)), \qquad (2.3)$$

where, ρ_w = Resistivity of the fluid at temperature T (Ωm),

   ρ_{wo} = Resistivity of the fluid at temperature T_0 (Ωm),

   α = Temperature coefficient of resistivity (°C), $\alpha \approx 0.023$°C,

   $T_0 = 23$°C (room temperature).

At high temperatures, there is a decrease in dielectric permittivity of water, resulting in decrease in the number of dissociated ions in solution. This effectively increases the

16

fluid resistivity. At temperatures about 300°C, fluid resistivity starts to increase as in Figure 1.8 (Hersir and Björnsson, 1991).

1.10 Pressure

The effects of pressure on electrical resistivity is dependent on the porosity of the rock medium; at low pressure, a partially saturated rock becomes less resistive, whereas saturated rock becomes more resistive as the pressure increases. Porosity is the sole property which determines the high pressure resistivity of water saturated rocks composed of non-conducting minerals. For a rock composed of conductive minerals, pressure at first decreases resistivity sharply and then has almost no effect. For rocks in which pressure causes collapse of pores, resistivity may either increase or decrease with pressure depending on initial connectivity of pores. Coarse-grained rocks containing calcite become abnormally resistive at high pressure owing to flow of the minerals sealing off the spaces (Brace and Orange, 1968).
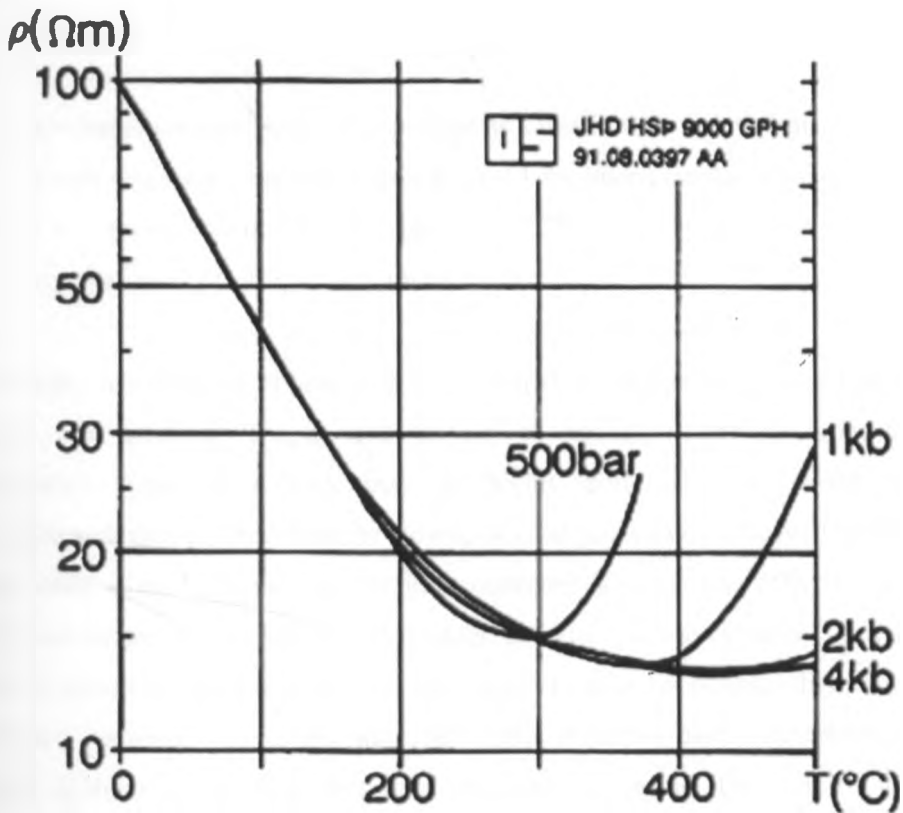
Figure 1.8: Electrical resistivity of water as a function of temperature at different pressures (Hersir and Björnsson, 1991)

1.11 Porosity and permeability of a rock

Porosity is a measure of the void spaces in a material, and is measured as a fraction, between 0–1, or as a percentage between 0–100 percent. More specifically, porosity of a rock is a measure of its ability to hold fluid. Permeability, on the other hand, is a measure of the ability for fluid flow through a rock. Both porosity and permeability are important for electrical conductivity of rocks. Porosity creates the spaces to hold the fluids as permeability allows the fluids to flow through the rock. Therefore, the degree of fluid saturation (dictated by porosity) is of importance to the bulk resistivity of the rock. It has been observed that resistivity varies approximately as inverse powers of the porosity when the rock is fully saturated with water (Keller and Frischknecht, 1966).

This observation has led to the wide spread use of an empirical function relating resistivity and porosity known as Archie's law given by the formula:-

$$\rho = a\,\rho_w\,\varphi^{-m} , \tag{2.4}$$

where,

ρ = bulk resistivity,

ρ_w = resistivity of the pore fluid,

φ = Interconnected porosity expressed as a fraction per unit volume of rock,

a = an empirical parameter varies from < 1 for inter-granular porosity to slightly

> 1 for rocks with joint porosity,

m = cementing factor, usually about 2.

Permeability is a measure of how well fluids will flow through a material. Just as with porosity, the packing, shape, and sorting of granular materials control their permeability. Although a rock may be highly porous, if the voids are not interconnected, then fluids within the closed, isolated pores cannot move. The degree to which pores within the material are interconnected is known as effective porosity. Rocks such as pumice and shale can have high porosity, yet can be nearly impermeable due to the poorly interconnected voids. The range of values for permeability in geologic materials is extremely large. The most permeable materials have permeability values that are millions of times greater than the least permeable. Permeability is often directional in nature. Secondary porosity features, like fractures, frequently have significant impact on the permeability of the material. In addition to the character of the

host material, the viscosity and pressure of the fluid also affect the rate at which the fluid will flow (Lee et al., 2006).

1.12 Water-rock interaction and alteration

Geothermal water reacts with subsurface ambient rock to form alteration zones. The distribution of an alteration zone provides information on the magnitude of the geothermal system and the flow path of the geothermal water. The alteration mineralogy provides information on the physicochemical characteristics of the geothermal water. The alteration intensity is normally low for temperatures below 50-100°C. At temperatures lower than 220°C, low temperature zeolites and the clay mineral smectite are formed (Árnason et al, 2000).

The range where low temperature zeolites and smectite are abundant is called the smectite-zeolite zone. In the temperature range from 220°C to about 240-250°C, the low temperature zeolites disappear and the smectite is transformed into chlorite in a transition zone, the so-called mixed layered clay zone, where smectite and chlorite coexist in a mixture. At about 250°C the smectite disappears and chlorite is the dominant mineral, marking the beginning of the chlorite zone. At still higher temperatures, about 260-270°C, epidote becomes abundant in the so-called chlorite-epidote zone. This zoning applies for fresh water systems. In brine systems, the zoning is similar but the mixed layered clay zone extends over a wider temperature range or up to temperatures near 300°C (Árnason et al, 2000).

Normally, resistivity decreases with increasing temperature but in high temperature volcanic areas, the situation is the reverse in the chlorite and chlorite-epidote alteration zone, where resistivity increases with increasing temperature. This high resistivity exhibited by chlorite and epidote could be due to an extremely low concentration of mobile cations. Figure 1.9 demonstrates the relationships between resistivity, alteration and temperature both for saline and fresh water systems.

Resistivity Structure summarised
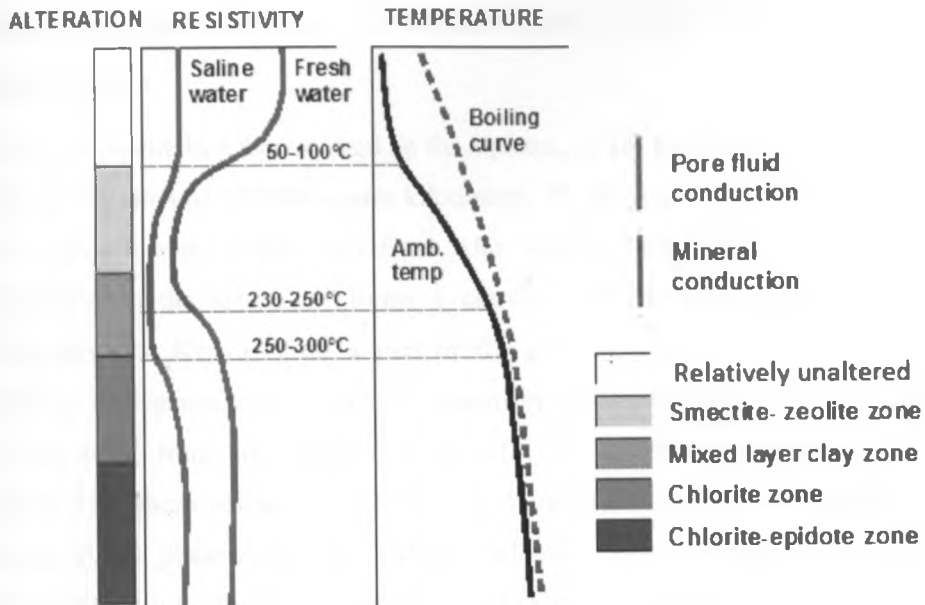
Figure 1.9: General resistivity structure of high temperature geothermal field showing resistivity variation with alteration and temperature (modified from Árnason et al., 2000)

When alteration is in equilibrium with temperature, then the reservoir temperature is expected to be above 250 °C. If the geothermal system has cooled down, then alteration remains and the resistivity structure can be misleading since it reflects the alteration that was formed in the past.

CHAPTER TWO

2.0 REGIONAL AND LOCAL SETTING OF THE STUDY AREA

2.1 Introduction

Kenya is a republic in Africa located on the equator, on the continent's east coast. It has a total surface area of 582000 square kilometers. The Kenya rift is one of the arms of the African rift system that runs from Afar triple junction in the north to Beira, Mozambique in the south. It forms a classic graben averaging 40-80 km wide. Geologically, the Kenya rift is a part of the great African rift, which is an intra-continental divergence zone where rift tectonism accompanied by intense volcanism, has taken place from late Tertiary to Recent. The rift floor comprises mainly the eruptives from these volcanoes (Figure 2.1). Most of the volcanic centers had one or more explosive phase, including caldera collapse. Some centers are dotted with hydrothermal activity and are envisaged to host extensive geothermal systems driven by their still hot magma.

The development of the Kenya rift started during early Miocene (14-23 Ma ago) with volcanism in Turkana followed by activity southwards. The faulting that accompanied rifting occurred in several stages starting with faulting on the western side accompanied by basaltic and phonolitic volcanism on the crust of uplift (Baker et al., 1987). Major faults extended along the western side forming half graben bounded by monoclinic flexure on eastern side and development of major basaltic-trachytic shield volcanoes occurring. Major faults developed on the eastern side with the half graben changing into full graben accompanied by basalt-trachyte volcanism.

The formation of the graben structure started about 5 million years ago and was followed by fissure eruptions in the axis of the rift to form flood lavas by about 2 to 1 million years ago. During the last 2 million years, volcanic activities became more intense within the axis of the rift. During this time, large shield volcanoes, most of which are geothermal prospects, including Silali volcano, developed in the Kenya rift axis.
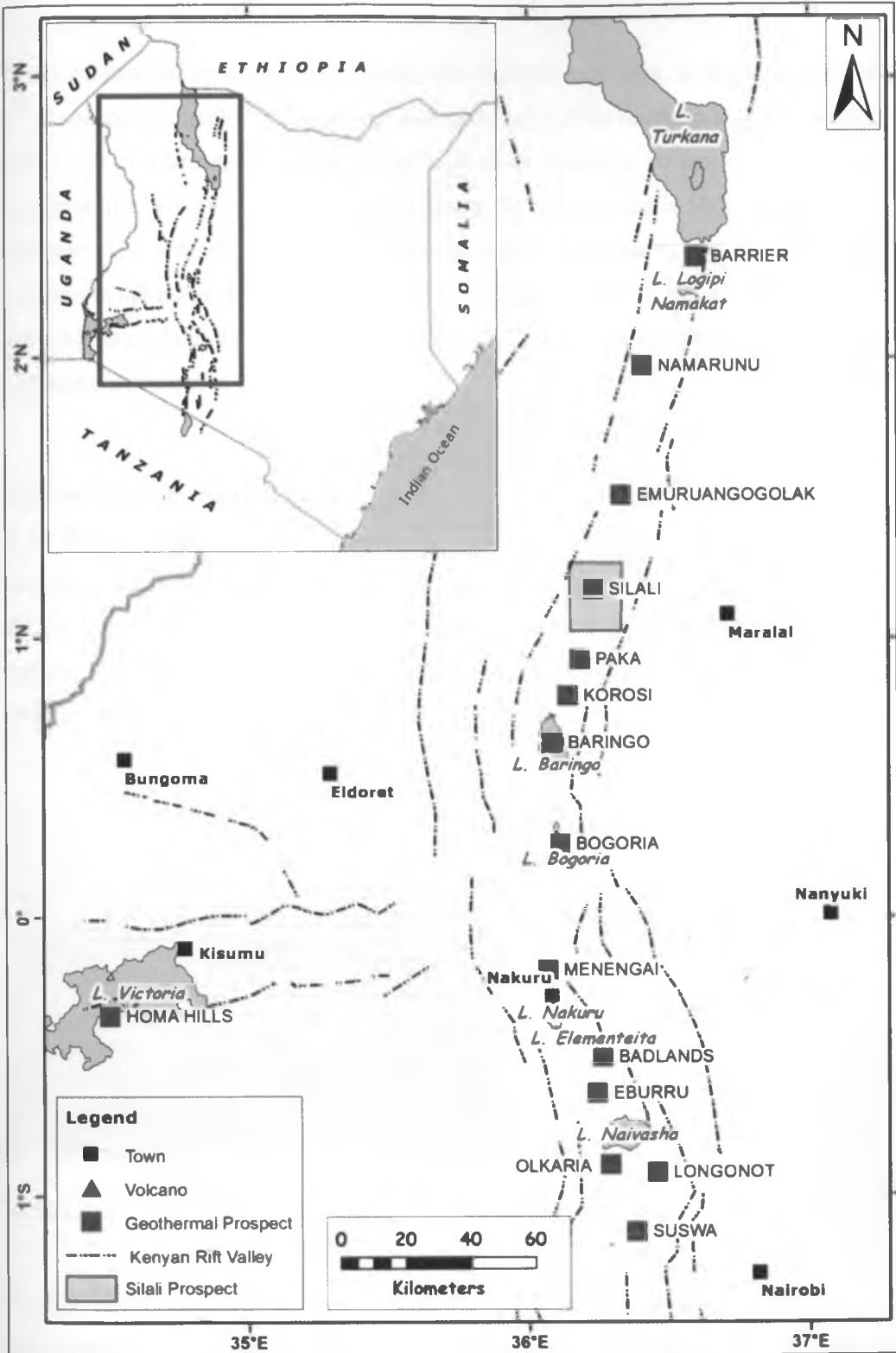
Figure 2.1: Map of part of the Kenya rift showing Silali and other northern rift sector volcanoes

2.2 Location

Silali geothermal prospect, herein referred to as the study area, is the largest and the most spectacular trachytic caldera volcano in the axis of the northern Kenya Rift Valley (KRV). It is a broad, low angle shield, with basal diameter 30 km x 25 km slightly elongate in a N-S direction. It is located along the rift axis and is 50 km north of Lake Baringo. The volcano is adjacent to Paka volcano to the south and Emurungogolak volcano to the north (Figure 2.1). The geographical positioning places the study area at approximately latitude $1°10'$ and longitude $36°12'E$ on the geological map of Silali volcano sheet number 91/2000.

2.3 Physiography and drainage

2.3.1 Physiography

Silali caldera is a major physiographic feature in the north rift floor. The spectacular caldera rim forms a complete circular cliff that breaks at few locations (Plate 1). The caldera floor, which is fairly flat except for a few explosive crater cones, covers an area of about 88 km^2 and is mainly covered by pyroclastics.

Plate 1: The general physiography of Silali caldera

2.3.2 Drainage

The simplified drainage map of the area between Lake Baringo and Silali is shown in Figure 2.2. Most of the rivers within the region are seasonal except for Suguta, Kerio and Mukutan, which flow throughout the year. The drainage in the area is strongly

controlled by the structural elements of the region. The crest of the eastern shoulder of the rift acts as a watershed between rivers that flow westwards through steep gorges into the inner trough, and the rivers that drain the high plateau and flow eastwards into EwasoNgiro and eventually into the Indian Ocean.
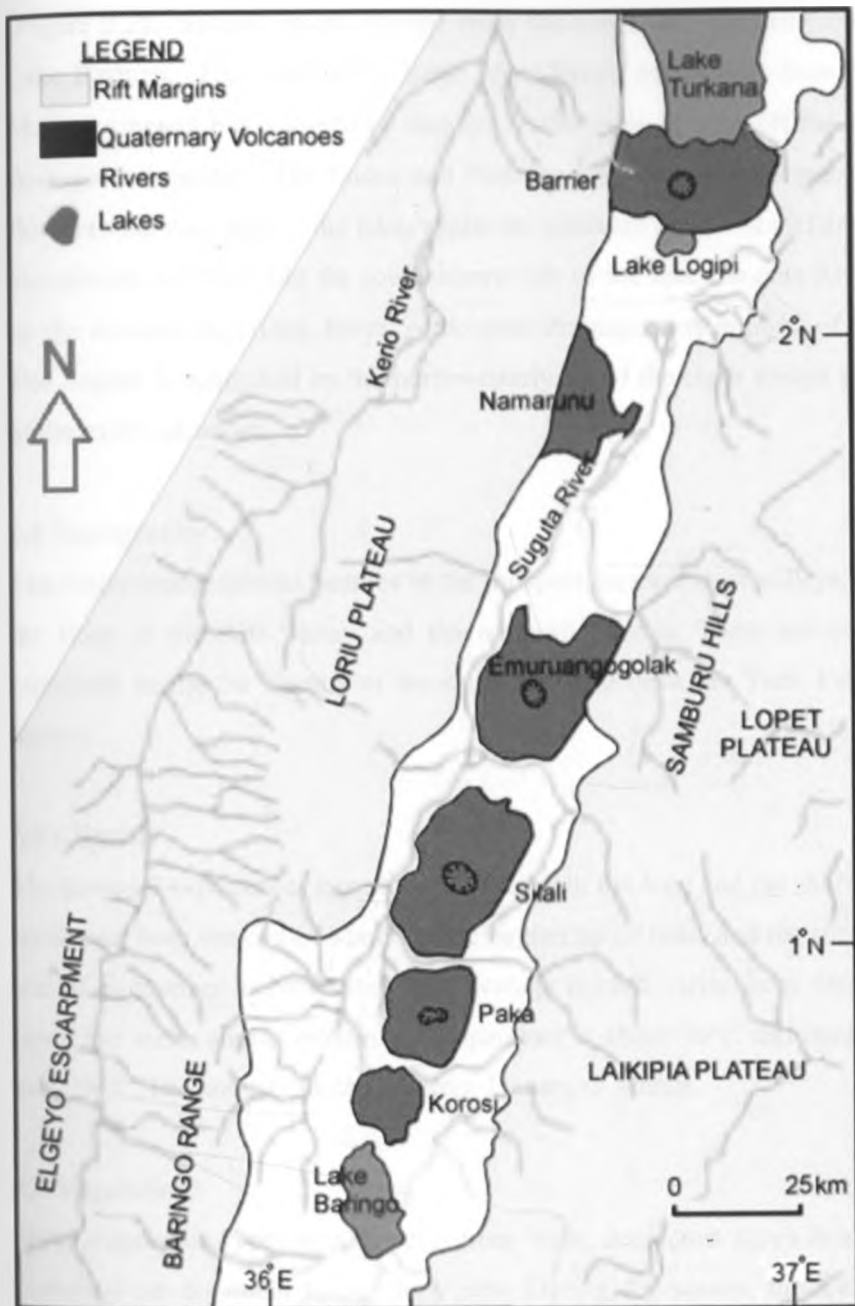
Figure 2.2: The map of the drainage system in the area between Lake Baringo and Lake Turkana (modified from Dunkley et al., 1993)

The crest of the western shoulder of the rift marked by Baringo Hills to the south and Loriu Plateau to the north acts as drainage divide between the Kerio system to the west and drainage into the inner trough to the east. The inner trough consists of two major drainage systems, namely Lake Baringo and Suguta River to the north of the study area (Figure 2.2). Several rivers flowing from the south, the southeast and the west feed Lake Baringo. The main feeder is the Molo River, which rises from the south on the Mau escarpment but is joined by numerous tributaries flowing off the eastern flanks of Baringo escarpment. The Endau and Perkerra also drain the Baringo escarpment and flow into the west side of the lake, whilst the Mukutan and OlArabel drain the Ngelesha escarpment and flow into the southeastern side of the lake. Suguta River, which is fed by the seasonal Nginyang River, is the main drainage system north of the project area. The Suguta is controlled by the northwesterly tilt of the inner trough and the locations of the axial volcanoes.

2.4 Topography

The major topographical features in the prospect area are river valleys, plains, the hills, the floor of the Rift Valley and the northern plateau. There are several volcanoes especially in the the vicinity of the study area and these are Tiati, Paka, Kamugo and Korosi.

2.5 Climate

The prospect experiences two seasons of rainfall; the long and the short rains. The long rains start from the end of March to the beginning of June, and the short rains from the end of September to November. The average rainfall varies from 486 to 755 mm per year. The mean annual maximum temperature is about 30°C and occasionally rises to over 35°C. The hottest months are from January to March.

2.6 Vegetation

Three vegetation types namely; evergreen bush, deciduous shrub land and chrysopon grassland are dominant in the study area. During dry season, the area is mostly bare ground. Other vegetation noted in the area is the geothermal grass (*fibrilytis exillis*) which is found in hot grounds and around the fumaroles.

2.7 Land use and land resources

The study area is 100% Arid and Semi-Arid Lands (ASAL). The local community (Pokots and Turkanas) in the study area are mainly pastoralist; however, a few have settled down to farming. Some crop farming is being done in agro-pastoralist livelihood zones found in Churo, Tangulbei and Koloa division.

2.8 Geology of the study area

Silali is a large Quaternary caldera volcano in the axis of the northern Kenya rift at the border between Turkana and Pokot East Districts at $1^{\circ}10'$N, $36^{\circ}12'$E (Figure 1.1). The volcanic shield covers an area of about 850 km^2 and rises to 760 m above the rift floor. The summit of the volcano is at 1528 masl and is occupied by a caldera that measures 7.5 km by 5 km and is bounded by 300 m cliffs.

The development of the 30 km wide Silali trachyte shield volcano was initiated during the early Quaternary times with the eruption of largely basaltic lavas. Subsequent activity comprised both basaltic and trachytic volcanism, which resulted in the formation of a low shield volcano. The eruptions composed predominantly of basalts, trachytes, hawaiite, mugearite, benmoreite and phonolite (Dunkley et al., 1993). Activity continued and culminated in the incremental collapse of the caldera at the summit with NW alignment. The simplified geological map of the area is shown in Figure 2.3.

Basalt and trachyte (Katenmening lavas) erupted along the circumferential fissure zone and from a major meridional summit fissure forming a series of flat summit benches and ponded in summit depressions before overflowing. The continuing inward collapse of the summit area and the lateral drainage of magma from a high level reservoir finally culminated in the formation of a large caldera at around 63 ka. During the Katenmening activity, three large pit craters formed on the southern flanks of Silali, probably as a result of phreatomagmatic activity. The largest Katemening crater is mantled by a basaltic agglutinate containing many thousands of dorerite blocks (McCall and Hornung, 1970). Post caldera activity utilized pre-existing weaknesses within the caldera, erupting basalt and trachyte lavas until around 7 ka within the caldera, and was contemporaneous with the eruption of trachyte lava domes (9-7 ka).
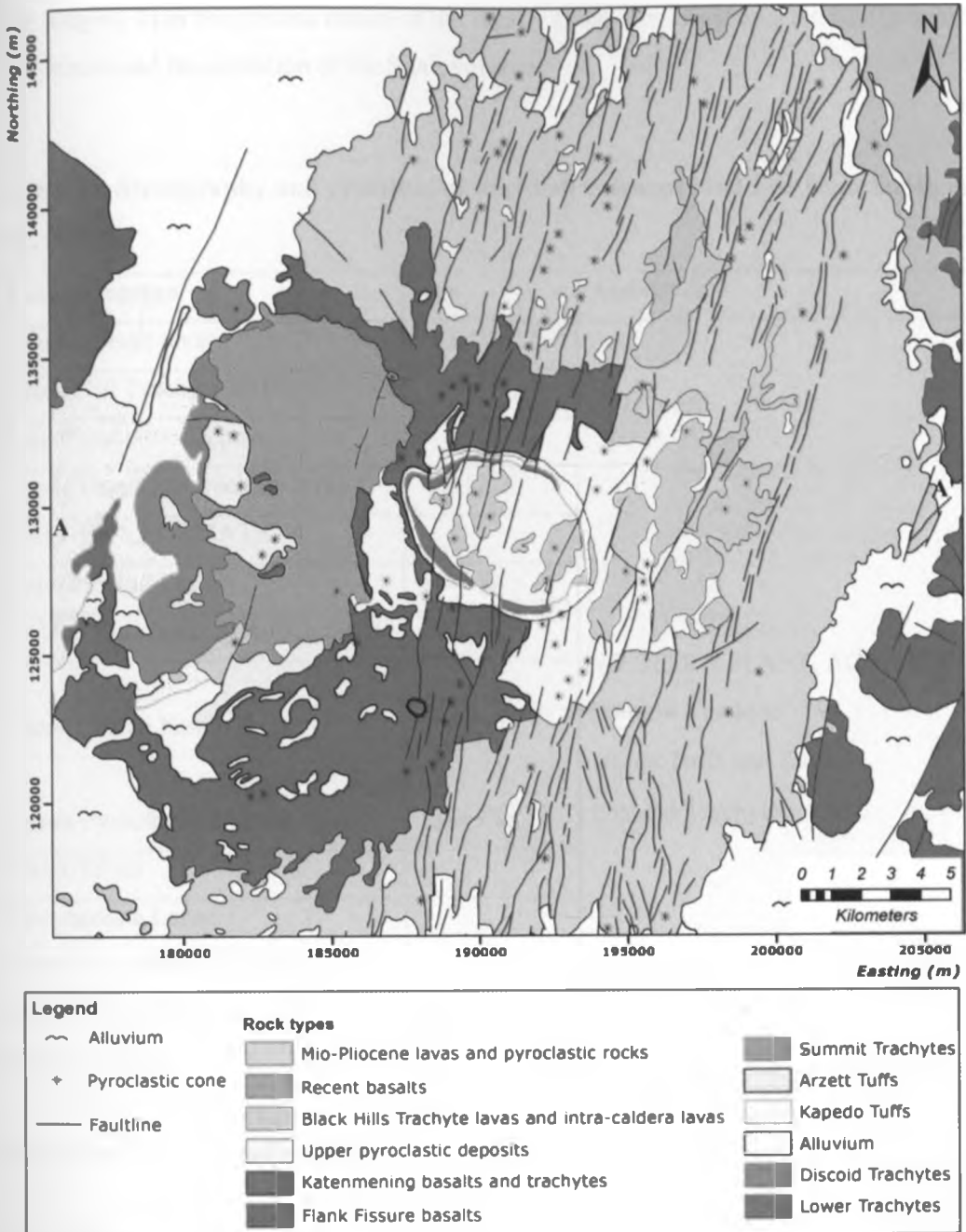
Figure 2.3: Simplified geological and structural map of Silali volcano. Modified from Williams et al., (1984).

BlackHills trachytes on the eastern flanks and some late tongues of basalt on the outer slopes are the latest eruptions in Silali and are not dated but are probably about 200 yrs

BP judging from the pristine nature of the lavas. Table 1 below shows the stratigraphic sequences and the evolution of the Silali volcano.

Table 1: Stratigraphy and evolution of the Silali volcano. Modified from Smith et al., (1995).

Event/eruption	Age	Activity
Young Basalt lavas	4±2-10±2 ka	
Black Hill Trachyte lavas		
Late Pyroclastic Deposit		
Upper basalt and trachyte lavas	7±3 ka	
CALDERA FORMATION		
Katenmening Lavas	64±2 ka	
FAULTING AND SUBISDENCE		
Flank Fissure basalt		WESTERN FLANK ACTIVITY Summit Trachyte Arzett Tuffs and Lavas
Upper Pyroclastic Deposit	133±3 ka	Discoid Trachyte
FAULTING		
Intermediate Lavas Lower Pyroclastic Deposit Lower Trachyte Lavas Mission Basalt	224±9 ka	Kapedo Tuff

2.8.1 Structural setting of Silali

The main structures in the area surrounding Silali include the NNE-SSW trending faults and the caldera. The axial rift zone which has played an important part in the younger phases of volcanism in Silali shows a change in orientation across the volcano. In the north, it is parallel to the rift margin and trends NNE-SSW at 018°, whereas in the south individual deformation belts become narrower, trend more N-S and are oblique to the rift margins. The faults and fractures in the rift are curvilinear with strike lenghts of

upto 5 km, and are often composed of a series of en echelon segments linked by short up-faulted horsts or obliquely trending relay or transfer faults.

Figure 2.4: Tectonics of the Silali region with thin lines signifying the numerous faults while the bold dark lines are fissures (Modified from Smith et al., 1995).

Downthrow directions are distributed equally between east and west and displacements vary from 10-20 metres. Changes in diaplacement directions along individual faults are not uncommon, particularly on the northern flanks. Post caldera within this zone is also indicated by numerous faults which cut the caldera walls and the lavas on the caldera floor. Figure 2.4 below shows the structural setup of Silali.
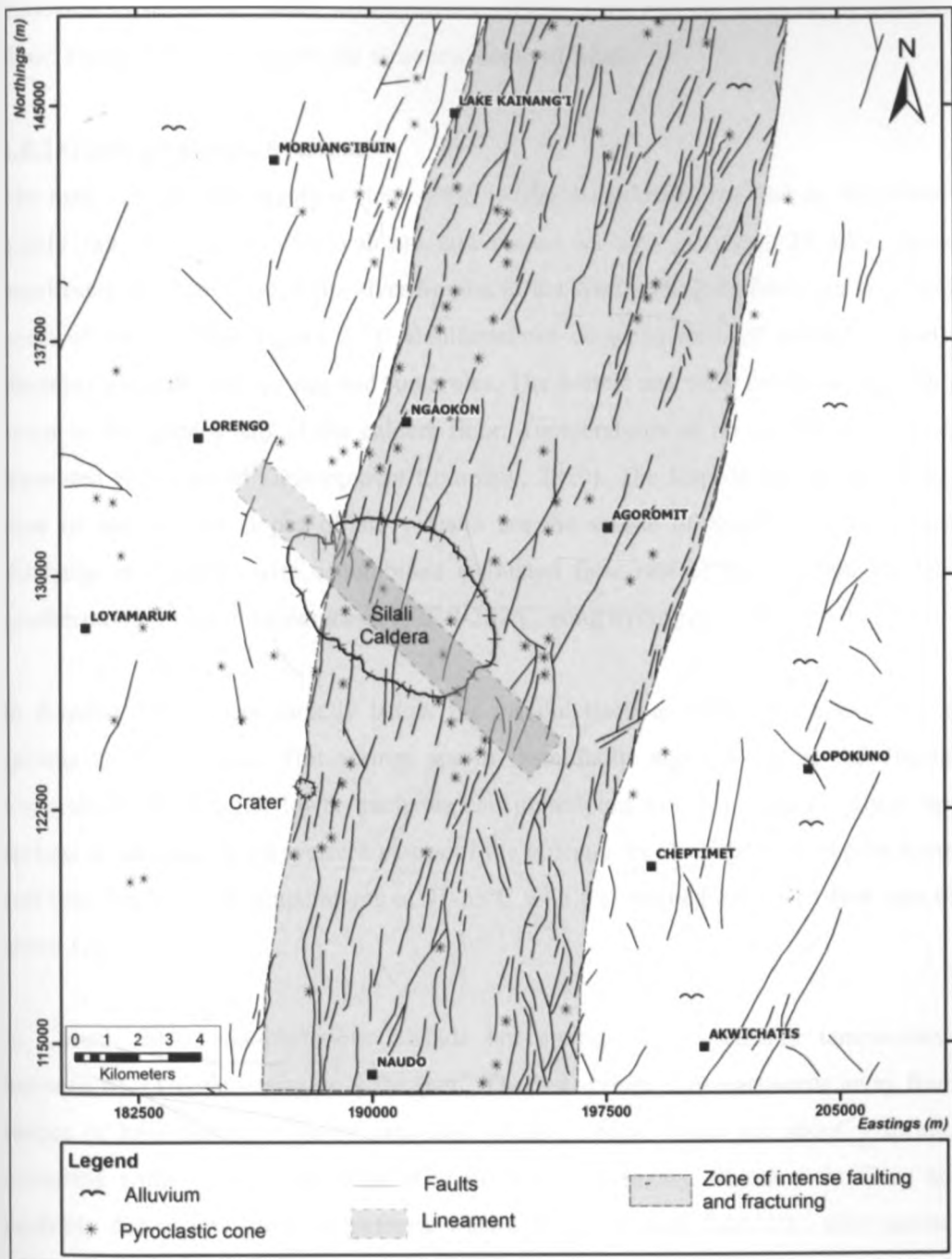
2.8.2 Geothermal manifestations

The major geothermal manifestations occur within the caldera floor and on the eastern highly faulted slopes of the volcano and covers an area of about 20 km^2. Some manifestations also occur along river Suguta in the west and along fractures in the far north of the volcano (Figure 2.5). Manifestations occur in form of altered grounds, steaming grounds, hot springs and fumaroles. The hottest and most extensive activities occur in the eastern half of the caldera floor. Temperatures of up to 97°C have been measured (Geothermal Development Company, 2010). The Kapedo hot springs at the base of the western slopes of the volcano are the source of Suguta river and they discharge at 45-55°C with a combined estimated flow rate of about 1,000 l/s. Gas geothermometry gave temperatures of 238-287°C using hydrogen (GDC, 2010).

In Kapedo, fault zones directly below the discoid trachyte result in a series of hot springs at the riverbed. Hot springs sprout from faults and fissures in the discoid trachytes, Kapedo tuffs, lower trachytes and underlying Mission basalts. These hot springs at the base of the western slopes of the volcano are the source of Suguta River and they discharge at temperatures of 45-55°C with a combined estimated flow rate of about 1,000 l/s.

In Lorusio Main manifestations include hot springs with measured temperatures between 65-74°C occurring on a flat pan. The hot springs flow eastwards away from ranges of hills hosting dyke swarms and volcanic cones. There are about 5 springs occurring within a discharge area of about 1 km^2 of highly altered rock. They are probably due to upwelling of meteoric waters along a fissure/fault zone after contact with deep hot rocks.
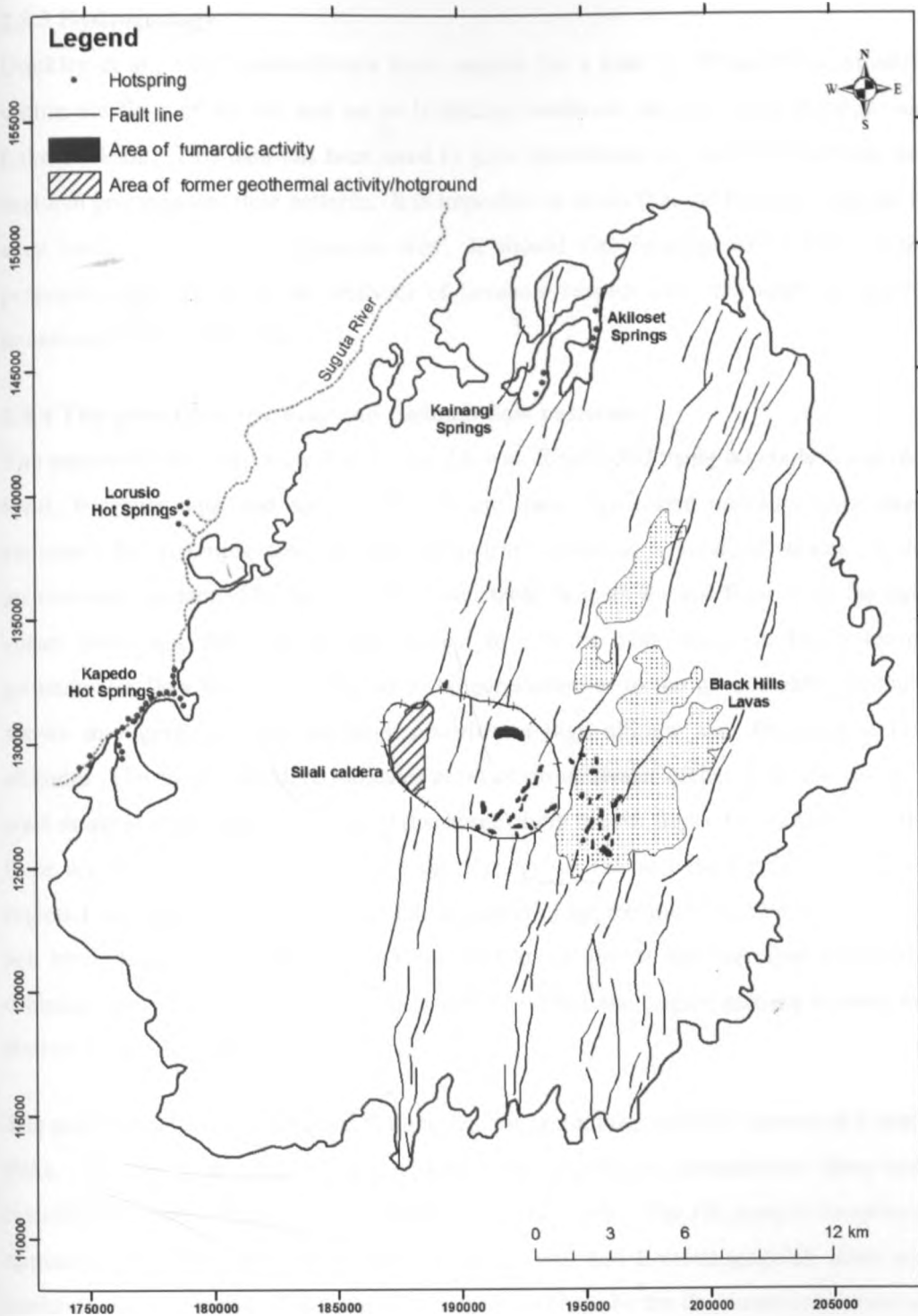
Figure 2.5 Map showing the geothermal manifestations in the Silali geothermal prospect

2.8.3 Hydrogeology

Dunkley et al., 1993 obtained data from records for a total of 70 boreholes, situated within the floor of the rift and on its bounding intefluves between Lake Baringo and Lake Turkana. This data has been used to gain information on aquifer properties and regional groundwater flow patterns. It is important to stress that the borehole data set is very limited for such an expansive area. It should also be emphasized that aquifer properties determined by the analyses of borehole records can only apply to depths penetrated by the boreholes.

2.8.4 The potentiometric map and regional flow patterns

The potentiometric map shown in Figure 2.6 was constructed using borehole water rest level, borehole data and spring data. Where data was scarse contours have been estimated by assuming that the potentiometric surface is a subdued replica of the groundwater surface. The depth to the water table beneath the rift floor from the data varies from less than 50 m near Korosi to 100 m near Silali. In broad terms, groundwater flow lines are expected to be perpendicular to the groundwater contours shown in Figure 2.4, with recharge occuring at high altitude and discharge at low altitudes. The figure therefore indicates areas of groundwater recharge on the east and west margins of the rift and a zone of discharge along the rift floor. Flows along the rift floor are directed northwards from Lake Baringo as far as Lake Logipi which is a regional discharge area with a water surface level of approximately 270 m above mean sea level. Lake Turkana lies at an altitude of about 365 m and therefore subsurface drainage from the lake is directed southwards towards Lake Logipi, passing beneath the Barrier Volcanic Complex.

The potentiometric data indicates that the regions around the volcanic centres of Korosi, Paka, Silali and Emuruangogolak are likely to be subjected to groundwater flows both laterally from the rift margins and axially from the south. The rift margin component appears to be dominantly from east for Paka, Silali and Emuruangogolak areas and perharps also for Korosi. Lake Baringo water is likely to be the dominant component of axial flow within the rift floor in the south of the area, but decreases northwards. The potentiometric map (Figure 2.4) indicates that the axial flow is mainly directed along the western side of the inner trough as far north as Emuruangogolak.

The Namarunu area appears to be one of the easterly groundwater flow, with a component of axial flow, although it is unlikely that Lake Baringo water persists in a readily identifiable form in this area. In the north of the area, around the Barrier Volcanic Complex, groundwaters are likely to be dominated by southerly subsurface flow from Lake Turkana with a strong component of easterly flow from the eastern margin of the rift around Ngiro.

The hydrogeological model for the system can be explained in terms of upflow and outflow within the caldera. The recharge is from the rains and mainly from the East, the fluid then outflows mainly to the west and to the north through formation contacts and faults and fractures discharging on the surface at the Kapedo springs. The recharge of the system is mainly from the east which is intensely faulted and to some extent from the south axially from Lake Baringo and the west.
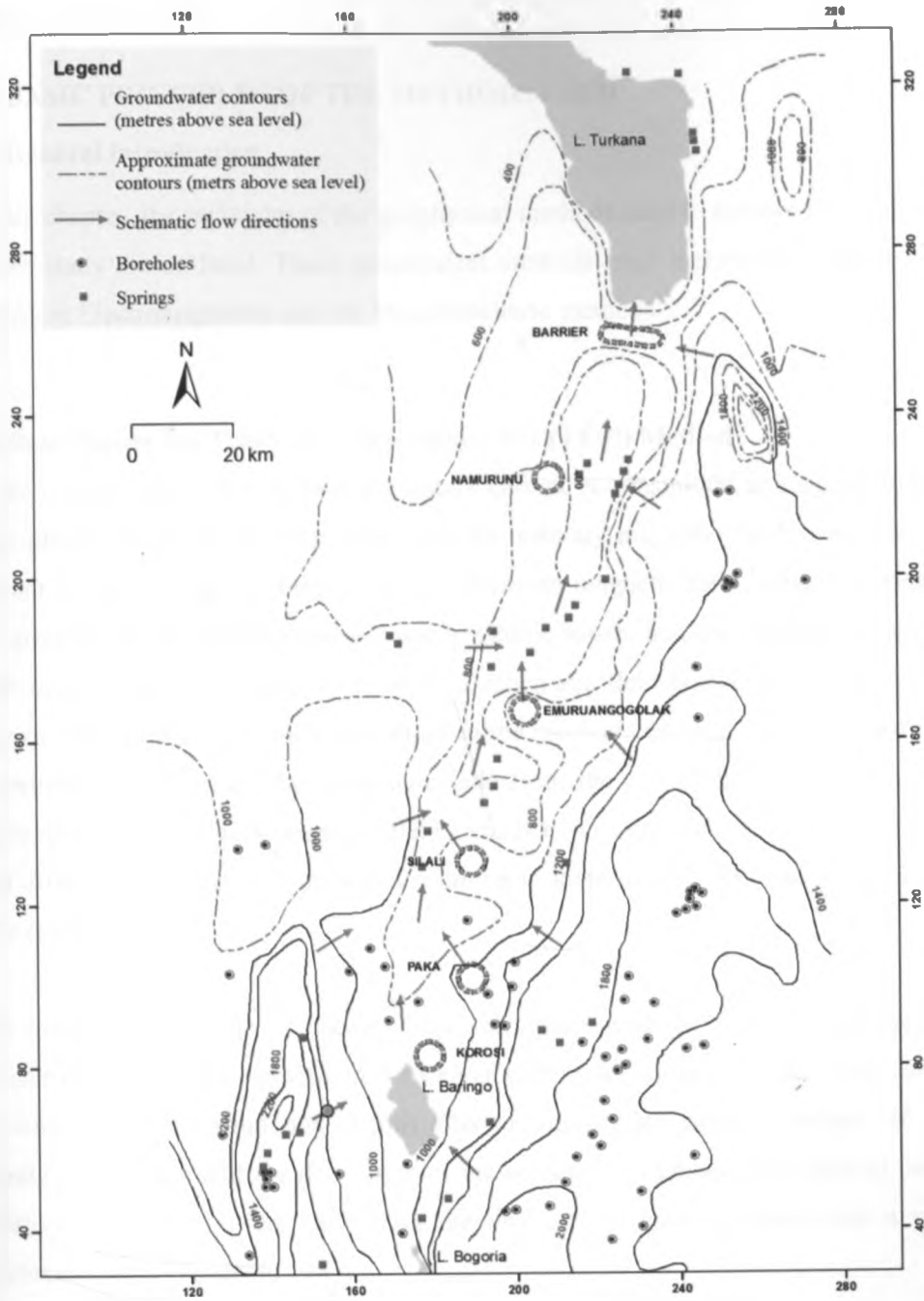
Figure 2.6: The potentiometric map between Lake Baringo and Lake Turkana (after Dunkley et al., 1993)

34

CHAPTER THREE

3.0 BASIC PRINCIPLES OF THE METHODS USED

3.1 General introduction

In this chapter, the principles of the geophysical methods used to achieve the objectives of the study are outlined. These geophysical methods used include the Central Loop Transient Electromagnetics and the Magnetotelluric methods.

3.2 Basic theory for Transient Electromagnetics (TEM) Method

In the central loop TEM method, a constant current is transmitted in a square loop of wire placed on the ground generating a static primary magnetic field around it. The current is then turned off abruptly and the decaying magnetic field induces currents in the ground. These currents decrease, due to Ohmic losses, and the secondary magnetic field decays with time. Figure 3.1 shows a schematic field layout and Figure 3.2 the current waveform and the induced voltage in the receiver coil. Just after the transmitter is switched off, the secondary magnetic field from the current in the ground will be equivalent to the primary magnetic field (which is no longer there) but, with time, it will diffuse downwards and outwards resulting in increasing depth of penetration with time (Figure 3.1).

The magnitude and rate of decay of the secondary magnetic field is monitored by measuring the voltage induced in a receiver coil usually placed at the centre of the transmitter loop, as a function of time after the transmitter current is turned off. The current distribution and the decay rate of the secondary magnetic field depend on the resistivity structure of the earth with the decay being more gradual over a more conductive earth (Árnason, 1989).

The depth of penetration in the central loop TEM-sounding is dependent on how long the induction in the receiver coil can be traced before it is drowned in noise. At the so called late times (described later), the induced voltage in the receiving coil on a homogeneous half space of conductivity, σ, is (Árnason, 1989)

$$V(t, r) \approx I_0 \left(C (\mu_0 \sigma r^2)^{3/2} / 10 \pi^{1/2} t^{5/2} \right), \tag{3.1}$$

where,

$C = A_r n_r A_s n_s \, \mu_0/2\pi r^3,$

n_r = Number of turns on the receiver coil,

A_r = Area of the receiver coil [m^2],

A_s = Area of the transmitting loop [m^2],

n_s = Number of turns in transmitter loop,

t = Time elapsed after the current in the transmitter is turned off [s],

μ_0 = Magnetic permeability [Henry/m],

$V(t,r)$ = Transient voltage [V],

r = Radius of the transmitter loop [m],

I_0 = Current in the transmitting loop [A].

This shows that the transient voltage for late times after current in the transmitter is abruptly turned off, is proportional to $\sigma^{3/2}$ and falls off with time as $t^{-5/2}$. This leads to the definition of the late time apparent resistivity by solving for the resistivity in equation 3.1 leading to the equation

$$\rho_a = \mu_0/4\pi (\, 2I_0\mu_0 A_r n_r A_s n_s/5t^{5/2} \, V(t,r) \,)^{2/3}. \tag{3.2}$$

Depth of probing increases with time after the current is turned off.

Apparent resistivity, ρ_a, is a function of several variables:

- Measured voltage,
- time elapsed from turn off,
- area of loops/coils,
- number of windings in loops/coils,
- magnetic permeability.

For half-space, apparent resistivity, ρ_a, (and the true resistivity for homogenous earth) is expressed, in terms of induced voltage at late times after the source current is turned off, as

$$\rho_a(t) = \frac{\mu_0}{4\pi} \left| \frac{2\mu_0 I A_r A_s}{5t^{5/2}V(t)} \right|^{2/3};$$

where,

ρ_a = Apparent resistivity,

μ_0 = Magnetic permeability [Henry/m],

A_r = Area of the receiver coil [m^2],

36

A_s = Area of the transmitting loop [m^2],

$V(t,)$ = Transient voltage [V],

t = Time elapsed after the current in the transmitter is turned off.
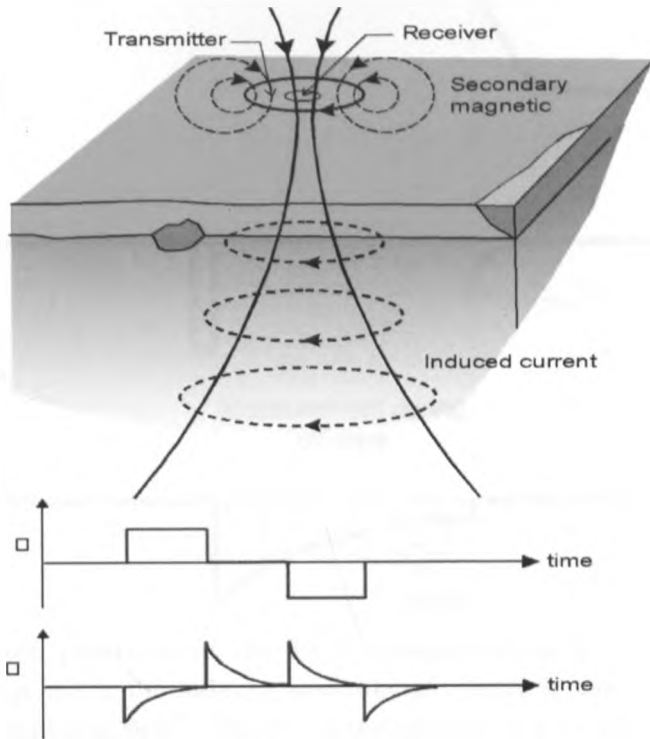
Figure 3.1: The central loop TEM configuration (from Hersir and Björnsson, 1991)
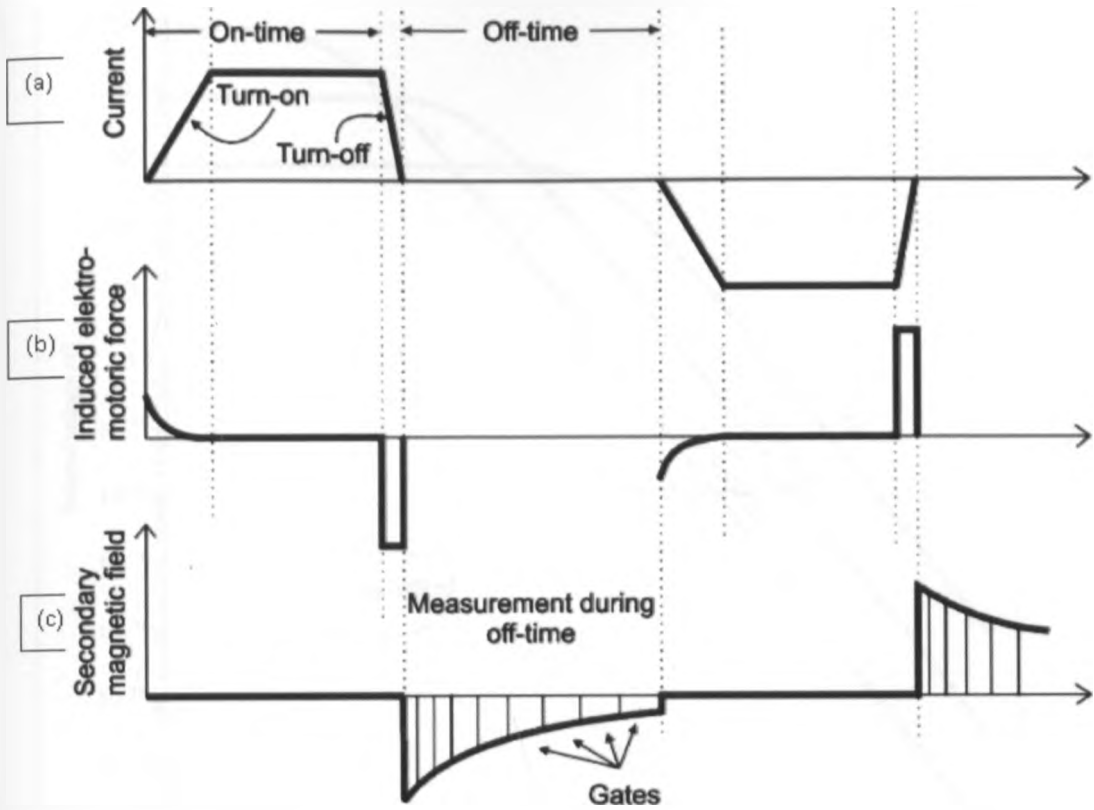
Figure 3.2: Basic principles of the TEM method (a) Shows the current in the transmitter loop. (b) Is the induced electromotive force in the ground, and (c) is the secondary magnetic field measured in the receiver coil (from Christensen et al., 2006).

The time behavior of the diffusing current is divided into three phases according to their characteristics as illustrated on Figure 3.3 which shows the induced voltage as a function of time for a homogeneous earth. In the early phase, the induced voltage is constant in time. In the intermediate phase, the voltage starts to decrease with time and with steadily increasing negative slope on log-log scale until the late time phase is reached where the voltage response decreases with time in such a way that the logarithm of the induced voltage decreases linearly as a function of the logarithm of time. The slope of the response curve in the late phase is -5/2 in accordance with equation 3.1 which is only valid for the late-time phase.
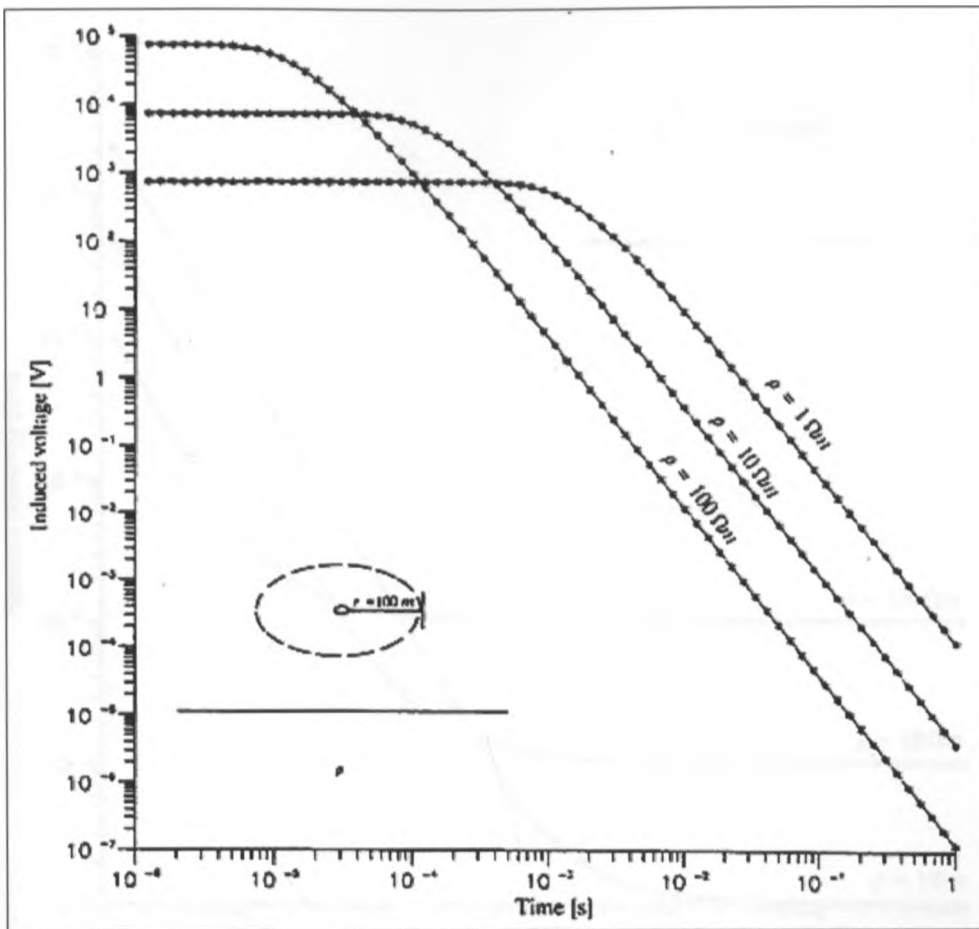
Figure 3.3: Voltage response for homogenous half space of 1, 10, and 100 Ωm (from Árnason, 1989)

The apparent resistivity at early time increases with decreasing resistivity of the half space and also that the transitions from early to late time get shifted towards earlier times as the resistivity of the half space increases (Figure 3.4). However, it should be noted that the response curve has the same shape for the different half space resistivities. When the apparent resistivity for a homogenous half-space is plotted as a function of time, it approaches asymptotically the true resistivity of the half-space for late times.
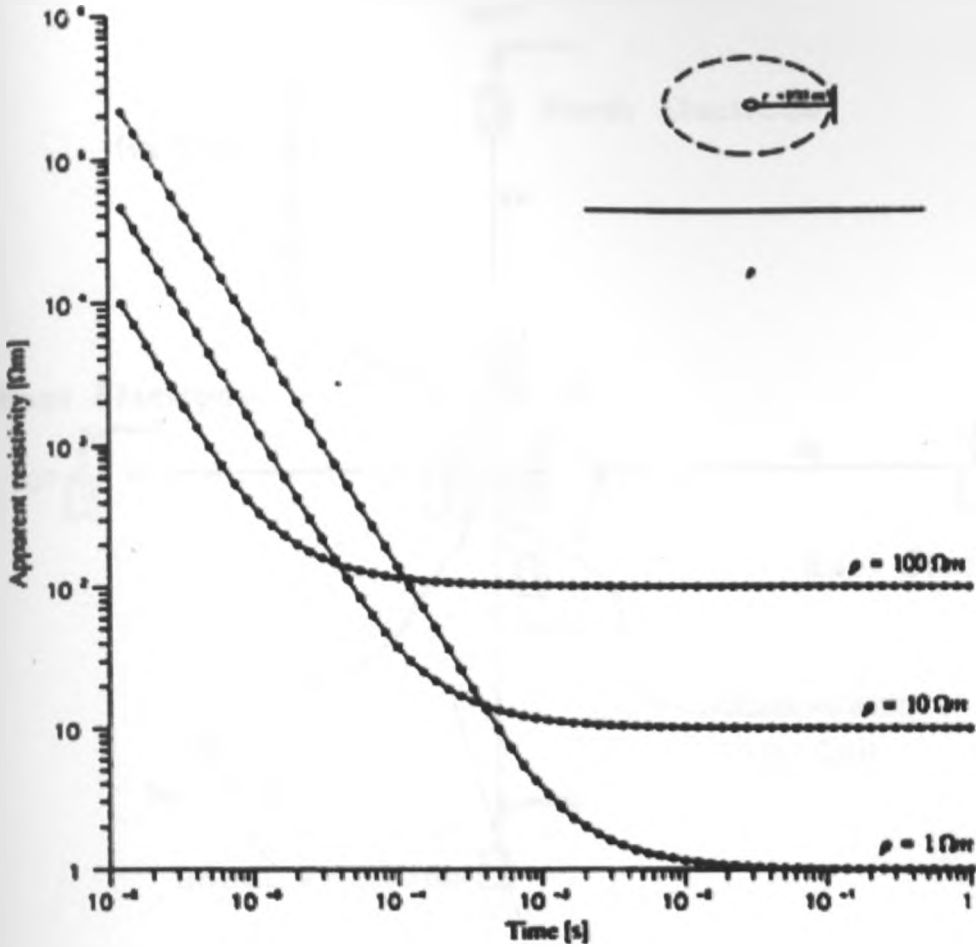
Figure 3.4: Late time apparent resistivity for homogenous half space of 1, 10 and 100 Ωm (from Árnason, 1989)

3.4 Basic theory of magnetotelluric method

The magnetotellurics method is a natural-source, electromagnetic geophysical method of imaging structures below the earth's surface, where natural variations in the earth's magnetic field induce electric currents (or telluric currents) under the Earth's surface. Both magnetic (H_x, H_y and H_z) and electric (E_x and E_y) fields are measured in orthogonal directions giving two impedance tensors and their phase which are used to derive the resistivity structure of the subsurface (Figure. 3.5).
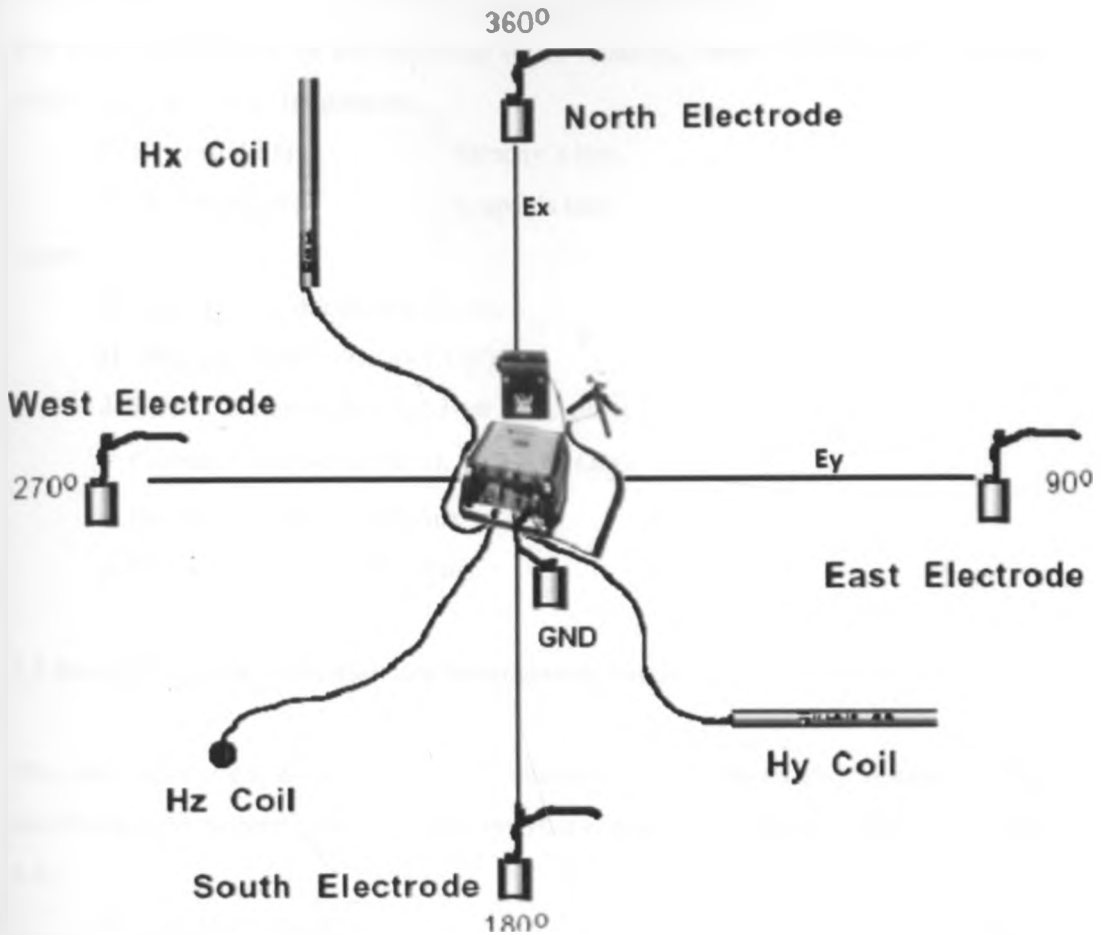
Figure 3.5: MT-soundings Layout

The ratio of the electric field to magnetic field can give simple information about the subsurface conductivity. The high frequency gives information about the shallow subsurface with the low frequency providing information about the deeper earth.

The magnetic and electric fields are measured in the frequency range 10^3 Hz to 10^{-4} Hz. This time varying magnetic field comes from two sources with high frequencies (>1 Hz) coming from lightening discharges in the equatorial belt while the low frequencies (<1 Hz) comes from the interaction between the solar wind and the earth's magnetosphere and ionosphere. These natural phenomena create strong MT source signals over the entire frequency spectrum.

The MT method can explore down to hundreds of kilometres, which makes it the EM method which has the most exploration depth of all the EM methods, and is practically

the only method for studying resistivity deeper than few kilometres. The propagation of EM fields is described by the following set of relations, called the Maxwell equations which hold true for all frequencies.

$$\nabla \times E = -\mu(\partial H/\partial t) \qquad \text{Faraday's law,} \qquad (4.1)$$

$$\nabla \times H = J + \varepsilon(\partial E/\partial t) \qquad \text{Ampéres law,} \qquad (4.2)$$

where,

E: Electrical field intensity (V/m),

H: Magnetic field intensity (A/m),

J: Electrical current density; $J = \sigma E$ (A/mm^2),

σ: Conductivity (Siemens/m); $\rho = 1/\sigma$ (Ωm),

ε: Electrical permittivity (F/m),

μ: Magnetic permeability (H/m).

3.5 Electromagnetic induction in a homogenous earth

The ratio of electric to magnetic field intensity is a characteristic measure of the electromagnetic properties often called the characteristic impedance (Equation 4.3 and 4.4)

$$Z_{xy} = E_x/H_y = i\omega\mu_0/k, \qquad (4.3)$$

$$Z_{yx} = E_y/H_x = -i\omega\mu_0/k, \qquad (4.4)$$

where,

Z_{xy}, Z_{yx} = Characteristic impedance in x and y directions,

ω = Angular frequency ($2\pi f$) where f is frequency (Hz),

μ_0 = Magnetic permeability (H/m),

$E_{x,y}$ = Electric field intensity (V/m) in x, y direction,

$H_{x,y}$ = Magnetic field intensity (Tesla) in x, y direction,

$k = \sqrt{(i\omega\mu(i\omega\varepsilon + \sigma))}$ stands for the wave propagation constant,

ε = Dielectric permittivity (C/Vm),

σ = Conductivity (Siemens/m).

The term $\omega\varepsilon$ in wave propagation constant k is much smaller than conductivity σ and can be ignored, therefore, $k = \sqrt{[i\omega\sigma]}$. Putting this into equations 4.3 or 4.4 we get:

$$Z_{xy} = E_x/H_y = i\omega\mu/k \approx i\omega\mu/\sqrt{[i\omega\sigma]} = \sqrt{i}\,\sqrt{[\omega\rho\mu]} = \sqrt{[\omega\mu\rho]}\,.e^{i\pi/4} \qquad (4.5)$$

42

$$Z_{yx} = E_y/H_x = -i\omega\mu/k = -Z_{xy} \qquad (4.6)$$
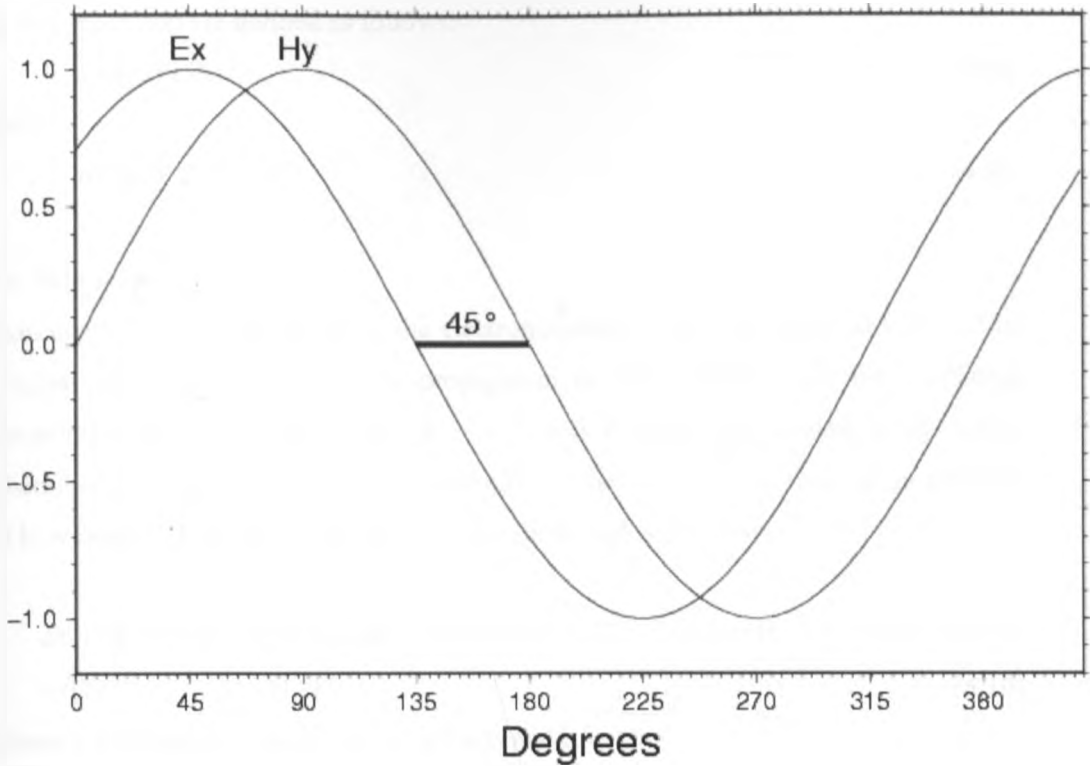
Figure 3.6: Homogenous half space response of electric and magnetic field describing the 45° phase difference of the E and H fields, their amplitude are not the same.

Where, $\pi/4$ is the phase angle by which H_y lags E_x as explained on Figure 3.6.

If the earth is homogenous and isotropic, then the true resistivity of the earth is related to the characteristic impedance through the following relation (e.g. Hermance, 1973).

$$\rho = 1/\mu\omega |Z_{xy}|^2 = 1/\mu\omega |Z_{yx}|^2 \qquad (4.7)$$

For a non-homogeneous earth, an apparent resistivity (ρ_a) can be defined as if the earth were homogeneous using this same formula.

In practical units, for homogeneous earth the resistivity, ρ in the above equation can be written as:

$$\rho_a = 0.2T |Z|^2 = 0.2T |Ex/By|^2, \qquad (4.8)$$

and phase angle $\theta = \arg(Z) = \pi/4$ or 45°,

where E' is the electrical field in mV/km, $E' = E \times 10^{-6}$, $B = \mu H$ is magnetic field in Tesla, $B = 10^{-9}$ Tesla, T is period in seconds and $\mu = 4\pi \times 10^{-7}$,

43

For a non-homogeneous earth, the apparent resistivity (ρ_a) and phase (θ_a) are functions of frequency and are defined as follows:-

$$\rho_a=0.2T|Z_0|^2 \qquad\qquad\qquad (4.9a)$$

and

$$\theta_a=\arg(Z_0)\neq 45°. \qquad\qquad\qquad (4.9b)$$

3.6 Skin depth

Skin depth, δ, is the depth where the electromagnetic fields have reduced to e^{-1} of its original value at the surface. The propagation is time dependent on the oscillating electromagnetic fields, that is $\mathbf{H}$, $\mathbf{E} \sim e^{i\omega t}$, and is vertically incident plane wave. Therefore skin depth is used as a scale length for the time-varying field, or an estimate of how deep such a wave penetrates into the earth, and is given by:

$$\delta= 1/Real(k)= 1/Real\,(i\omega\mu\sigma)= \sqrt{[2/\omega\mu\sigma]} = \sqrt{[2T\rho/(2\pi\times4\pi\times10^{-7})]}= 10^3/\pi\times\sqrt{[20/8]}$$
$$\times\sqrt{[T\rho]},\text{ or}\qquad \delta\approx500\,\sqrt{[T\rho]}, \qquad\qquad (4.10)$$

where δ is in metres, T is period in seconds and ρ in Ωm

3.7 MT dead band

MT data acquisition is prone to a number of problems, one of them being the dead band problem. This occurs in the frequency band between 0.1 Hz to 10 Hz in which natural signals are typically weak. The power spectrum of these fluctuations plummets in the frequency range 0.5 − 5 Hz minimizing at 1Hz. This problem is attributable to the inductive source mechanisms, one effective below ~1Hz and another above ~1Hz which causes reduction in data quality. Induction magnetic coils used in MT data acquisition are not sufficiently sensitive in the dead band to detect the natural background.

However, it is to be noted that the dead band problem, due to the weak and fluctuating signals with dominant noise in that band, does not get resolved satisfactorily by robust processing with the site itself so remote reference processing is used to minimize distortions at this band and improve on signal to noise ratio. This leads to poor inherent geometric resolution of target structures at depths near the subsurface (Garcia and Jones, 2002).

44

CHAPTER FOUR

4.0 DATA AQUISITION AND PROCESSING OF DATA

4.1 Brief Outline

In this chapter, the methods and instruments used during the field surveys and the data processing procedures are presented.

Section 4.2 gives an outline of the general approach used in project administration right from inception to completion. This is a procedure to guide the research in planning, collecting, analyzing and interpreting observed facts.

Section 4.3 discusses the instrumentation used during the field surveys. The main focus is on the foundation of each instrument used during the resistivity survey.

Section 4.4, discusses methods used to collect the data used to determine variations in electrical conductivity of the sub-surface both laterally and with depth at the scale of field mapping.

A procedure for processing all field data so as to achieve the results of the study is also discussed critically in section 4.5.

4.2 Research Design

This study involved four main stages, namely;

- Review of available data,

- Fieldwork,

- Data processing and interpretation,

- Reporting.

1.**Review of available data:** This step involved the collection and review of all relevant available literature from existing files, reports, libraries, and the databases for a wide range of information on Silali, such as:

➤ Topographical maps, aerial photographs and satellite images,

➤ Geographical and geological data,

> Reports of previous geophysical studies (magnetic, seismic, gravity and electrical resistivity) in the area,

> MT and TEM data files,

> Data on the present energy use and the future energy demand.

The findings of this survey were used to plan the fieldwork in a way that:

> duplication of earlier investigations is avoided,

> data are collected in the significant locations,

> the best results are obtained for the least cost.

2. Fieldwork: The fieldwork involved the execution of magnetotellurics and transient electromagnetic resistivity sounding at a number of points in the study area.

3. Data processing, interpretation and geothermal modelling: This stage involved the processing of all the data collected both from the archive and from the fieldwork. Geophysical anomaly maps and 1D apparent resistivity pseudo-section models were made using the software packages Winglink from Phoenix Geophysics. Integration and overlay analysis of the processed field results were carried out using the GIS software, ArcGIS 9.3 from ESRI, and software Surfer of Golden Software Inc.

4. Reporting: This stage included the reporting on the entire work (data collection, data analysis and interpretation) and establishment of recommendations for future developments.

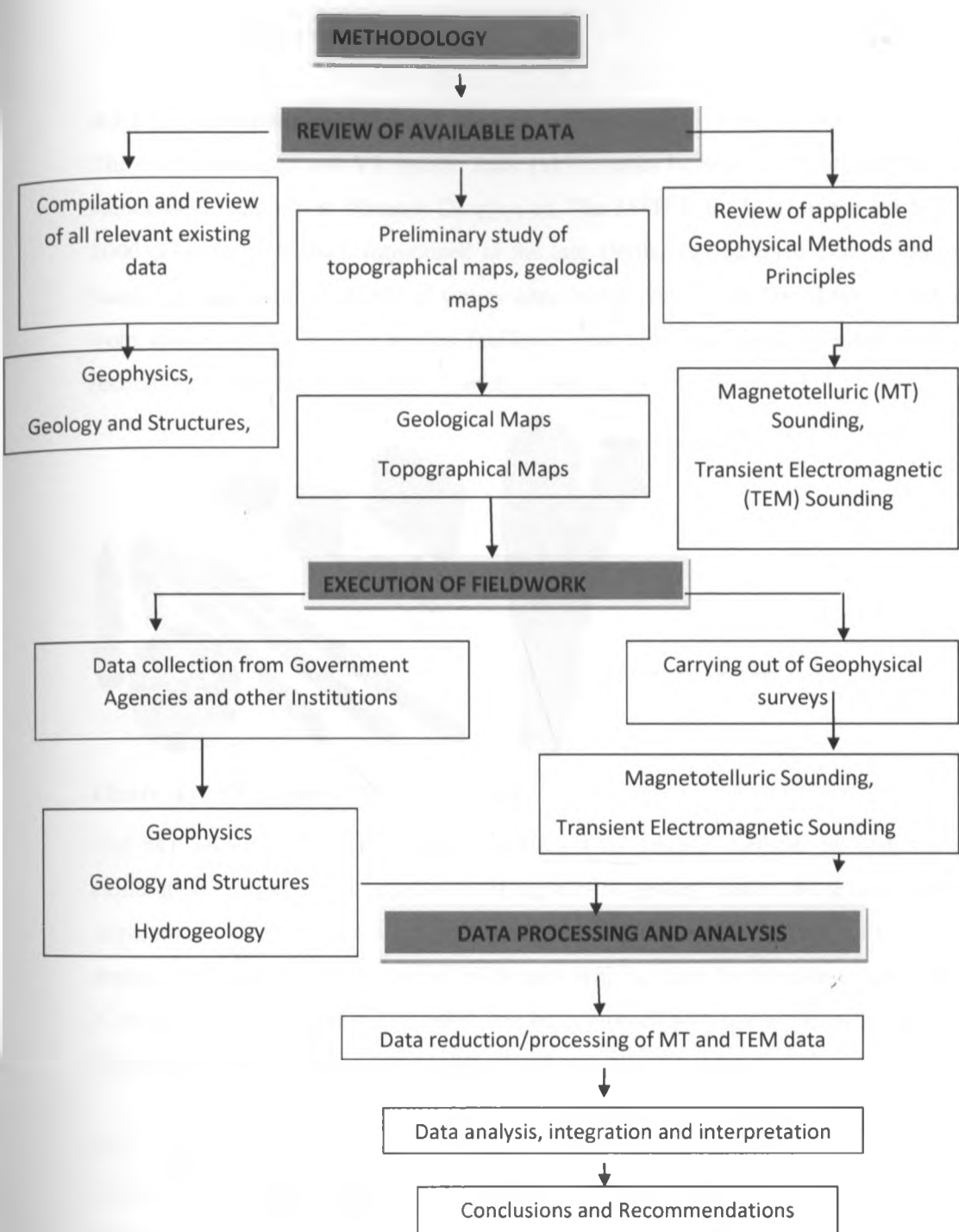This approach has been summarized as shown in Figure 4.1.

Figure 4.1: A schematic illustration of the approach used for during research project.

4.3 Field Instrumentation

4.3.1 Magnetotelluric (MT) method

The instrument used was V5 System 2000 (MTU series i.e Satellite-Synchronized Data Acquisition Units) from Phoenix Geophysics. The MTU is the heart of the V5 System 2000 (Figure 4.2 below). Introduced in the late 1990s, this patented system has now been used at tens of thousands of survey sites worldwide. Flexibility of station spacing from kilometres to tens of metres facilitates cost-effective broad reconnaissance or resolution of fine details in a variety of applications.

Figure 4.2: V5 System 2000(MTU series)

The MT techniques are excellent supplements to seismic methods in hydrocarbon exploration, but can also be used alone if logistics or geology makes the seismic method impractical. GPS synchronization means that multiple stand-alone units can be deployed simultaneously in almost any terrain, with no need for interconnecting cables. A small number of magnetic channels can be combined with many electric channels to form an economical system of virtually any size.

The deployment of synchronized remote reference stations permits sophisticated noise-reduction methods during processing. Several channel complements are available—electric (E) only, magnetic (H) only, or 2E + 3H combined. The units can be purchased for MT alone (MTU) or for selectable MT/AMT (MTU-A). Acquisition setup files are stored on the removable industrial-grade Compact Flash card for automatic operation. Data files are stored on the same card for easy transfer to the processing PC.

4.3.2 Transient Electromagnetic method

The TEM equipment used is manufactured by Zonge Engineering and consists of a current transmitter, Transmitter Controller (XMT), GDP-32 receiver, a receiver coil with effective area of 10000 m^2, a voltage regulator and a transmitter loop and a 120VA three phase power generator as shown in figure 4.4 below.

The transmitter can transmit either frequency domain (100% duty cycle) or time domain (50% duty cycle) waveforms. This transmitter is suitable for surveys ranging from laboratory-scale (like core samples) to deep mining, geothermal, or petroleum exploration. Figure 4.3 below shows a Zonge TEM transmitter used during the field work.
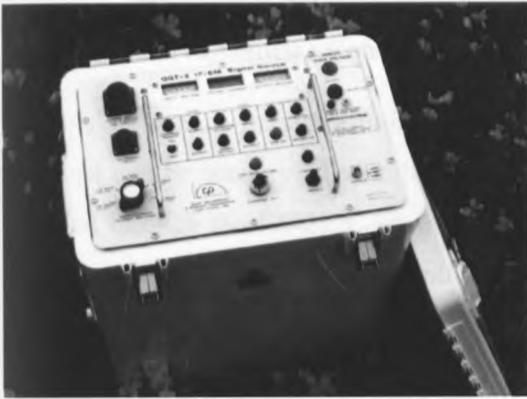

Figure 4.3: Zonge TEM transmitter
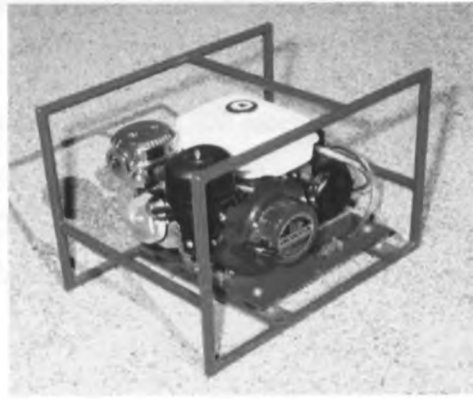
Figure 4.4: Three phase generator

The XMT-32 Transmitter controller (Figure 4.5) produces timing signals for controlling all of the Zonge Engineering GGT, ZT, and NT transmitters

Figure 4.5: Transmitter Controllers

Provision is made for synchronizing multiple controllers and GDP receivers. Frequency control can be accomplished either manually or by a time sequence program which is loaded through the RS-232C port. The GDP-32 is Zonge Engineering's multi-channel receiver for acquisition of controlled- and natural-source geoelectric and EM data (Figure 4.6).

Figure 4.6: GDP-32 Receiver

The Geophysical Data Processor receivers perform broadband synchronous time or frequency domain measurements on both controlled-source (i.e., signals generated by transmitting current into grounded dipoles or wire loops) and on natural fields.

Performance advantages:

- multifunction capability,
- synchronous timing,
- unique multi-channel acquisition.

Unique capabilities:

- Remote control operation,
- Broadband time-series recording,
- High-speed data transfer.

4.4 Field Data Acquisition and Processing

4.4.1 Magnetotelluric (MT) field survey

A total of 134 MT soundings are considered for interpretation in the Silali prospect covering an area of about 81 km^2 as shown in Figure 5.6. The data was acquired using 5-channel MT data acquisition system (MTU-5A) from Phoenix Geophyics.

The layout was made such that the electric dipoles were aligned in magnetic North-South and East-West, respectively, with corresponding magnetic channels in orthogonal directions and the third channel positioned vertically in the ground as can be seen in Figure 3.5. Before data acquisition, a start-up file was prepared with parameters like gains, filters, time for data acquisition and calibrations for both equipment and the coils and stored on a flash disk in the equipment. The ground contact resistance is generally measured to gauge the electrode coupling to the ground and both high pass filter and antialiasing filter used with a corner frequency of 0.005Hz to remove the effect of self potential from the electric dipoles. The electric field was measured by lead chloride porous pots and the magnetic sensors were buried about 20 cm below the surface to minimize the wind effect.

MT data was acquired in frequency range from 10^3 Hz to 10^{-4} Hz for a period of about 20 hrs which ensures that deeper investigation of the subsurface is achieved. In this survey, long period data was not realised in most of the stations because signals were drowned in noise at low frequencies. The penetration depth of the electromagnetic wave depends on the frequency.

4.4.2 TEM field survey

In this study a total of 100 Central Loop TEM soundings were carried out in the Silali area spread over about 65 km^2. The stations were scattered within the prospect area with denser coverage inside the caldera as shown in Figure 5.6 using the TEM equipment described earlier.

Before data acquisition, both the receiver and the transmitter controller high-precision crystals were warmed up for a period of about an hour and then synchronized to ensure that induced voltage is measured by the receiver at the correct time after the current turn off. In the field setup, a 300m x 300m transmitter wire loop was used and a 9 ampere half-duty square wave current was transmitted at frequencies 16 Hz and 4 Hz. The transient signal was recorded in the time interval of 36.14µsec to 96.85msec at logarithmically spaced sampling gates after the current turn-off. For each frequency several repeated transients were stacked and stored in a memory cache inside the Zonge data logger and later transferred to a personal computer for processing.

4.4.3 Data processing

4.4.3.1 General introduction

For magnetotelluric data a Fourier transform was applied to the time series data collected and then processed into cross-power estimates. Processing was done and the cross-powers were then analyzed to obtain an estimate of impedance, resistivity and phase which was later converted to Electronic Data Interchange (EDI) format using the Phoenix SSMT processing software. The raw Transient Electromagnetic (TEM) data were converted to average (AVG) files appropriate for importing into the Winglink software database for interpretation.

The EDI files were then imported to WinGlink software for interpretation. Here Magnetotelluric data (MT) data were decomposed to principle axes to minimize the diagonal elements of the impedance tensor.

For the Transient Electromagnetic data, raw data files were read and downloaded from the GDP-32 receiver by using TEM SHRED (a Zonge Geophysics program) and the TEM-AVG (also a Zonge Geophysics program) was used to calculate averages and standard deviations of repeated transient voltage measurements and late time apparent resistivity as a function of time. WingLink (Geosystem) interpretation program was used to perform one dimensional inversion (1D) on the data. TEM data were then included to correct for static shifts in MT data. A one dimensional inversion was initially run for MT and TEM data and later, a one-dimensional (1D) joint inversion of MT and TEM was run, and finally a two-dimensional (2D) MT inversion.

4.4.3.2 Magnetotelluric static shift correction using Transient Electromagnetic

One of the common problems in interpreting MT data is static-shift. Static-shift is caused by the presence of small-scale heterogeneities near the ground surface at stations. The shift is basically a constant vertical displacement of the MT apparent resistivity curves on a log scale at all frequencies. These shifts are common to almost all electrical methods where electrode-ground contact is allowed. MT data interpretation can be very misleading if these shifts are not addressed (Meju, 1996).

Resistivity methods that do not use electrodes, like the transient electromagnetic (TEM), are less affected by these localized resistivity contrasts (Pellerin and Hohmann, 1990; Cumming and Mackie, 2010). However, on the other hand, the TEM method is limited by its shallow depth of investigation (usually less than 1km) and can sometimes be affected by near surface heterogeneities at the initial times of recording. This is because at initial times, the response corresponds to the very local geology near the wire loop (Pellerin and Hohmann, 1990). In this study, TEM data were used to correct for static shifts on MT data that result from near surface conductivity heterogeneity.

The other possible cause of distortion on MT data is topographic changes (Cumming and Mackie, 2010). However, this effect can easily be handled by including topographic information during the inversion process. Thus, TEM data were used entirely to correct for galvanic distortion on MT data.

Appendix I show some examples of the static shift corrections made to MT data using TEM data. The static shifts varied across stations in this region. In this figure, the plots labeled as (i) are the uncorrected apparent resistivity plots while the ones labeled as (ii) are the static shift corrected resistivity data. It can be observed that only the apparent resistivity curves incur this shift while the phases of the MT and TEM correlate.

The plots of the apparent resistivity and phases with time show that, the apparent resistivity determined from the electric field in the north direction (Ex) and the magnetic field in the east direction (Hy) that is XY, and the other curve which plots the data for the other two orthogonal horizontal fields, Ey and Hx that is YX values overlap, but at lower frequencies (longer periods) the values are different (split curves) with the exception of station silMT24 whose values appear relatively the same at all frequencies (Appendix I). This shows that, the dimensionality can be detected from the apparent resistivity plots. For 1D subsurface (resistivity only varies with depth) the XY and YX apparent resistivity plots will be similar to the station silMT24. The curves display a similar trend. However, for a 2D or 3D subsurface (resistivity varies both horizontally and vertically) the XY and YX data separate, as displayed on stations silMT55, silMT180, and silMT75. A careful analysis of the onset of these separations provides the depth at which the subsurface deviates from a 1D structure. At geothermal systems this information can help to determine the depth extent of the clay cap *(Onacha, 2006)*.

CHAPTER FIVE

5.0 DATA ANALYSIS AND DISCUSSION OF RESULTS

5.1 Introduction

In this chapter data obtained from methods deployed in chapter 4 are analyzed and results are discussed. The chapter is divided into four sections 5.1, 5.2, 5.3 and 5.4.

Section 5.1 introduces the general approach used during data analysis and discussion of results. This is a procedure to guide the research in analyzing and interpreting observed facts so as to achieve the objectives of the study.

Section 5.2 gives an outline used in one dimension (1D) inversion and interpretation.Further, results in form of iso-resistivity maps at varying elevations are also presented.

Section 5.3, discusses the two dimension (2D) resistivity inversion results showing significant variations in the resistivity distribution both vertically and horizontally on all profiles.

Section 5.4, discusses the essential features considered while the conceptualized geothermal model was being modelled.

5.2 One dimension (1D) inversion and interpretation

For 1D inversion, it is assumed that the resistivity only varies in the vertical direction and is laterally constant. In this study, rotational invariant determinant MT data were used for the 1D Occam (minimum structure) inversions (Constable et al., 1987) (Figure 5.1). These data have the capability to reproduce 3D resistivity structures (Arnason et al., 2010; Cumming et al., 2000). 1D Occam inversions were run for MT and TEM data separately using the WinGlink software. Then the TEM plots were incorporated into the MT for static shift correction as shown in Appendix 1.

Studies have shown that 1D joint inversion/interpretation of MT and TEM data not only solves the static shift problem but also enhances the resolution of the subsurface resistivity when inverted together for geological structures (Cumming and Mackie, 2010; Arnason et al., 2010). The integrated approach involves two related data (resistivity) sets to optimize a model with better constraints on the inversion. In this way, the problem of layer suppression is reduced while mitigating the highs and lows in

the resistivity equivalences that may be encountered without incorporating the TEM data. Examples of typical 1D Occam inversion models of MT data after correcting for static shift are shown in Figure 5.1.

The resistivity models show a resistive top layer overlying a conductive (less resistive) layer at about 500 m depth. The base of the conductive layer is at about 1000 m depth. The resistive layer overlies a less resistive layer at a depth below 2000 m. In general, most of the MT soundings in this region have a similar trend where a conductor exists at 1000 m depth. This is interpreted as hydrothermal alteration product (clay cap) (Wright et al., 1985). This lateral conductor overlies a resistive zone that is interpreted as a region of higher temperature altered rocks (Onacha 2006; Spichak and Manzella, 2009; Ingham, 2004).
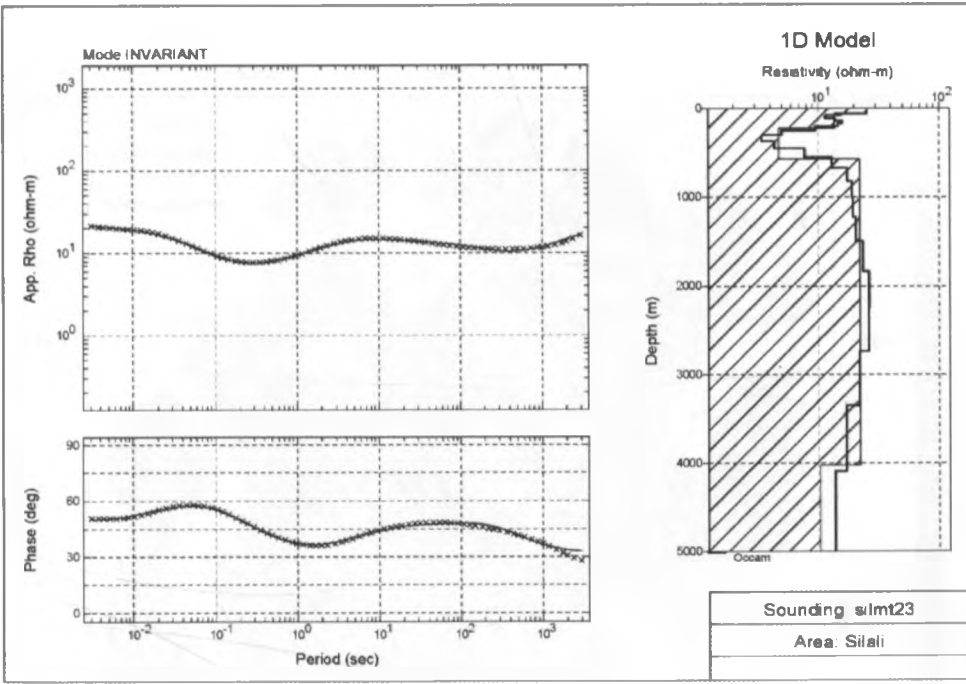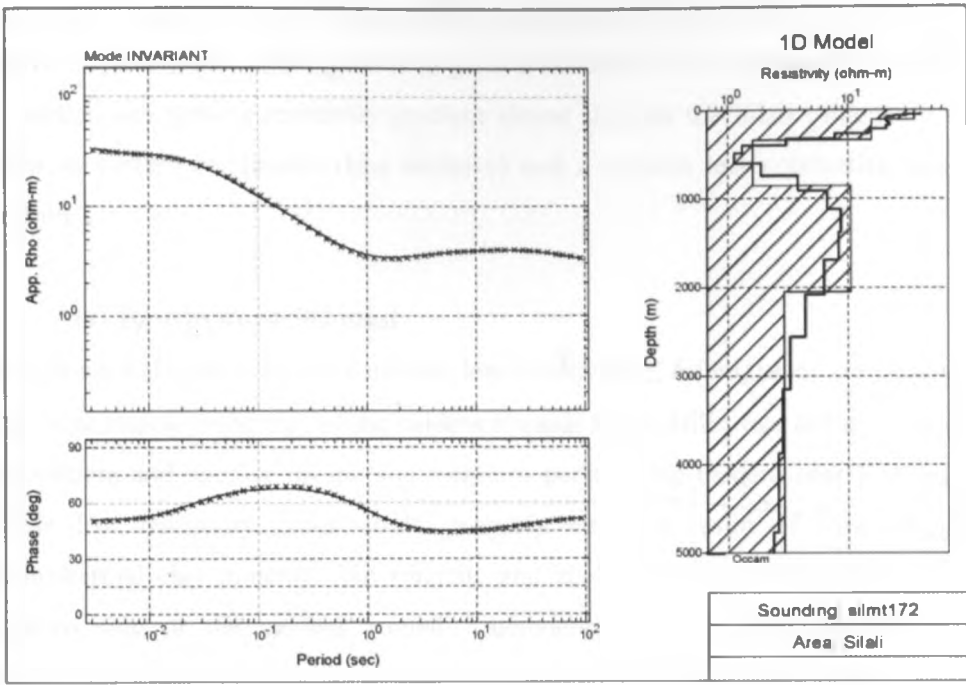
Figure 5.1: One-dimensional Occam resistivity inversion models of MT data at station silMT172 and silMT23.

Maps of resistivity versus elevation were generated from the 1D Occam inversion result (Figures 5.2-5.5). These maps show the lateral resistivity distribution around the Silali region at a particular elevation. These figures show resistivity at depths of 500, 1000

57

meters above sea level and 2000 and 5000 m below sea level. At shallow depths (500 m above sea level), the Silali region is in general conductive (low resistivity) (Figure 5.2). A north-south striking resistivity gradient almost dissects the Silali calderas in two to form an eastern conductive (less resistive) and a western less conductive (resistive) section.

(a) Resistivity at 500 masl

At 500 masl (Figure 5.2), three distinct low resistivity ($\leq$ 6 Ωm) areas are clearly seen; one large region to the east of the caldera towards Black Hills, one to the north-east of the caldera and another on the south-eastern parts of the caldera near Kuttung area. These low resistivity zones could probably be as a result of low temperature hydrothermal clay minerals like smectite and zeolite. On the other hand, the south-western side of the caldera around Katenmening area is characterized by high resistivities which are probably as a result of un-altered rocks near the surface.
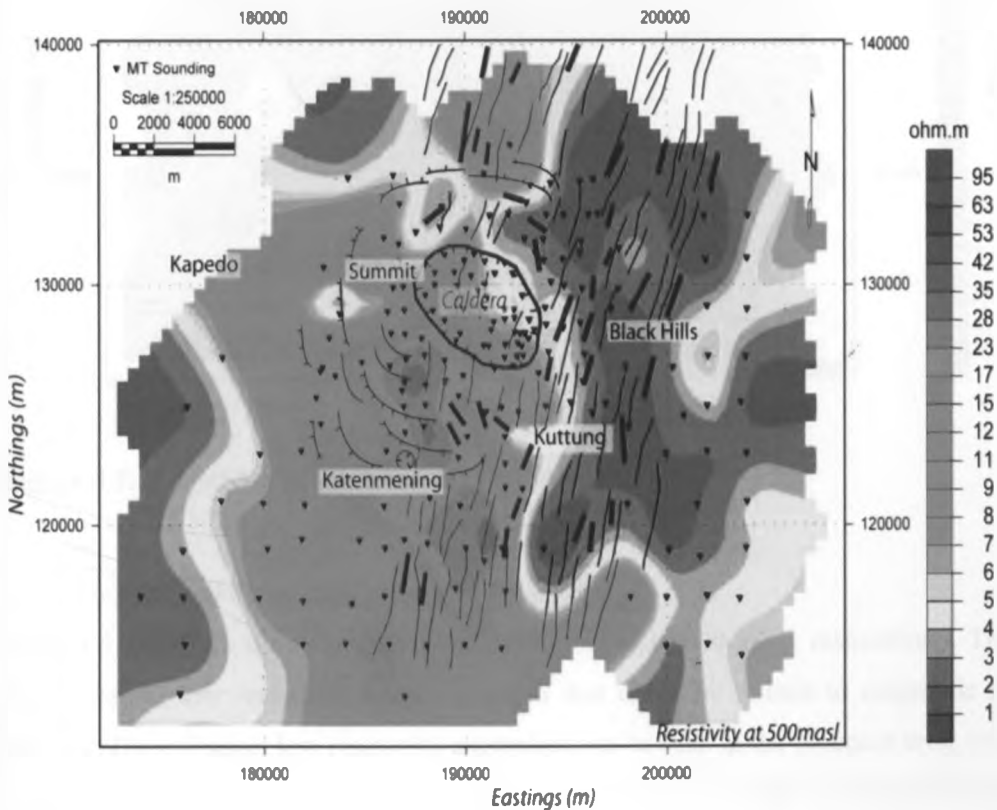

Figure 5.2: Resistivity at 500 m above sea level

58

(b) Resistivity at sea level

At sea-level (Figure 5.3), the general resistivity structure of the prospect indicate a high resistivity (about 49 ohm-m) particularly within the caldera and in the south western s ide in the Katenmening area. This high resistivity portion could probably be associated with high temperature alteration minerals such as chlorites and epidotes. Some higher resistivity zones can be seen appearing on the southern part of the prospect area and another in the north-western side of the caldera aligning in the NE-SW direction. Slighty low resistivity values are still seen on the eastern part around Black Hills area.
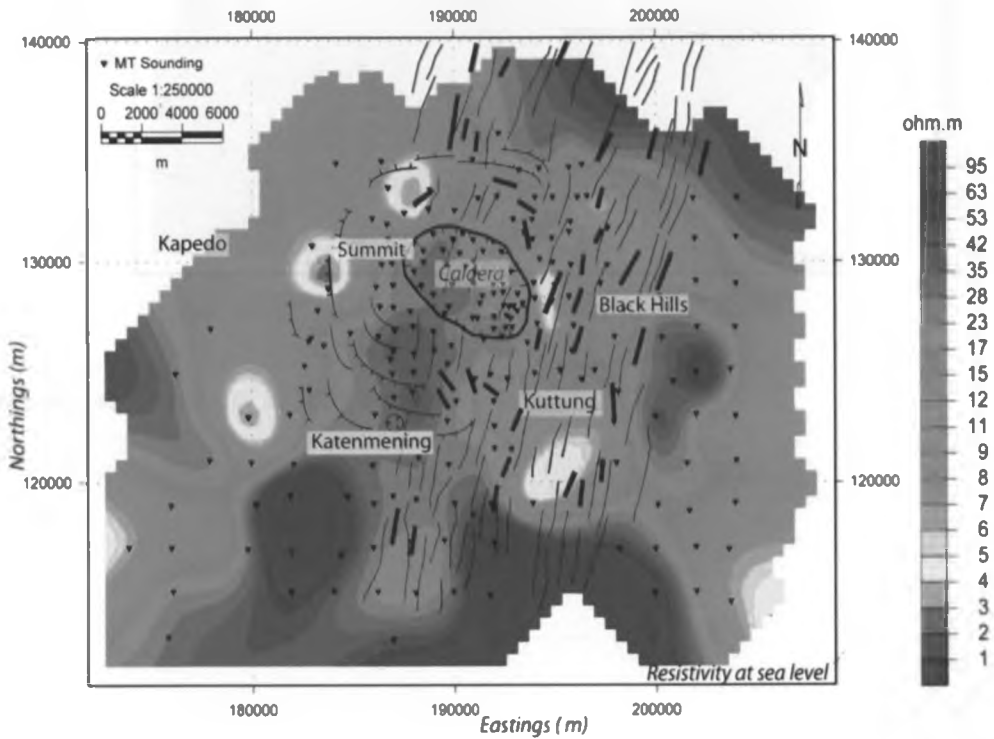

Figure 5.3: Resistivity at sea level

(c) Resistivity at 2000 mbsl and 5000 mbsl

Figures 5.4 and 5.5 shows resistivity at 2000 mbsl and 5000 mbsl, respectively. These figures reveal low resistivity bodies at depth that could be related to magmatic heat sources. Three distinct low resistivity anomalies can be seen in the prospect area, one in the eastern part of the caldera towards the Black Hills , the other in the north eastern part of the caldera and the third towards Kuttung area.
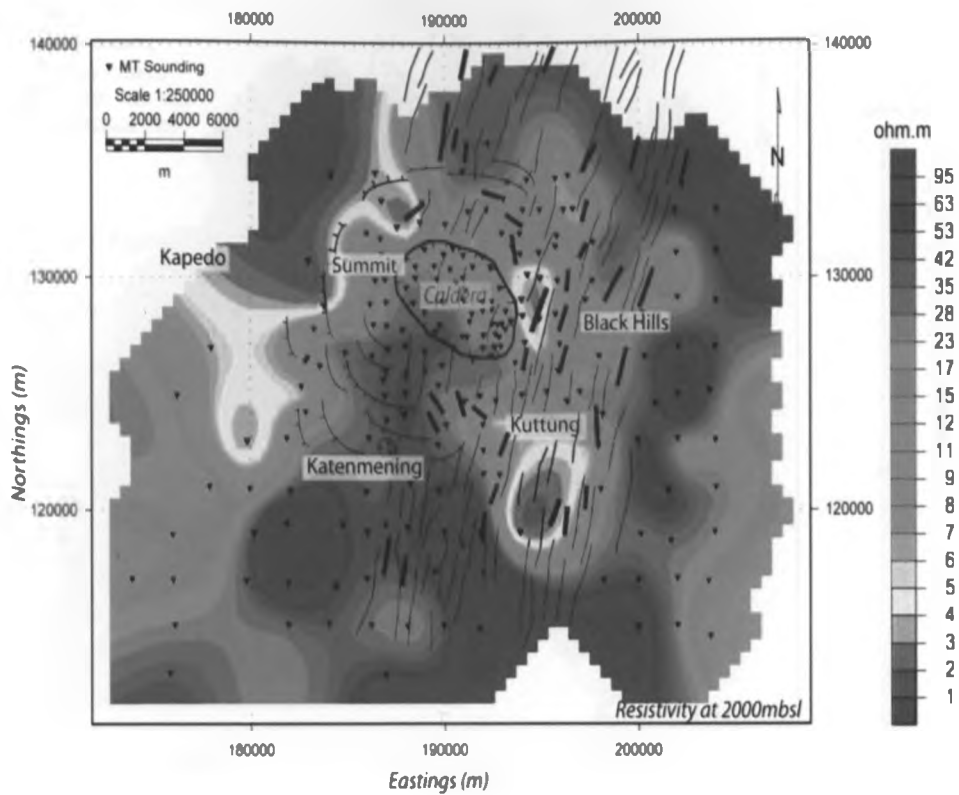
59

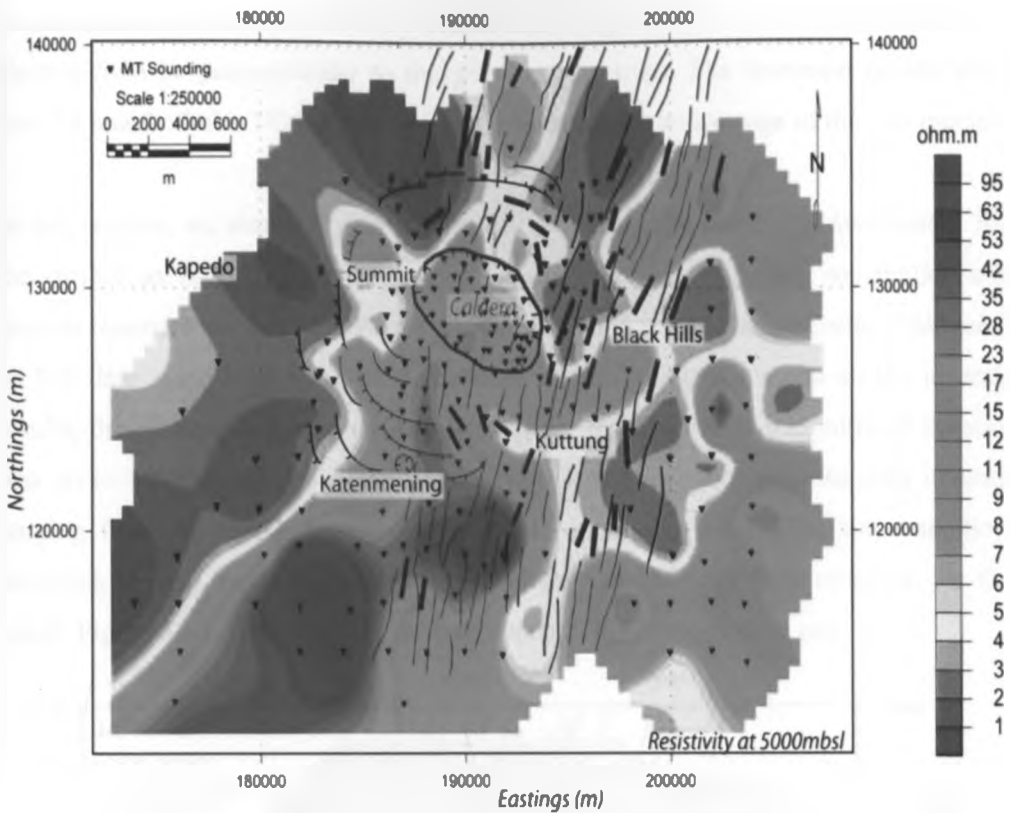Figure 5.4: Resistivity at 2000 m below sea level

Figure 5.5: Resistivity at 5000 m below sea level

A low resistivity anomaly spreads almost in the entire survey area with more prominence in the eastern part of the prospect area from the centre of the caldera (Figure 5.5). This probably is a heat source extending towards the eastern part of the prospect area. The relatively high resistivity seen in the upper elevation is still present which shows that the heat source is structurally controlled.

5.3 Two dimension (2D) inversion and interpretation

In 2D inversion process, it is assumed that the resistivity varies vertically (z) and in one lateral (either x or y) direction while in the other lateral direction (either y or x), the resistivity is constant. It is also assumed that the soundings along a profile are perpendicular to the geo-electric strike. During data collection, the MT instrument layout has the E lines and H coils oriented in the north-south and east-west directions, respectively, which does not necessarily coincide with the geo-electric strike (Figure 3.4). The data is rotated so that one axis is perpendicular and the other parallel to the geo-electric strike before running the inversions. Hence the data is polarized in two modes. The Transverse Electric (TE) mode is achieved when the electric field is parallel

to the geo-electric strike while the Transverse Magnetic (TM) mode requires that the electric field be perpendicular to the geo-electric strike. The inversion results shown here include both the TE and TM modes (assumed to be an average of the two modes).

In this section, we aim to obtain 2D images and show the resistivity distribution from the surface to 7000 m below sea level. To achieve this objective, we applied a 2D smooth inversion for both transverse electric (TE) and transverse magnetic (TM) modes on MT data along several profiles as shown in the figures below. In all the inversion results, the root mean square (RMS) errors were less than 5. The number of iterations was set to 45. This number was picked after running several inversions with iterations ranging from 30 to 60. We realized that 45 iterations were good since additional iterations beyond this value either did not change or had very little effect on the final result. Figure 5.6 below shows lines over which 2D inversions were run.
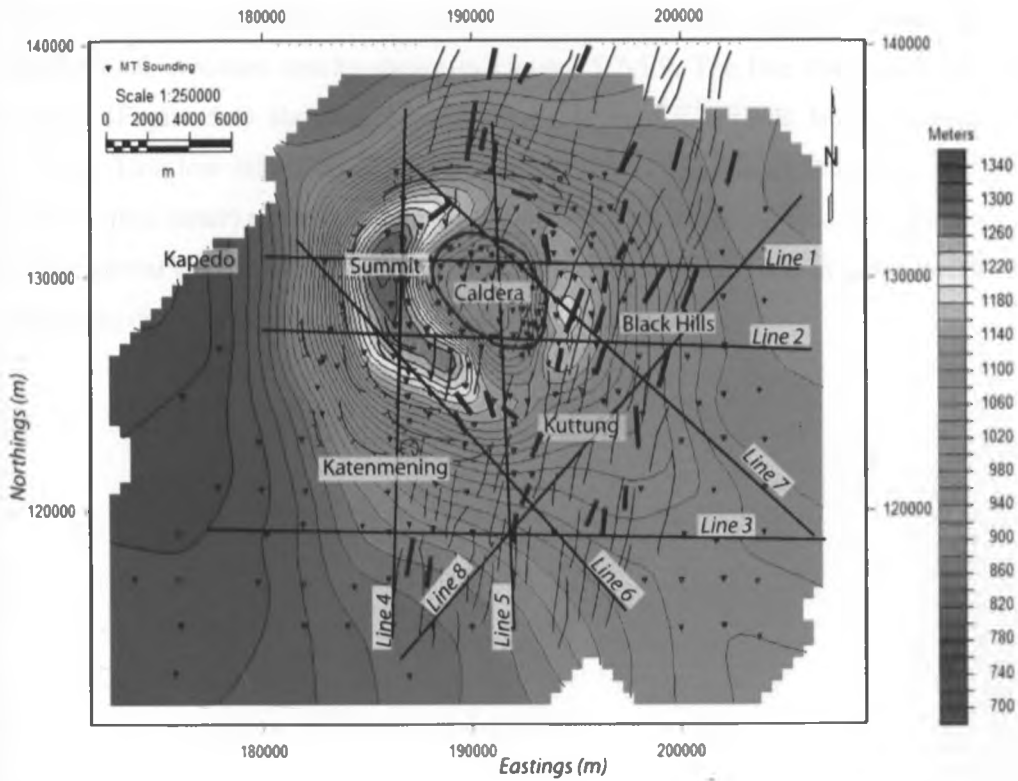

Figure 5.6: Silali contour map showing the sounding points

In general, the 2D resistivity inversion results show significant variations in the resistivity distribution both vertically and horizontally on all profiles. A lateral

62

conductor at about sea level shows up on all profiles. The conductor displays a varied thickness at all profiles. In high temperature geothermal systems, a shallow (about 1000 m depth) lateral conductor is after a hydrothermal alteration product (clay) (Cumming and Mackie, 2010; Spichak and Manzella, 2009; Ingham, 2004). The lateral conductor overlies a resistive zone in almost all the two-dimensional resistivity models (Figures 5.7-5.12). In several profiles (i.e., Figures 5.7, 5.8, 5.9), the resistive zones have signatures of nearly vertical conductors. The nearly vertical conductors are interpreted as fluid filled fracture systems/faults.

We group the 2D resistivity inversion models into four categories: profiles that trend east-west, profiles that trend north-south, the profiles that trend northwest-southeast, and profiles that trend northeast-southwest.

5.3.1 The east-west oriented profile lines.

a) Three east-west profile lines were drawn as shown in Figure 5.6 and their two dimensional inversion results shown in Figures 5.7-5.9. The line that cut through the caldera (Figure 5.6) shows a low resistivity layer that spreads laterally across the caldera. This low resistivity layer (conductor) shows significant low resistivity (less than 15 ohm meter) to the immediate west and far right of the caldera. The depth extent of this lateral conductor varies across the profiles from about 1000 m depth near to the caldera to over 3000 m away from it as shown in figure 5.7.
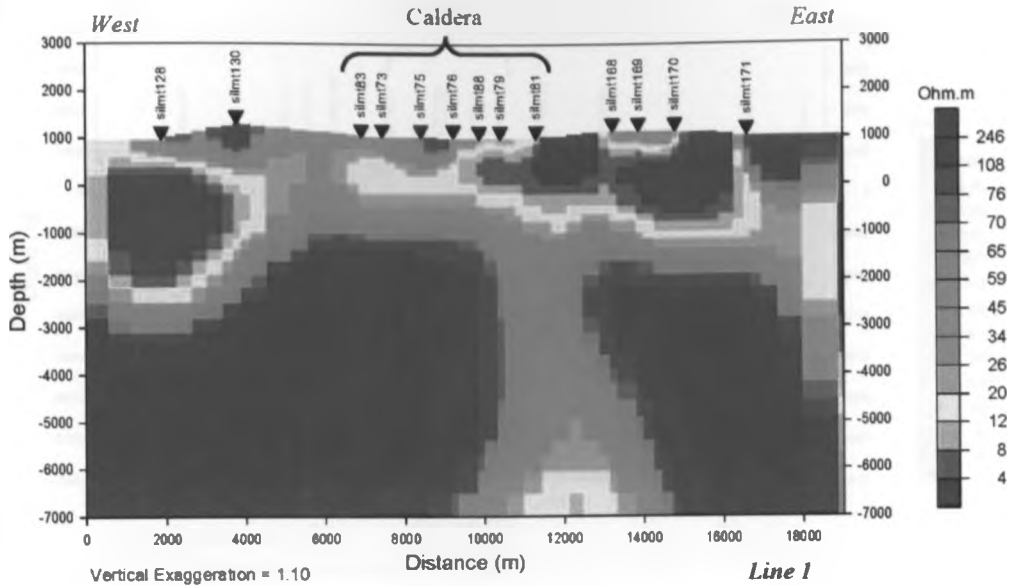
Figure 5.7: Two-dimensional resistivity cross-section along E-W Line 1 cutting through the Silali prospect in the north of the caldera.

Figure 5.8 also shows a nearly vertical conductor located at the central east section of the caldera. This low resistivity is thin at shallow elevations and the thickness increases with increasing depth. The resistivity variation trending east of the caldera was also observed on elevation slices of the resistivity maps (Figure 5.8 and 5.9). The vertical conductor zone is interpreted as a fault zone with fluid abundance. This interpretation applies to the north trending profiles (Figure 5.6).
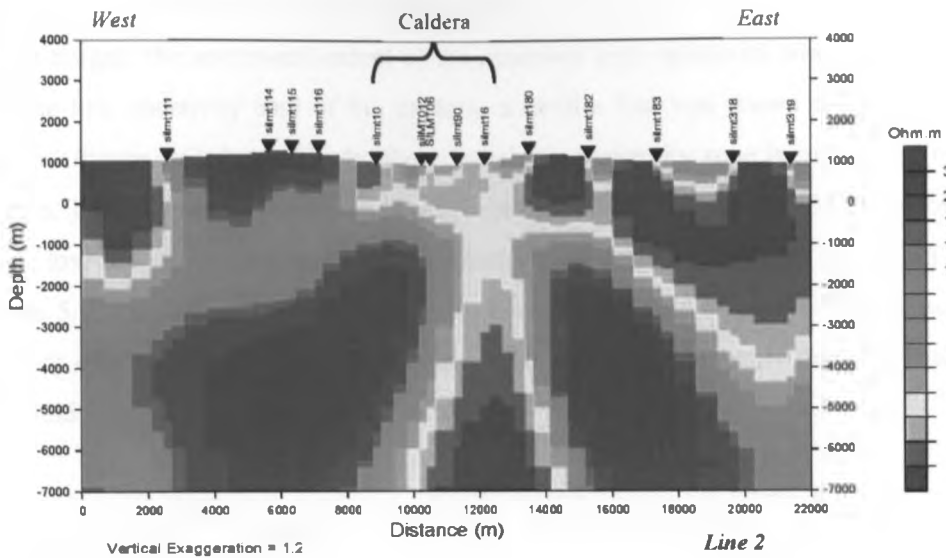
Figure 5.8: Two-dimensional resistivity cross-section along E-W Line 2 cutting through the Silali prospect in the south of the caldera.
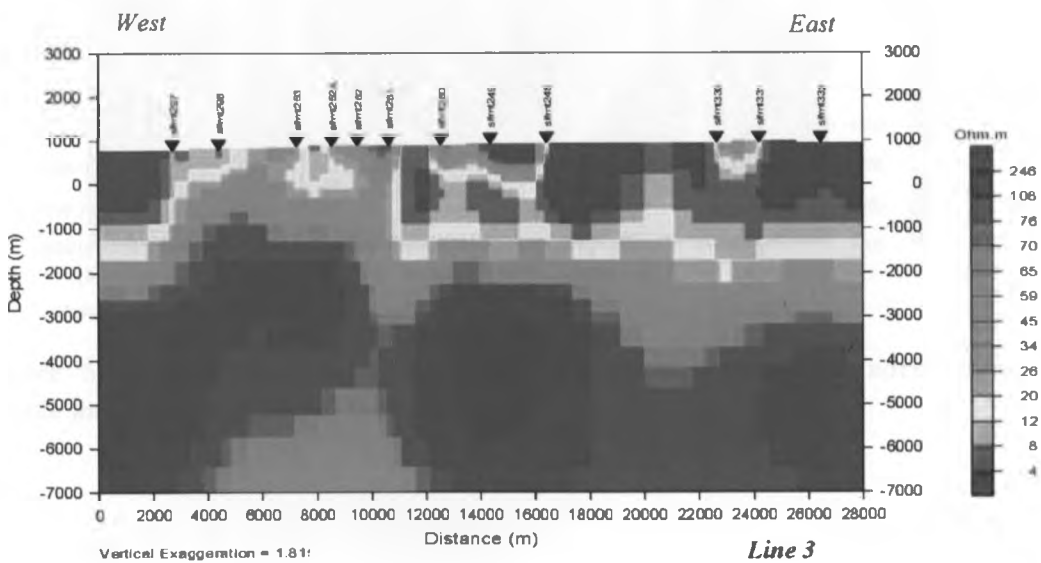

Figure 5.9: Two-dimensional resistivity cross-section along E-W Line 3 cutting through the Silali prospect in the south of the caldera.

5.3.2 The North-South oriented profile lines.

To investigate the southward extent of the observed high resistivity west of the caldera and the low resistivity east of the caldera, a profile line was drawn far south of the caldera (Figure 5.6). Interestingly, the vertical low resistivity zone is suppressed in this section. There appears to be a connection between the shallow (about 1000 m below sea level) low resistivity zone and the low resistivity at depths is 6000 m below sea level Figure 5.9. The top and bottom resistivity connection could suggest a fault; however, the lack of a significant low as in Figures 5.10 & 5.11 could imply that this fault has less fluid.
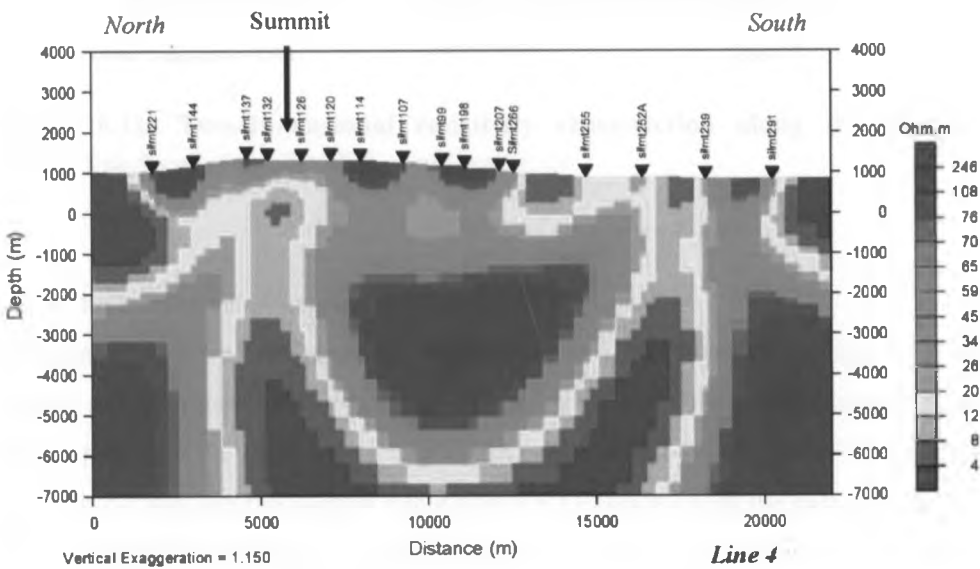

Figure 5.10: Two-dimensional resistivity cross-section along the north-south profile line 4 running west of the caldera.
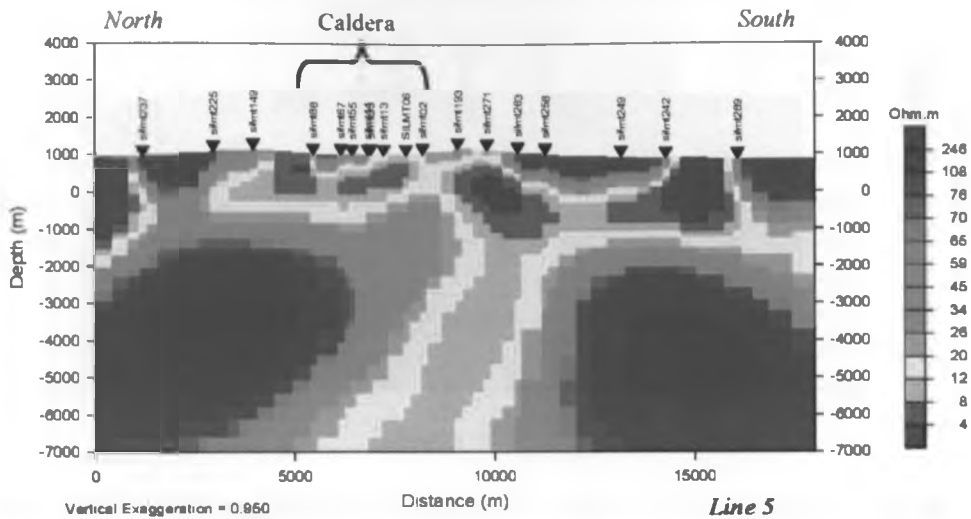
Figure 5.11: Two-dimensional resistivity cross-section along the north-south profile line 5 running east of the caldera.

5.3.3 The northwest-southeast oriented profile lines.

The general trend of faults around the Silali area is northeast from Figure 2.4 above. Hence, to investigate the depth extent of these faults, northwest trending profiles lines shown (Figure 5.6) were drawn. Figure 5.12 is a profile southwest of the caldera and does not cut through the caldera while figure 5.13 cuts through the caldera. The base of the clay cap (low resistivity) is shallow near the caldera (less than 1000 m below sea level) and extends to deeper levels away from the caldera along this profile. There are dipping conductors that are almost vertically oriented east of the caldera. These conductors are interpreted as faults.
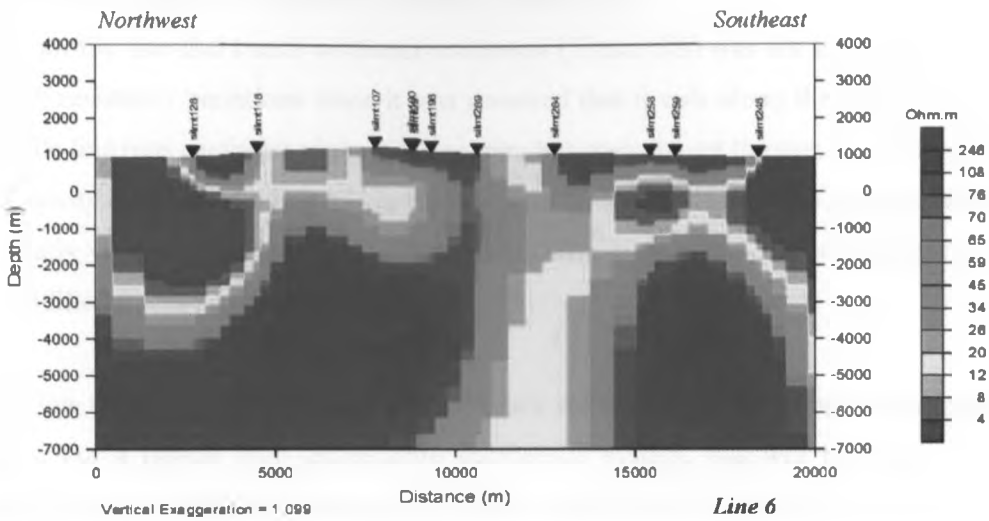
Figure 5.12: Two-dimensional resistivity models of the northwest-southeast profiles cutting west of the caldera and the Silali summit.
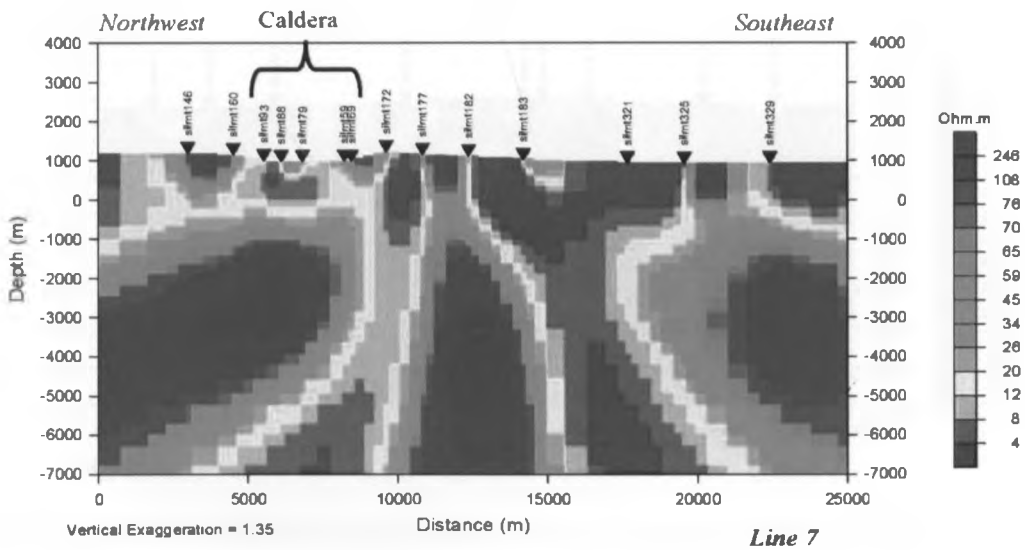

Figure 5.13: Two-dimensional resistivity models of the northwest-southeast Line7 cutting through the caldera.

5.3.4 The southwest-northeast oriented profile lines.

The profile line that trends northeast-southwest (Figure 5.6) was not expected to show much resistivity variations since it was assumed that it cuts along the fault line. This profile line runs southeast of the Silali caldera but does not cut through the caldera. The resistivity distribution along this profile shows a lateral conductor (cap rock) above and a nearly vertical conductor in an otherwise resistive zone below and is interpreted as a fluid filled fracture system (Figure 5.14).

The low resistivity layer at about 1000 m below sea level spreads throughout the profile lines. For a typical high temperature geothermal system, this will be clays rich in smectite and or zeolite (Cumming et al., 2000). The resistive zone that lies immediately below this conductor represents high temperature clays (Arnason et al., 2010; Spichak and Manzella, 2009).
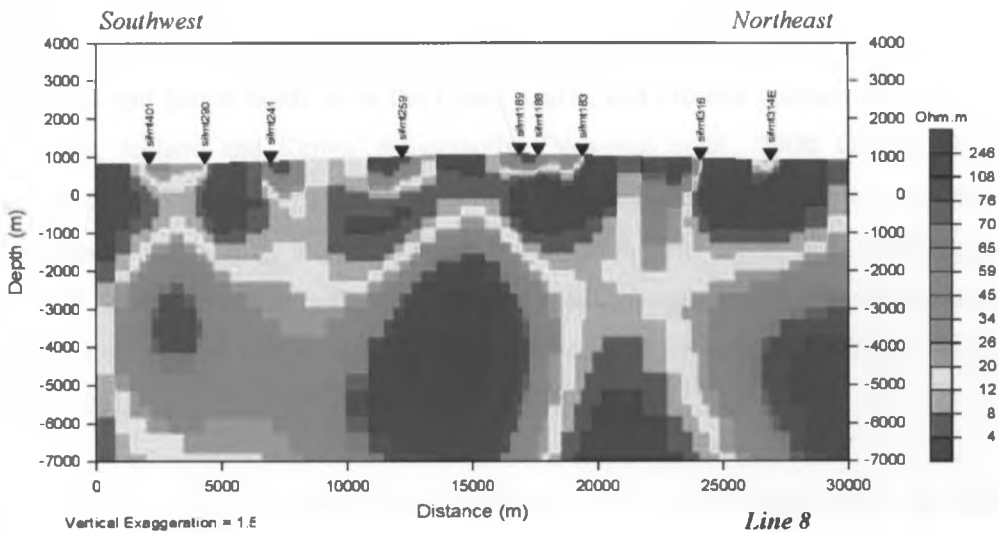

Figure 5.14: Two-dimensional Resistivity cross-section along NW-SE Line 8.

A proposed resistivity conceptual model for high temperature geothermal system requires that a conductive hydrothermal alteration zone (clay cap) overlies a less conductive (resistive) zone (Pellerin et al., 1996; Cumming et al., 2000). The resistivity of these zones is related to temperature dependent hydrothermal alteration processes (Flovenz et al., 2005). At low temperatures (but above 70^0C), clay minerals like smectite and zeolite are the dominant hydrothermal alteration products (Cumming et al.,

2000). High concentration of smectite and zeolite minerals within the rock matrix will reduce its electrical conductivity. At higher temperatures (up to 180^0C), chlorite and illite minerals form from hydrothermal effect. These minerals do not conduct electricity. And hence, high amounts of illite and chlorite within the rock matrix will increase its electrical resistivity. The concentration of illite and chlorite minerals increases with increasing temperature. At temperatures of about 220^0C and 240^0C, smectite and zeolite are never present and the only minerals are illite and chlorite (Flovenz et al., 2005; Cumming et al., 2000).

The reduced resistivity in the smectite dominated zones is attributed to the electrical double layer otherwise known as surface conduction (Flovenz et al., 2005). This surface conduction happens because of the movement of free mobile ions through the system. The freedom of ions is suppressed in the chlorite and illite rich zones and hence increases in resistivity (Flovenz et al., 2005). In the high resistivity region, low resistivity zones can occur and this has often been related to an increased porosity (fractures) and hence fluids as in the Coso, Krafla, and Olkaria geothermal system in California, Iceland and Kenya, respectively, (Newman et al., 2008, Onacha, 2006; Lichoro, 2009). However, the high resistivity in the chlorite- illite mineral dominated zone does not necessarily imply the absence of hydrothermal fluids. This could happen when the conductivity due to the hydrothermal fluids is suppressed by the abundance of the chlorite and illite and sometimes epidote minerals (Cumming et al., 2000; Flovenz et al., 2005).

In this study, MT data together with TEM data were used to characterize the Silali volcanic zone for its geothermal potential. Both 1D and 2D inversion models reveals a picture of a typical high temperature geothermal system around the Silali caldera (Arnason et al., 2010; Cumming et al., 2000; Spichak and Manzella, 2009). The resistivity data show a low resistivity (conductor) at shallow depth (about 0 -1000 m below sea level) which sits on top of a high resistivity zone. This conductor could be related to high temperature hydrothermal alteration product: the clay cap (Cumming and Mackie, 2010; Cumming et al., 2000; Wright et al., 1985). The conductivity in these regions is probably enhanced by smectite and/or zeolite minerals.

The increase in the resistivity of the underlying layer can be attributed to the transition from the conductive smectite mineral to resistive illite and chlorite minerals. This high resistivity zone is generally perceived to be the geothermal reservoir (Pellerin et al., 1996; Flovenz et al., 2005). Hence the conductivity of the reservoir is influenced most by the resistive illite clays than by the fluids confined within the reservoir fractures. However, in complex geothermal systems where faulting, hydrothermal alteration, fluid distribution, and fluid salinity affect resistivity, it is difficult to isolate unique relationships on resistivity signatures. In turn, this will often give room for unambiguous interpretation to the observed resistivity signatures.

In some cases, a low resistivity may occur in the illite-chlorite dominated zones. Our data show this type of anomalies as nearly vertical conductors. Similar conductors have been observed at Coso geothermal field and Olkaria geothermal field and were interpreted as zones of high fracture porosity and fluid abundance (Lichoro, 2009; Newman et al., 2008). We place a similar interpretation to the vertical conductor observed east of the Silali caldera.

From the ground surface to the base of the clay cap, the apparent resistivity plots show 1D characteristic (XY resistivity overlies the YX resistivity) as shown in Figure 4.8. However, at depth below the base of the clay cap rock, most of the stations show a separation of the XY and YX resistivity values (Figure 4.8). Onacha (2006) suggests that the splitting of these data begins at the base of the clay cap rock and the split is an indicator of the deviations from one dimensionality.

Results from the resistivity cross-sections derived from the 1-D joint MT and TEM inversions in the study area reveals three layers namely: a very shallow high resistivity layer of > 100 Ωm, an intermediate low resistivity layer of > 10 Ωm underlying the upper high resistivity layer, and a deep high resistivity layer with values greater than 50 Ωm underlying the low resistivity layer. MT resistivity cross-section also shows low resistivity at few kilometres depth below sea level that could be related to heat sources for this part of the field.

5.4 Conceptualized Geothermal Model

5.4.1 Silali Hydrothermal System

The apparent indicators for essential features for development of geothermal system(s) are discussed below.

5.4.2 Heat source

The continued eruption (post, intra caldera) indicates that the magma chamber below Silali caldera is still active (molten and hot). The Silali trachytes contain both silica-oversaturated and silica under-saturated varieties. The oversaturated types occur in the western flanks with the pre-caldera group while the caldera wall and post caldera groups are under-saturated (Macdonald et al., 1995). In the post caldera group, increasing differentiation is thought to have resulted in progressive silica under-saturation. The Blackhills trachytes are critically under-saturated with respect to silica. A general progression from two-feldspar trachytes to the dominant, one-feldspar varieties is accompanied by a decrease in phenocryst abundances with more evolved trachytes tending to be aphyric and glassy. The youngest activity on Silali erupted porphyritic olivine basalt on the north-eastern flanks of the caldera from a series of small scoria cones. There is lack of vegetation here suggesting that activity may have taken place only a few years ago probably 200-300 years ago (Dunkley et al., 1993).

5.4.3 Recharge and permeability

Silali prospect is located on the rift floor where hydrogeologic regime comprises of recharge of meteoric waters from the higher rift scarps mainly from the east, i.e., the Laikipia ranges and to some extent from the west, i.e., the Tiati hills. The intense rift floor fracture/faulting resulting from extensional tectonics of regional rifting in this area i.e., NNE and some EW structures, provide a good structural set up that allows water from the rift scarps to penetrate deep into the crust towards the magma bodies under the rift floor and normal faults conducting hot fluids from deep into possible geothermal reservoirs at shallower depth. The E-W lineament and the NNE fissure swarm may be such an important conduit of deep fluids, thus important geothermal controlling features in the area.

5.4.4 System capping:

Silali Volcano eruption included issue of several extensive blankets of pyroclastics. The spread of this debris, preferentially to the north and NW, is evidenced by the way the rift floor faults are masked in the area. Glassy component pyroclastics are susceptible to alteration forming hydrated clays that are the cause of self-sealing and the layered pyroclastics formation becoming very good capping for geothermal systems.

5.4.5 Geothermal System

Studies reveal that a high temperature geothermal system exists under Silali caldera within the prospect. It is envisaged that the reservoir is hosted within fractured trachytes and associated pyroclastics of Silali formation and flood trachytes of the Kenya rift floor. The intense fracturing of the formations is likely to have created high permeability within the reservoir; however, it is expected that some regions could have effects of sealing by dyke intrusions. It is envisaged that the reservoir primarily exists in the central part of the caldera but extends to the eastern side.

The main upflow of the geothermal fluids is postulated to be around the centre of the caldera and extending mainly east and southeast of the caldera. Resistivity data indicates the eastern half of the caldera to have high potential as evidenced by lower values. The top of the reservoir is to be expected to be at a depth of between 800-3,500 m and outflows at shallow levels to the east. From the above, a conceptualized geothermal model of the study area has been developed and is shown in Figure 5.15.
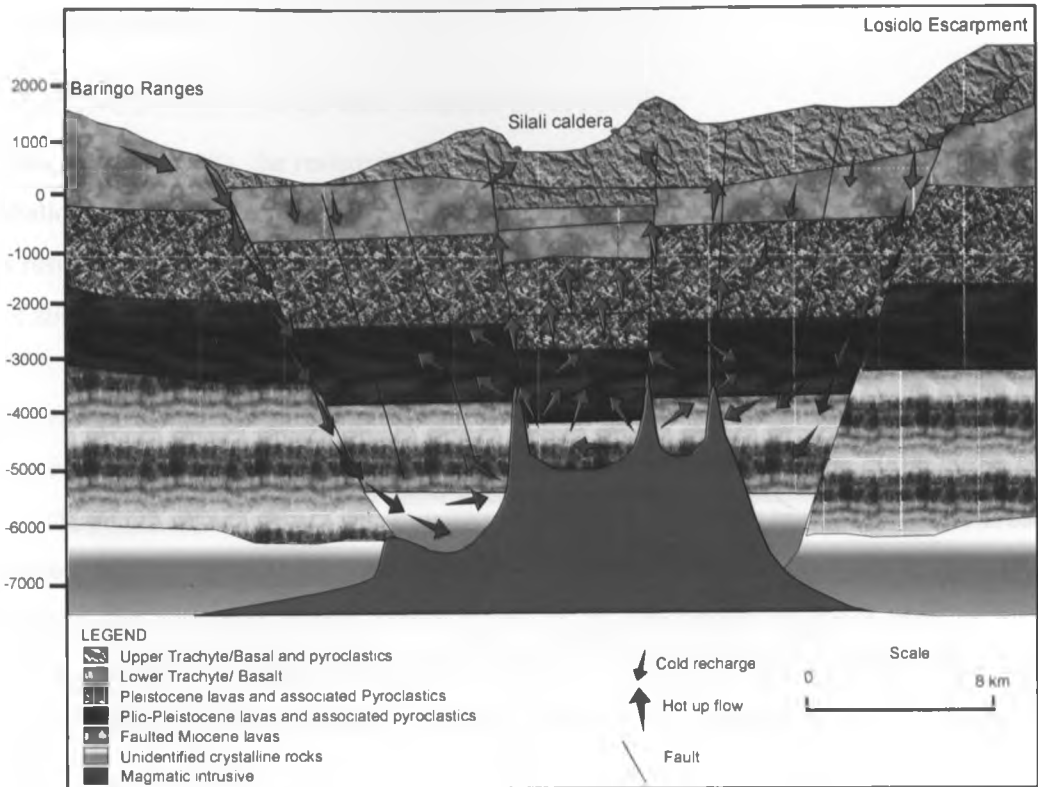
Figure 5.15: The E-W conceptualised geothermal model of Silali caldera along A-A'' in Figure 2.3

CHAPTER SIX

6.0 CONCLUSIONS AND RECOMMENDATIONS

Based on the results, the resistivity structure of the study area has been divided into 1) a shallow high resistivity zone (> 100 Ωm) to about 300 m below the surface which is as a result of unaltered rocks, 2) An intermediate low resistivity zone (10 Ωm) to depths of about 1 km which is as a result of low temperature hydrothermal alteration minerals, 3) A deeper high resistivity (> 50 Ωm), up to 3-4 km depth indicating high temperature minerals occurring at depth. The shallow boundary between an upper, low resistive layer and the underlying intermediate resistivity zone at depths of 800-3500 m appears to mark the change in clay mineralogy from low grade alteration mineralogy represented by smectite to high grade alteration mineralogy represented by chlorite, epidote and actinolite, which is interpreted as the geothermal reservoir zone of this study area, and 4) a deeper low resistivity region, at a depth of about 5000 m below sea level is inferred to be magmatic material or intrusion i.e., the heat source of this study area.

The resultant 2-D resistivity models showing significant variations in the resistivity distribution both vertically and horizontally on all profiles indicate major structural controls of the geothermal system.

Further, the study area seems to host a much larger geothermal resource under Silali caldera and extends to the eastern flanks covering an area of about 75 km^2 than previously thought. The system appears to cover much larger area than the coverage of soundings. The resource potential area has been determined using combined TEM and MT resistivity anomaly at 5,000 m depth. Using a conservative value of an average of 15 MWe per square kilometer, it is estimated that more than 1125 MWe can be generated from the identified resource at the study area.

It is therefore recommended that, more long period magnetotelluric (MT) and transient electromagnetic (TEM) data at the same area be acquired in order to define the extent of this field and 3-D interpretation be carried out to define three-dimensional features both laterally and vertically. However, to reduce ambiguities in resistivity data interpretations, constraints from other geophysical data (i.e. gravity and seismic),

geological, geochemical, and heat-flow data can greatly improve these interpretations before any drilling is done. In addition, exploratory wells should be drilled to about 3,000-m depth in the caldera and on the eastern flanks (Figure 6.1) of the caldera to confirm the characteristics and potential of the geothermal reservoir.
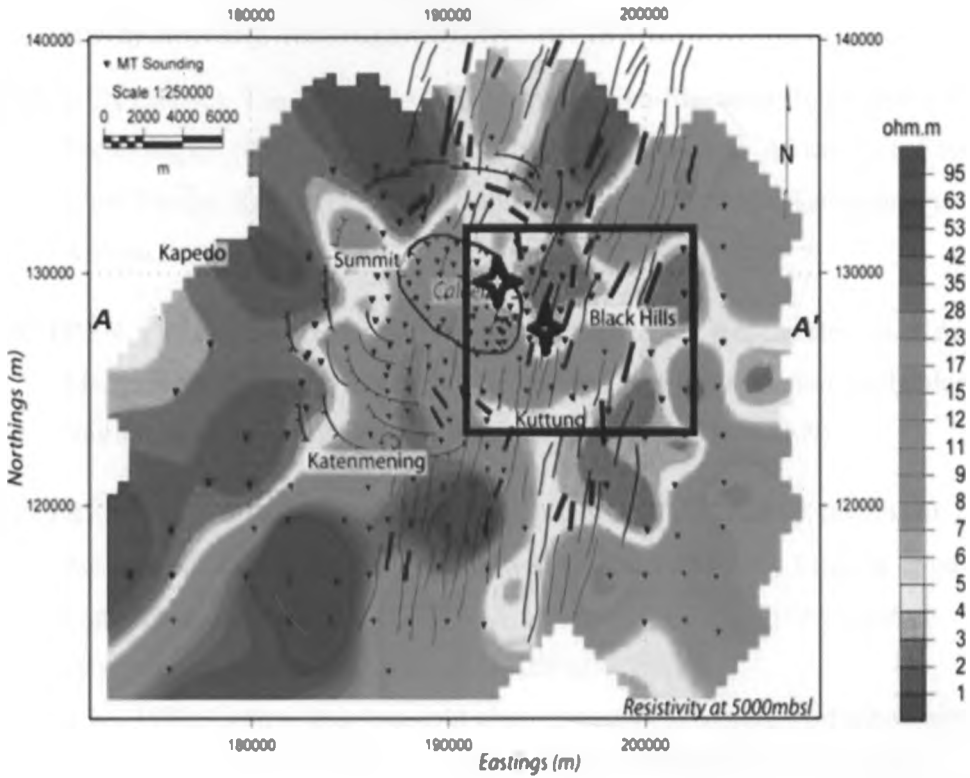

Figure 6.1: Resistivity anomaly map at 5000 mbsl showing the proposed wells.

REFERENCES

Achauer, U and the KRISP Teleseismic Working Group, 1994. New ideas based on the Kenya rift based on the inversion of the combined dataset of the 1985 and 1989/90 seismic tomography experiments. *Tectonophysics,. 236, p.305-329.*

Achauer, U., 1992. A study of the Kenya rift using delay-time tomographic analysis and gravity modeling. *Tectonophysics, 209: 197-207.*

AFREPREN (2004c). The Potential Contribution of Non-Electrical Renewable Energy Technologies (RET's) in Poverty Alleviation in Eastern Africa: The Case of Wind Pumps, Ram Pumps and Treadle Pumps in Kenya and Tanzania, Nairobi, African Energy Policy Research Network(AFREPREN)

AFREPREN (2005a) AFREPREN Occasional Paper 26. Renewables in Kenya's Electricity Industry: A Review of Geothermal and Cogeneration Technologies, Nairobi, African Energy Policy Research Network (AFREPREN)

AFREPREN/FWD (2006) Influencing policy through the Active Involment of a Reseach Institution in the Performance Contract Process- Lessons from the Experience of AFREPREN/FWD, Nairobi, Energy, Environment and Development Network for Africa (AFREPREN/FWD).

Árnason, K., 1989: Central-loop transient electromagnetic sounding over a horizontally layered earth. Orkustofnun, Reykjavík, report OS-89032/JHD-06, 129 pp.

Arnason, K., Eysteinsson, H., Hersir, G. P., 2010. Joint 1D inversion of TEM and MT data and 3D inversion of MT data in the Hengill area, SW Iceland. *Geothermics, 39, 13-34.*

Árnason, K., Karlsdóttir, R., Eysteinsson, H., Flóvenz, Ó.G., and Gudlaugsson, S.Th., 2000: The resistivity structure of high-temperature geothermal systems in Iceland. Proceedings of the World Geothermal Congress 2000, Kyushu-Tohoku, Japan, 923-928.

Balla, P. (2005) National Study on Small Hydropower Development Status and Potential of Small Hydropower Development in the Tea Industry in Kenya, unpublished report, Nairobi and Mombasa, UNEP/GEF and East African Tea Trade Association (EATTA).

Balla, P. (2005) The Potential Contribution of Non-Electrical Renewable Energy Technologies (RETs) towards Poverty Alleviation: Non-Electrical water pumping technologies for irrigation, Nairobi, Energy, Environment and Development Network for Africa (AFREPREN/FWD).

Berktold, A. (1983). Electromagnetic studies in geothermal regions. *J. Geophys. Surv 6.173-200*

Brace, W.F., and Orange A.S. 1968: Further studies of the effects of pressure on electrical resistivity of rocks, *J. Geophys. Res. 73-16*, 5407–5420.

Brace, W.F., and Orange A.S. 1968: Further studies of the effects of pressure on electrical resistivity of rocks, *J. Geophys. Res. 73-16*, 5407–5420.

Christensen, A., Auken, E., and Sørensen, K., 2006. The transient electromagnetic method. *Groundwater Geophysics, 71*, 179-225.

Clarke, M.C.G., Woodhall, D.G., Allen, D., and Darling, G., 1990: *Geological, volcanological and hydogeological controls of the occurrence of geothermal activity in the area surrounding Lake*

Constable, S., Parker, P., Constable, C., 1987. Occam's inversion: a practical algorithm for generating smooth models from electromagnetic sounding data. Geophysics 52. pp. 289– 300.

Cumming, W., Mackie, R., 2010. Resistivity imaging of geothermal resource using 1D, 2D, and 3D MT inversion and TDEM static shift correction illustrated by a Glass mountain case history. Proceeding World Geothermal Congress, 2010.

Cumming, W., Nordquest, G., astra, D., 2000. Geophysical exploration for geothermal resources: an application for combined MT –TEM. In: Society of exploration Geophysics Annual Meeting Teaching program expanded Abstracts, 6-11 August, Canary, Canada, pp. 1071-1074.

Dakhnov, V.N., 1962: Geophysical well logging. *Q. Colorado Sch. Mines, 57-2*, 445 pp.

Dunkley, P.N., Smith, M., Allen, D.J. and Darling, W.G. 1993. The geothermal activity and geology of the northern sector of the Kenya Rift Valley. British Geol. Surv., Research Report. Ministry of Energy, Kenya.

Fairhead, J. D. and Stuart, G. W., 1982. The seismicity of the East African rift system and comparison with other continental rift, *In G. Palmason (editor), Geodynamic series AGU, Washington DC, 8:41-61.*
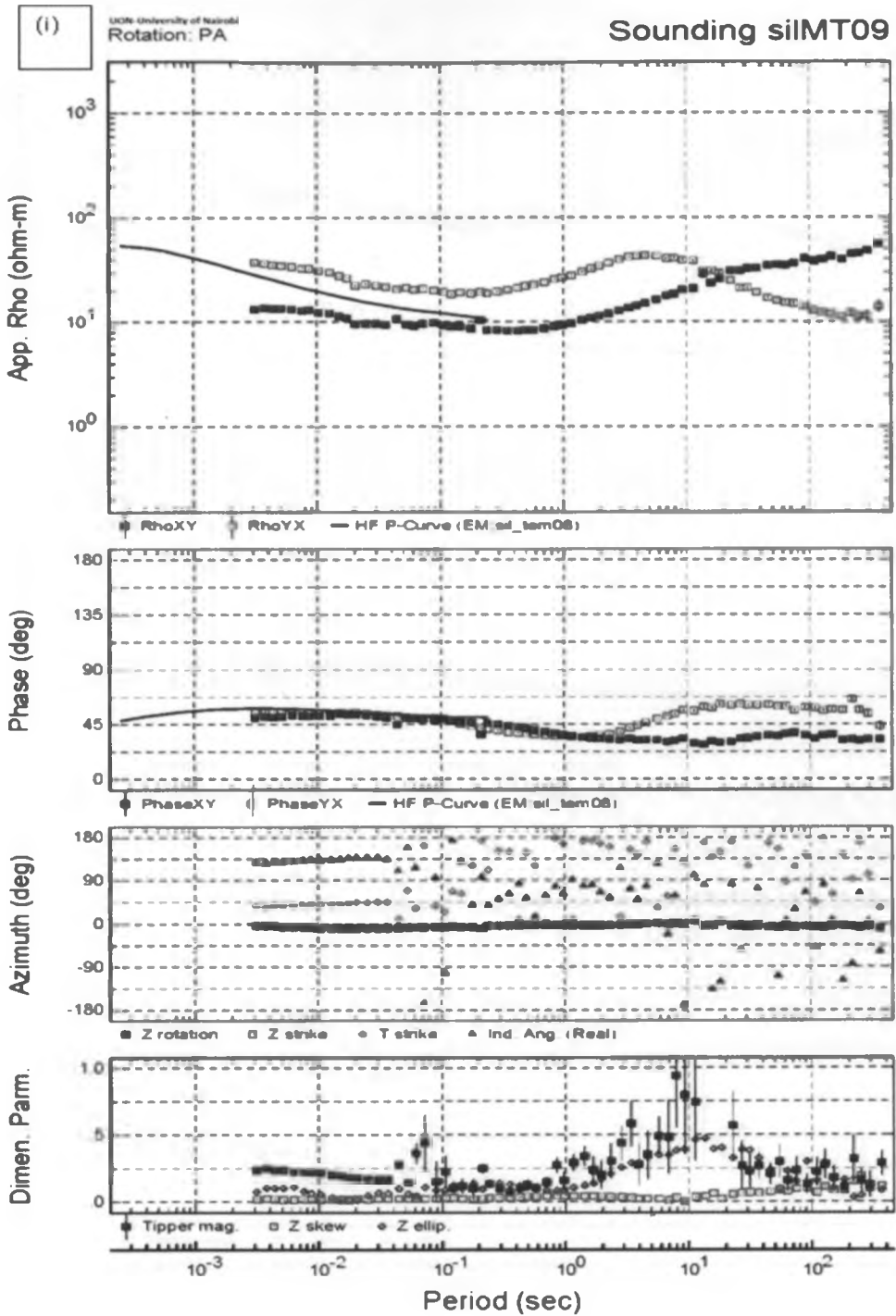
Fairhead, J. D., 1976. The structure of the lithosphere beneath the Eastern rift, East Africa, deduced from gravity studies. *Tectonophysics, 30: 269-298.*

Flovenz, O., Spangenberg, E., Kulenkampff, J., Anarson, K., Karlsdottir, R., and Huenge, E. 2005. The role of electrical conduction in geothermal exploration. Paper presented at the World Geothermal Congress, Antalya, Turkey.

Garcia, X., and Jones, A.G., 2002: Atmospheric sources for audio-magnetotelluric (AMT) sounding. *Geophysics, 67,* 448–458.

GOK (2002b) National Development Plan 2002-2008, Nairobi, Government of Kenya (GOK).

Hamilton R. M., Smith B. E., and Knopp F., 1973. Earthquakes in Geothermal Areas near Lakes Naivasha and Hannington (Bogoria), Kenya. Unpublished report to the UNDP/EAP&L.

Hamilton R.M. and Muffler, L. J. P. 1972. Micro-earthquakes at the Geysers Geothermal area, California. *J. Geophys. Res.,77, no. 11,* 2081-2086

Henry, W.J., 1987. A seismic investigation of the Kenya Rift Valley. PhD thesis, University of Leicester, Leicester. 214pp

Henry, W.J., Mechie, J., Maguire, P.K.H., Khan, M.A., Prodehl, C., Keller, G.R., and Patel, J., 1990. A seismic investigation of the Kenya rift valley. *Geophys. J. Int. vol. 100, pp.107-130.*

Hermance, J.F., 1973: Processing of magnetotelluric data. *Physics of the Earth and Planetary Interiors, 7,* 349-364.

Hersir, G.P., and Björnsson, A., 1991: Geophysical exploration for geothermal resources. Principles and applications. UNU-GTP, Iceland, report 15, 94 pp.

Ingham, M. 2004. High resolution electrical imaging of fault zones. Phy. of the earth and planetary interior. 150. p. 93-105

Kearey, P., and Brooks, M., 1994: An introduction to geophysical exploration (2nd edition). Blackwell Scientific Publ., London, 236 pp.

Keller, G. R., Mechie, J., Braile, L. W., Mooney, W. D. and Prodehl, C., 1994. Seismic structure of the uppermost mantle beneath the Kenya rift. In C. Prodehl, G. R. Keller and M.A Khan (Editors), Crustal and Upper Mantle structure of the Kenya Rift. *Tectonophysics, 236: 201-210.*
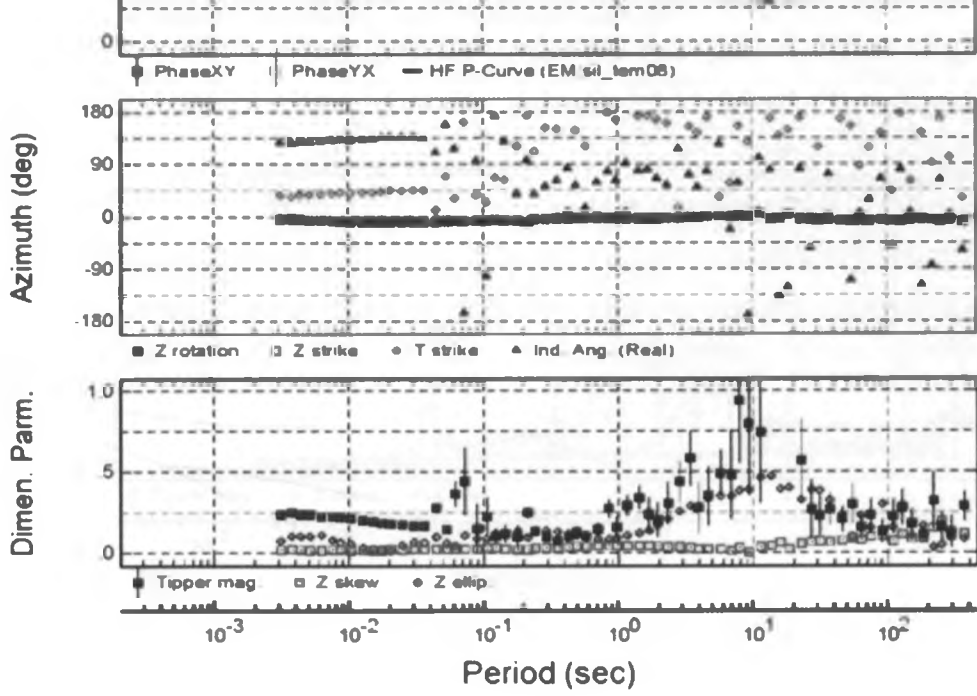
Keller, G.R., Prodehl, C., Khan M.A., Morgan, P., Braile, C.W., Ulsen, K.H., Wendlandt, R.F., and Baldridge W.S., 1994. The East African Rift system in the light of KRISP 90. *Tectonophysics, 236: 465-483.*

Keller, G.V., and Frischknecht, F.C., 1966: Electrical methods in geophysical prospecting. Pergamon Press Ltd., Oxford, 527 pp.

KNBS (2006) Kenya Facts and Figures, Kenya National Bureau of Statistics (KNBS)

KPLC (2006). Annual Report, 2006, Nairobi Kenya Power and Lightning Company (KPLC)

Lee Lerner, K., Lerner, B.W., and Cengage, G., 2003: *Porosity and permeability.* World of Earth Science, Retrieved from http://www.enotes.com/earth-science/

Lichoro, 2009., Joint 1-D inversion of TEM and MT data from Olkaria domes geothermal area, Kenya. *Paper presented at the UNU geothermal Training Programme.*

Mariita, N. O., Keller, G. R., 2007. An integrated geophysical study of the northern Kenya rift. J. Afr Earth Sc. 48, 80-94.

Mariita, N.O. 2003. An integrated geophysical study of the northern Kenya rift crustal structure: implications for geothermal energy prospecting for Menengai area. *A PhD dissertation, University of Texas at El Paso, USA.*

Meju, M. A., 1996. Joint inversion of TEM and MT data soundings: some effective practical considerations. *Geophysics, 61. 56-65.*

MOE, 2002. Study on Kenya's Energy Demand, Supply And Policy Strategy for Households, Small Scale Industries and Service Establishments, Ministry of Energy (MOE)

Newman, G. A., Hoversten, M.,Gasperikova, E., Wannamaker, P. E., (2008). Three-dimensional magnetotelluric characterization of the Coso geothermal field *Geothermics 37, 369-399*

Ngigi, A. and D. Macharia, IT Power East Africa.2006. Health Sector Policy Overview Paper.Nairobi, ENABLE.

NOCK 1987. Aeromagnetic data interpretation of the Winam Gulf and the east African Rift areas in Kenya. National oil Corporation of Kenya, unpubl report no. 26/2 16D.

Omenda, P.A., 2000: Anatectic origin for Comendite in Olkaria geothermal field, Kenya Rift; Geochemical evidence for syenitic protholith. *African Journal of Science and Technology, Science and Engineering series,* 1, 39-47.

Onacha, S.A.: The electrical resistivity structure of the Eburru prospect. KPC Internal report, (1990)

Pellerin, L., and Hohmann, G. W. 1990. Transient electromagnetic inversion: a remedy for magnetotelluric static shift. *Geophysics* 55. 1241-1250.

Pellerin, L., Johnston, J. M., Hohmann, G. W., 1996. A numerical evaluation of electromagnetic methods in geothermal exploration. *Geophysics. 61, 121-130.*

Quist, A.S., and Marshall, W.L., 1968: Electrical conductances of aqueous sodium chloride solutions from 0 to 800°C and at pressures to 4000 bars. *J. Phys. Chem., 72,* 684-703.

Simiyu, S. M., Keller, G. R 1997. An integrated analysis of the lithospheric structure across the east African plateau based on gravity analysis and recent seismic studies. *Tectonophysics* Vol. 278.

Simiyu, S. M., Keller, G. R., 2001. An integrated geophysical analysis of the upper crust of the Southern Kenya rift. *Geophys. J. Int.* 147, 543-561.

Simiyu, S.M., and Keller, G. R., 1997. Integrated geophysical analysis of the East African Plateau from gravity anomalies and recent seismic studies. *Tectonophysics, 278:291-314.*

Slack, P. D., Davis, P. M. and the KRISP Teleseismic Working Group. 1994. Attenuation and velocity of P-waves in the mantle beneath the East African rift, Kenya. In: C. Prodehl, G. R. Keller and M. A. Khan (Editors), Crustal and Upper Mantle Structure of the Kenya Rift. *Tectonophysics, 236, 179-199.*

Smith, M., 1994. Stratigraphic and structure constraints on the mechanism of active rifting in the Gregory rift Kenya. In: C. Prodehl, G. R. Keller and M. A. Khan (Editors), Crustal and Upper mantle structure of the Kenya rift. *Tectonophysics,*236, 3-22.

Spichak, V., Manzella, A. 2009. Electromagnetic sounding of geothermal zones. J. *Appl. Geophys.* 68, 459-478.

Swain, C. J. and, Khan, M. A., 1978. Gravity measurements in Kenya. *Geophys. J.R. Astron. Soc.,* 53, 427-428.

Swain, C. J., Khan, M. A., Wilton, T. J., Maguire, P. K. H., and Griffiths, D. H., 1981. Seismic and gravity surveys in the Lake Baringo-Tugen Hills area, Kenya rift valley. *J. Geol. Soc. London, 138, 93-102.*

Swain, C.J., 1992. The Kenya Rift axial high: a re-interpretation. *Tectonophysics, 204: 59-70.*

Swain, C.J., Maguire P.K., and Khan M.A., 1994. Geophysical experiments and models of the Kenya rift before 1989. *Tectonophysics, 236: 23-33.*

Tongue, J.A., 1992. Tomographic study of local earthquake data from the Lake Bogoria region of the Kenya Rift. *Geophys. J. Int., 109, 249-258.*

Tongue, J.A., Maguire, P.K.H., and Burton, P. 1994. An earthquake study in the Lake Baringo basin of the central Kenya Rift. *Tectonophysics, 236, 151-164.*

Wannamaker, P. E. 1999. Affordable magnetotellurics; interpretation in natural environments. In; Orastaglio, M., Spies, B. (Eds.), Three-Dimension Electromagnetic. Geophysical Development Series,. Society of exploration Geophysicist, *Tulsa, Vol. 7 p. 724.*

Williams, L.A.J., Macdonald,R., and Chapman, G.R. 1984. Late Quaternary caldera volcanoes of the Kenya Rift. *Journal of Geophysical research,* 89, B10, 8553-8570.

World bank, 2004. Africa Development Indicators. Washington D.C: The World Bank.

World bank, 2006. World Development Indicators, 2006. Washington D.C: The World Bank.

Wright, P. M., Ward, S. H., Ross, H. P., West, R. C., 1985). State-of-the-art geophysical exploration for geothermal resources. *Geophysics,* 55. 2666-2699.

Young P., Maguire P., Laffoley A., and Evans J., 1991. Implications of the distribution of seismicity near Lake Bogoria in the Kenya rift. *Geophys. J. Int., 105, 665-674.*

APPENDIX I: STATIC SHIFT CORRECTION OF MT USING TEM.
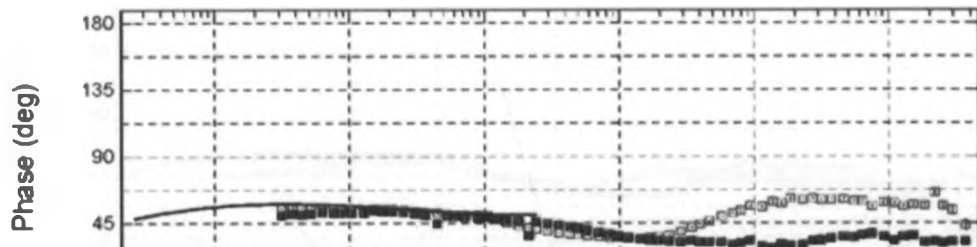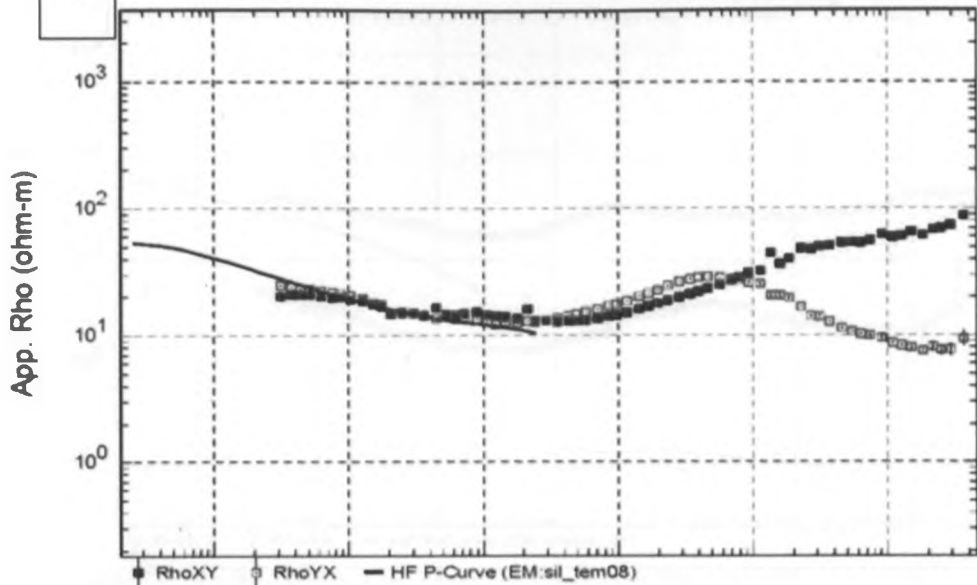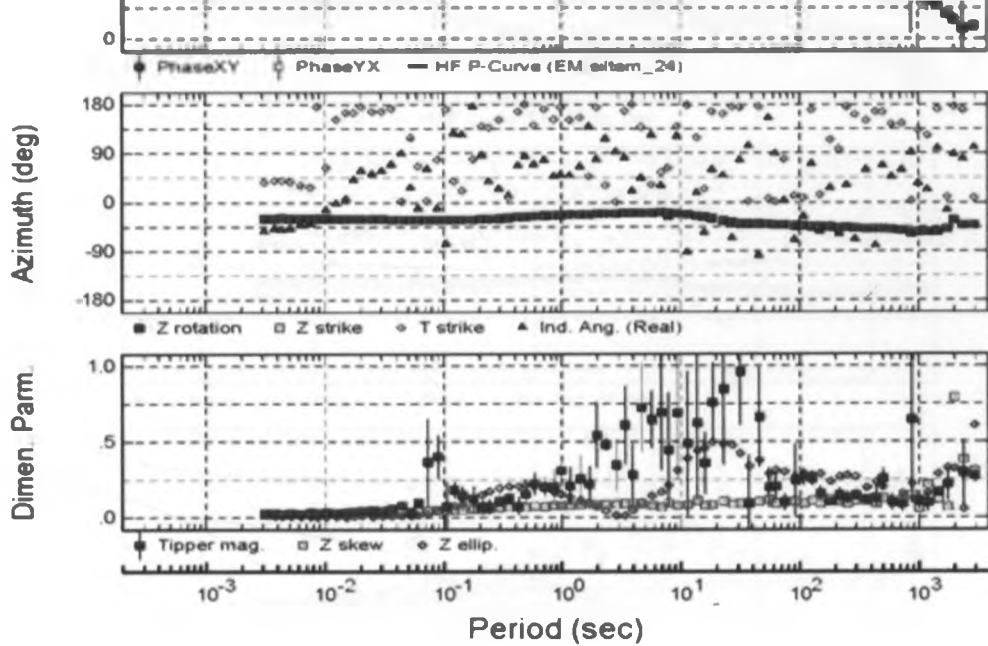
Sounding silMT09

(ii) UON-University of Nairobi
Rotation: PA

App. Rho (ohm-m)

10^3

10^2

10^1

10^0

■ RhoXY   □ RhoYX   — HF P-Curve (EM:sil_tem08)

Phase (deg)

180

135

90

45

85

Sounding silMT 24

86

(ii) Rotation: PA
UON-University of Nairobi

Sounding silMT24

App. Rho (ohm-m)

10^3
10^2
10^1
10^0
10^{-1}

● RhoXY   □ RhoYX   — HF P-Curve (EM sitem_24)

Phase (deg)

180
135
90
45

(I)

Rotation PA

Sounding silMT55

App. Rho (ohm-m)

10^3

10^2

10^1

10^0

10^{-1}
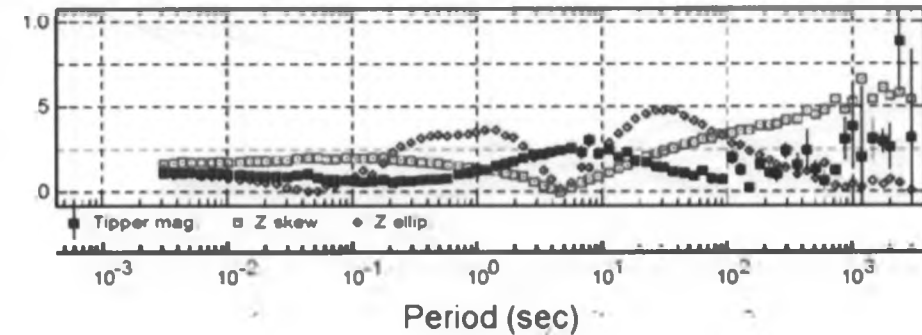
RhoXY   RhoYX   — HF P-Curve (EM:siltem_55)

Phase (deg)

180

135

90

45

(ii) UON-University of Nairobi
Rotation: PA

Sounding silMT55

PhaseXY   PhaseYX   — HF P-Curve (EM siltem75)

Z rotation   Z strike   T strike   Ind Ang (Real)

Tipper mag   Z skew   Z ellip

89
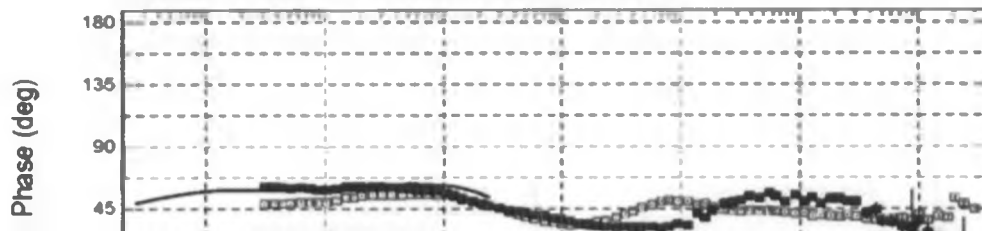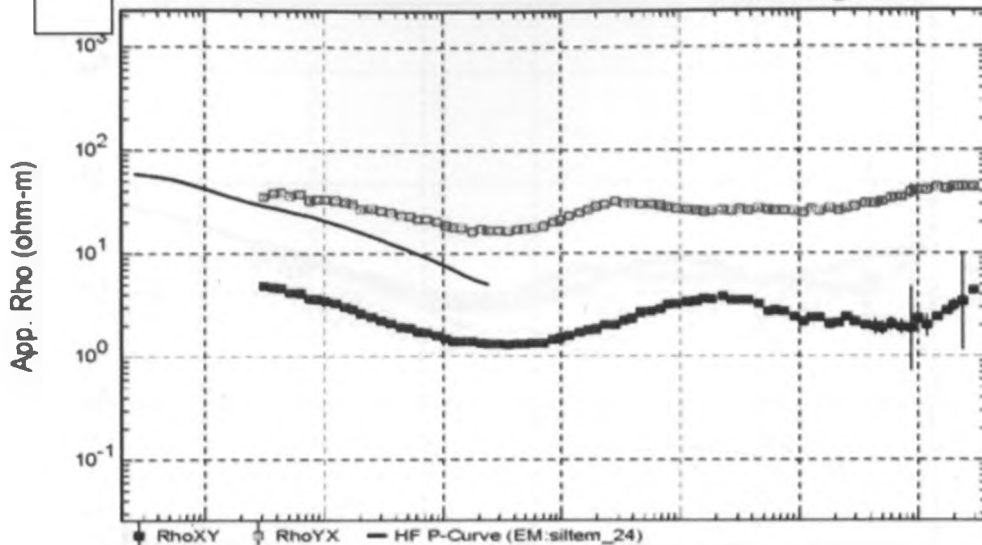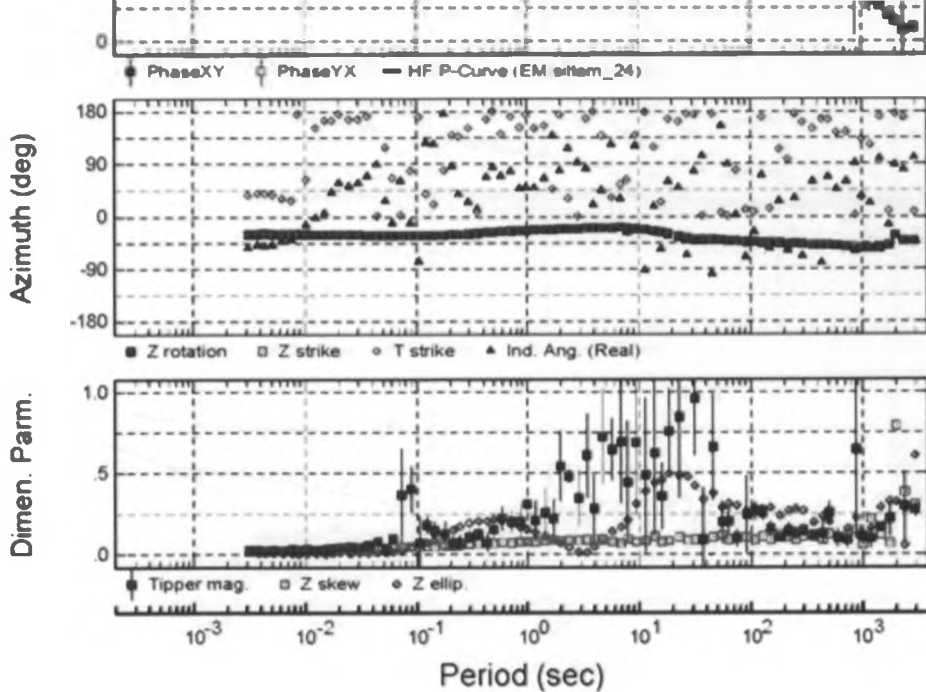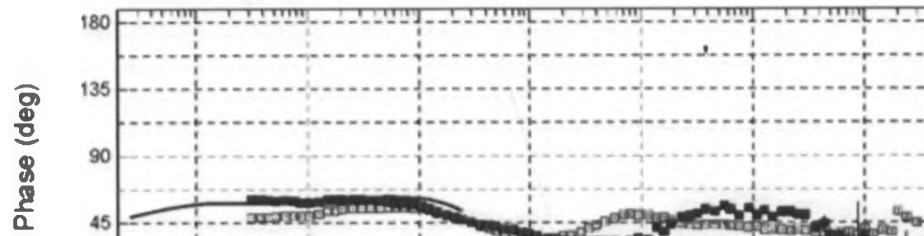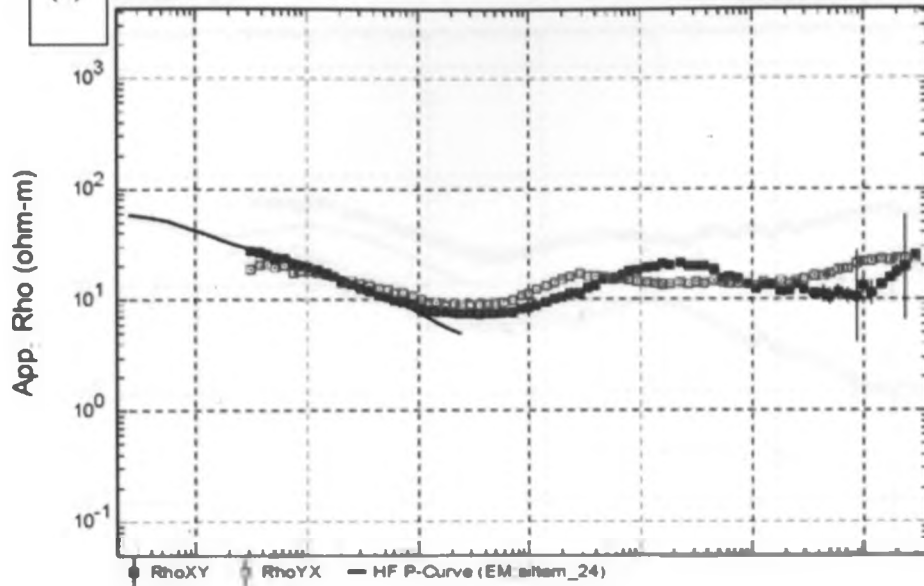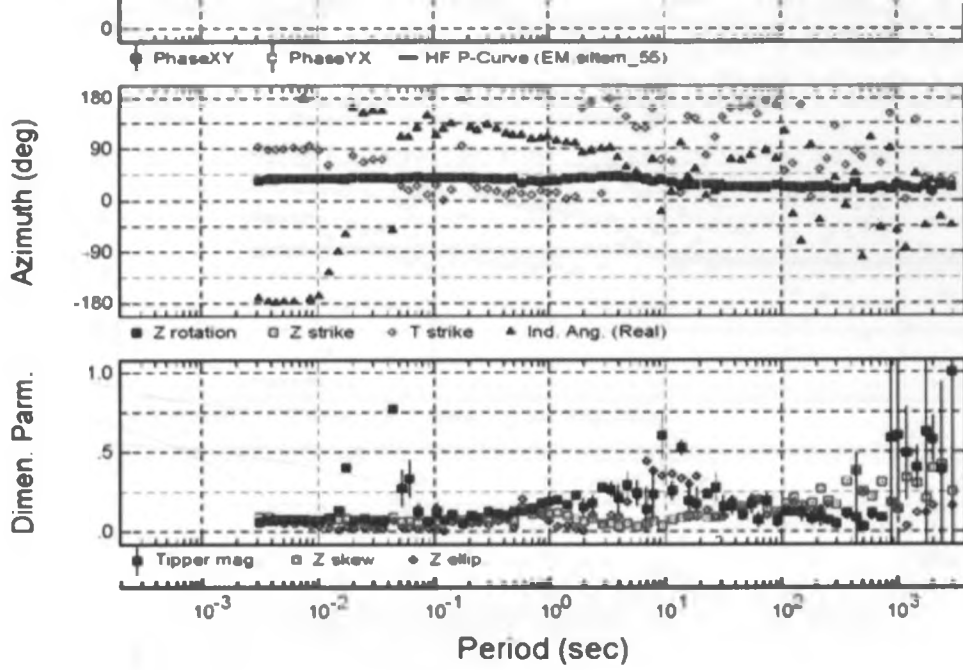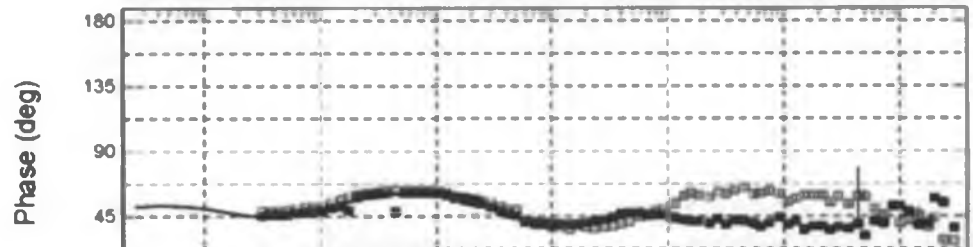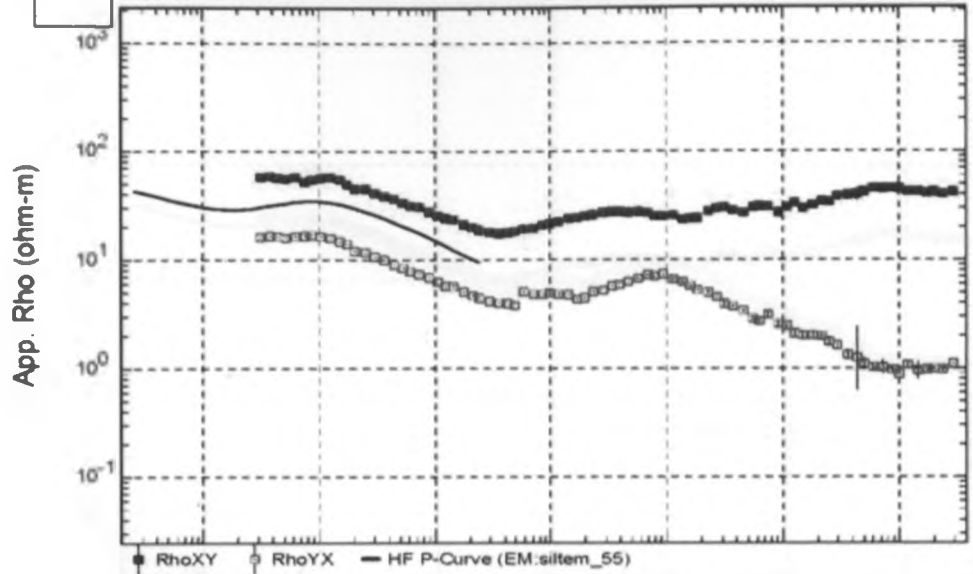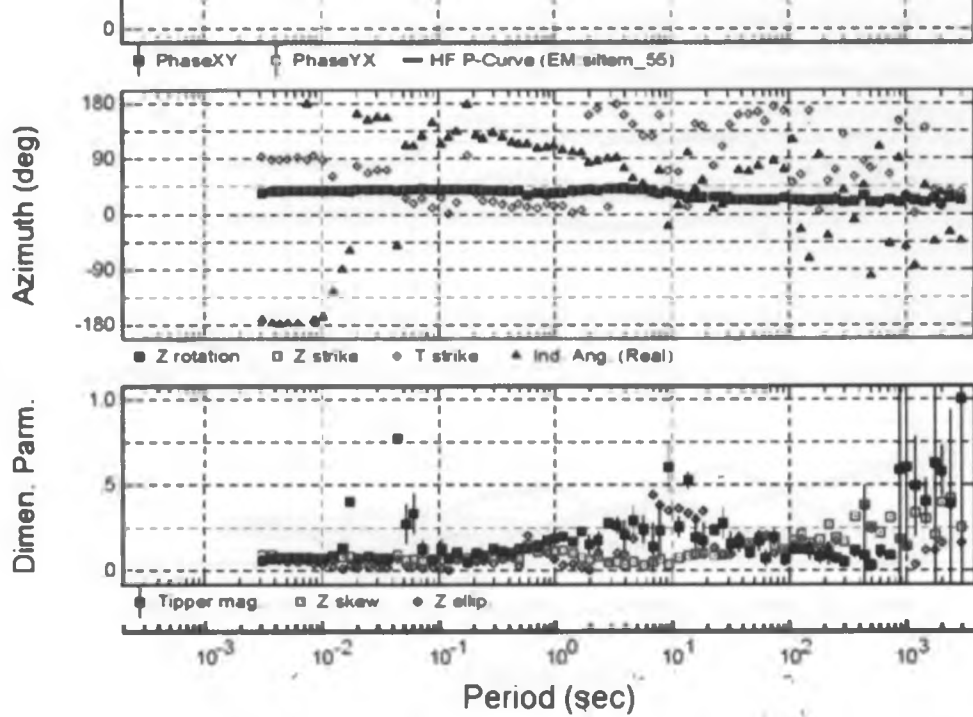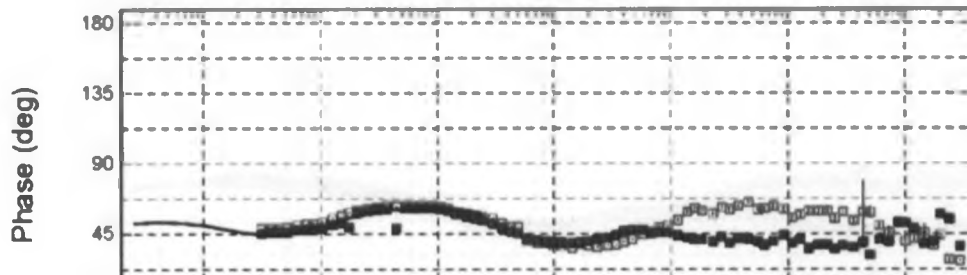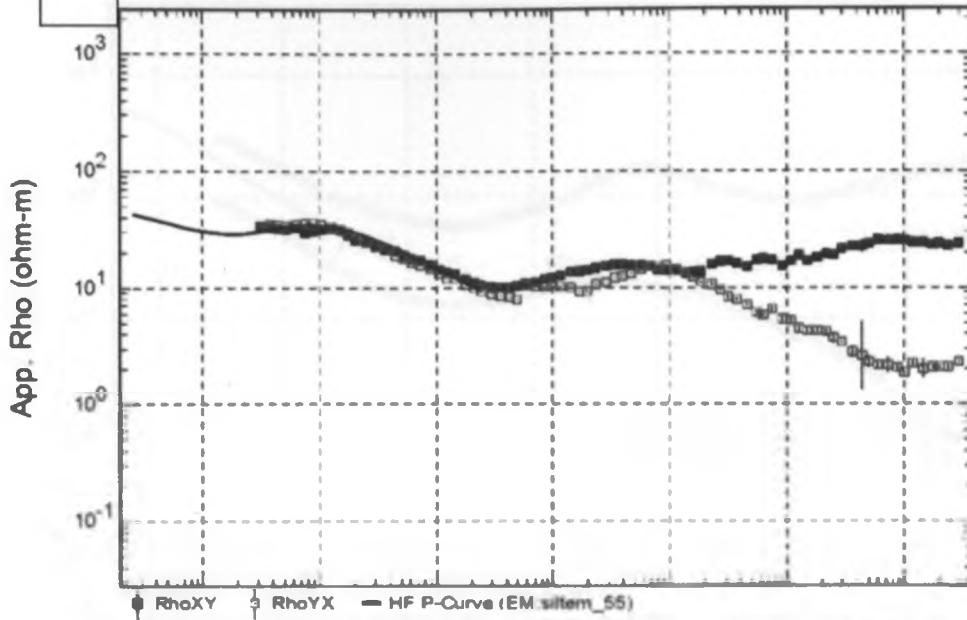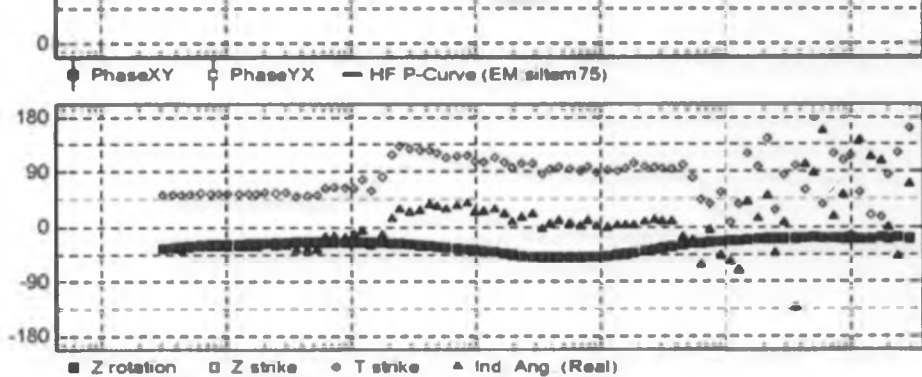
(i) UON-University of Nairobi
Rotation: PA

Sounding silMT75

App. Rho (ohm-m)

■ RhoXY   ♢ RhoYX   — HF P-Curve (EM:siltem75)

Phase (deg)

UON-University of Nairobi
Rotation: PA

Sounding silMT180

App. Rho (ohm-m)

10^2

10^1

10^0

● RhoXY   ╓ RhoYX   — HF P-Curve (EM:siltem 180)

Phase (deg)

180

135

90

45

0

● PhaseXY   ╓ PhaseYX   — HF P-Curve (EM:siltem 180)

Azimuth (deg)

180

90

0

-90

-180

■ Z rotation   □ Z strike   ◇ T strike   ▲ Ind. Ang. (Real)

Dimen. Parm.

1.0

.5

.0

■ Tipper mag.   □ Z skew   ◇ Z ellip.

10^{-3} 10^{-2} 10^{-1} 10^0 10^1 10^2

Period (sec)